UNIVERSITY OF CALIFORNIA
RIVERSIDE

# In Situ Surface Sensitive Analysis of Platinum Atomic Layer Deposition on Silicon-Based and Metal Substrates

A Dissertation submitted in partial satisfaction
of the requirements for the degree of

Doctor of Philosophy

in

Materials Science and Engineering

by

Clinton K. Lien

December 2018

Dissertation Committee:
Dr. Francisco Zaera, Chairperson
Dr. Elaine Haberer
Dr. Sandeep Kumar

Copyright by
Clinton K. Lien
2018

The Dissertation of Clinton K. Lien is approved:

______________________________________________

______________________________________________

______________________________________________
Committee Chairperson

University of California, Riverside

# ACKNOWLEDGEMENTS

I would like to express the deepest appreciation to my committee chair Professor Zaera, who continually and convincingly conveyed a spirit of adventure in regard to research and scholarship, and an excitement in regard to teaching. Without his guidance and persistent help this dissertation would not have been possible.

I would like to thank Professor Elaine Haberer and Professor Sandeep Kumar, for serving as my advancement & doctoral committees.

COPYRIGHT ACKNOWLEDGEMENTS

The text of this dissertation, in part or in full, is a reprint of the material as is appears in the publications below. Dr. Francisco Zaera directed and supervised the research which forms the basis for this dissertation.

[1] Lien, C.; Sun, H.; Qin, X.; Zaera, F. Platinum Atomic Layer Deposition on Metal Substrates: A Surface Chemistry Study. Surface Science 677, **2018**, 161–166.

[2] Lien, C.; Konh, M.; Chen, B.; Teplyakov, A.V.; Zaera, F. Gas-Phase Electron-Impact Activation of Atomic Layer Deposition (ALD) Precursors: $MeCpPtMe_3$. J. Phys. Chem. Lett 9, 16, **2018**, 4602-4606.

ABSTRACT OF THE DISSERTATION

# In Situ Surface Sensitive Analysis of Platinum Atomic Layer Deposition on Silicon-Based and Metal Substrates

by

Clinton K. Lien

Doctor of Philosophy, Graduate Program in Materials Science and Engineering
University of California, Riverside, December 2018
Dr. Francisco Zaera, Chairperson

Platinum (Pt) has been extensively used in the fuel cells due to their excellent catalytic activity; with high work function, it is also a possible candidate for the use in memory devices as charge storage medium, and thereby has generated interest in MOS structures. The Pt cost/availability is one of the major reasons limits it's commercialization. Scaling the film thickness or downsizing catalyst nanoparticles to single atoms could significantly increase their efficiency in energy aspect or lessen the impact of lateral coupling of charge storage layers, reduce the stress-induced leakage current in MOSFET applications.

Atomic layer deposition (ALD) is a thin film growth technique utilizing sequential self-limiting surface reactions to deposit films with atomic layer control that are usually extremely conformal to the initial substrate, and thereby is utilized in this study. However, the entire process still lacks detailed atomic-scale understanding including the formed

interface and the effect of substrate used on the metal growth, this is in part because the surface science involved in the first few layer is not easy to be identified; thereby the dissertation works aimed on using surface sensitive techniques to investigate the surface reactions taking place at the initial stage of film formation.

The primary goal of the study was to examine and identify the self-limiting mechanisms that drive the surface reactions involved in ALD Pt on the Si-based and transition metal surfaces using (methylcyclopentadienyl)-trimethyl platinum ($MeCpPtMe_3$) and $O_2$ as the reactants. The second phase of this portion of the investigation involved establishing an optimized process window for a steady growth regime by tailoring dosing conditions. The detailed controls were based on acquisitions of chemical information per dose, which is demonstrated through in situ X-ray photoelectron spectroscopy of $MeCpPtMe_3$ chemisorption by mapping the gradual atomic scale evolution in the surface composition, and further.

Pt thin films were grown on $SiO_2$ films with assistance of electron impact activation and have shown an enhancement in uptake of film depositions. An atomic ratio of 6.98:1 between C:Pt and the fragmentation pattern reproduced via mass spectrometry confirm that the entire process results in loss of methyl ligands only while retaining the MeCpPt moiety intact. The depositions of $MeCpPtMe_3$ on Si(100) with native oxide revealed a temperature window from 523 K to 573 K. The surface coverage of Pt films on 300 nm $SiO_2$ shows a linear relationship with the exposure. Molecular oxygen atoms dosed onto

the $SiO_2$ surface after $MeCpPtMe_3$ exposures lead to layered growth with steric hindrance during the first few cycles after which the growth per cycle shows trend becoming constant and the film thickness may increases linearly with the number of cycles.

The surface chemistry associated with the thermal ALD of platinum films on metallic nickel substrates using the identical recipe was discussed. The uptake of the $MeCpPtMe_3$ was found to be self-limiting between 525 and 625 K, but to lead to multilayer deposition at 675 K. The calculated C:Pt ratio of the adsorbed species, suggests that all methyl moieties are lost upon activated bonding to the surface while the MeCp group remains coordinated to the adsorbed Pt atoms. Oxygen treatment of that surface leads to the complete removal of the carbon-containing species from the surface and to the formation of a thin NiO film. Further dosing with $MeCpPtMe_3$, in the next ALD cycle, fully reduces that NiO film to metallic Ni(0) and adds more Pt to the surface. However, no Pt film buildup was seen after several ALD cycles.

The study also includes approaches of activating/passivating the starting surface by modifying the surface chemistry through liquid/gas phase pretreatment. The long nucleation delay observed from $Pt/SiO_2$ experiments could be partially reduced by generating hydroxyl groups as new adsorption sites via piranha cleaning process. On the other hand, the selective deposition was demonstrated by applying silylation step in gas phase, and the site-blocking was shown partially effective as the XPS studies revealing

the silylated samples required many more ALD cycles for nucleation and growth to achieve similar intensities compared with referenced samples.

## Table of Contents


CHAPTER ONE ... 1

1.1 Thin film scaling and nanostructured materials resizing ... 1

1.2 Atomic Layer Deposition (ALD) ... 3

1.3 Dissertation Works ... 5

1.4 References ... 9

CHAPTER TWO ... 14

2.1 Introduction ... 14

2.2 Film Depositions ... 15

2.3 Characterizations ... 17

2.4 References ... 20

CHAPTER THREE ... 21

3.1 Introduction ... 21

3.2 Experimental ... 23

3.3 Results and Discussions ... 24

3.4 Conclusions ... 33

3.5 References ... 35

CHAPTER FOUR ... 39

4.1 Introductions ... 39

4.2 Half Cycle Depositions of $MeCpPtMe_3$ on $SiO_2$ Surfaces ... 40

4.2.1 ALD temperature window ... 40

4.2.2 Surface Species Identifications ... 46

4.2.3 Surface Coverage ... 49

4.3 Cyclewise and Alternate Exposures ... 55

4.4 Surface Types ... 62

4.5 Conclusions ... 71

4.6 References ... 73

CHAPTER FIVE ... 75

5.1 Introduction ... 75

5.2 Experimental ... 76

5.3 Half cycle depositions of $MeCpPtMe_3$ on Ni surface ... 77

5.4 References ... 85

CHAPTER SIX ... 87
6.1 Introduction ... 87
6.2 Surface Modification by Silanes ... 89
6.3 Experimental ... 90
6.4 Characterization ... 92
6.4.1 X-Ray Photoelectron Spectroscopy (XPS) ... 92
6.4.2 Water Droplet Tests ... 92
6.5 Half cycle ALD HMDS on $SiO_2$/Si ... 93
6.5.1 Introduction ... 93
6.5.2 Results and Discussions ... 93
6.6 Multicylces of Hf on HMDS/$SiO_2$/Si ... 100
6.7 Conclusions ... 107
6.8 References ... 109
CHAPTER SEVEN ... 113
7.1 General Conclusions ... 113
7.2 Future Works ... 116
7.2.1 Studies on addition of surface adsorption sites ... 116
7.2.2 Studies on platinum thin films grown by ALD using $H_2O$ or $H_2$ as counter reactant ... 117
7.2.3 Attempting of different silylation agent for efficient employment of inhibiting layer on starting surface ... 117
7.3 References ... 119

**List of Figures**

**Figure 1.** Chemical formulas of the platinum precursor molecules: Linear Formula: $C_9H_{16}Pt$, Synonym: $MeCpPtMe_3$ [42]. ....................................... 7

**Figure 2.** Picture of the UHV system used in this dissertation. ....................... 15

**Figure 3.** Pictures of the ionization gauge used in this study. .......................... 16

**Figure 4.** (Left) Image and (Right) schematic of a Bayard-Alpert ionization gauge [27]. ........................................................................................ 24

**Figure 5.** Pt 4f XPS spectras from Si(100) film exposed to defined first half cycle dose of $MeCpPtMe_3$ with $T_s$ set at 673K. ....................................... 26

**Figure 6.** Chemical formulas of the platinum precursor molecules: Linear Formula: $C_9H_{16}Pt$, Synonym: $MeCpPtMe_3$. ............................................ 29

**Figure 7.** Electron-impact mass spectrum of $MeCpPtMe_3$ recorded with a quadrupole mass spectrometer. ................................................................ 31

**Figure 8.** Pt 4f XPS spectra of single cycle $MeCpPtMe_3$ deposition on a Si(100) sample at (a) 423 K, and (b) 573 K completed by two separated dosings.42

**Figure 9.** Pt 4f XPS of single half cycle saturated $MeCpPtMe_3$ deposition on Si(100) samples as a function of substrate temperature. .......................... 44

**Figure 10.** Uptake curves of given exposure (5.4 x $10^5$ L) of $MeCpPtMe^3$ on Si(100) samples, in form of quantified Pt 4f peak area versus exposure, deposition taking place at various substrate temperatures between 373 and 673 K. The half-reaction displays a near-saturating reaction between 523-573 K. ........................................................................................ 45

**Figure 11.** (a) Pt 4f, and (b) O 1s XPS spectra of single cycle $MeCpPtMe_3$ deposition on a Si(100) sample at 523 K, completed by three separated dosings. ........................................................................................ 48

**Figure 12.** (a) Pt 4f, and (b) Si 2p XPS spectra of single cycle $MeCpPtMe_3$ deposition on a Si(100) sample at 523 K, completed by three separated dosings. ........................................................................................ 50

**Figure 13.** Schemes of different phase growth mechanisms, (a) layer-by-layer growth, (b) island growth, and (c) mixed growth. .................................. 53

**Figure 14.** (a) O 1s, and (b) C 1s XPS spectra of single cycle $MeCpPtMe_3$ deposition on a Si(100) sample at 523 K. ... 56

**Figure 15.** Pt 4f XPS of $MeCpPtMe_3$ deposition on Si(100) samples as a function of the number of cycles. ... 58

**Figure 16.** Estimated thickness of platinum film in monolayer equivalent calculated via attenuations of Si signals versus the number of deposition cycle. ... 60

**Figure 17.** (a) Pt 4f XPS of single cycle $MeCpPtMe_3$ deposition on different thickness of $SiO_2$ covered on Si(100) at 673 K. (b) Uptake curves of given exposure of $MeCpPtMe_3$ on 300 nm $SiO_2$/Si(100) samples, in form of quantified Pt 4f peak area versus exposure, deposition taking place at various substrate temperatures between 373 and 673 K. The half-reaction displays a near-saturating reaction between 523-573 K. (c) Growth rate of half cycle exposure of $MeCpPtMe_3$ on 300 nm $SiO_2$/Si(100) conducted at 523 and 573 K. ... 65

**Figure 18.** Macrographs of the selected samples: (left) pristine, and (right) piranha cleaned 300 nm $SiO_2$/Si(100), showing various degree of hydrophobicity/ hydrophilicity with contact angles measured 41°, and 18°, respectively. ... 69

**Figure 19.** (a) Uptake curves of given exposure of $MeCpPtMe_3$ on pristine, and piranha cleaned 300 nm $SiO_2$/Si(100) samples, in form of quantified Pt 4f peak area versus exposure, deposition taking place at various substrate temperatures between 373 and 673 K. (b) Side by side comparisons on curve fitted area between two types of starting surface, with deposition underwent by introducing $9 \times 10^5$ L of $MeCpPtMe_3$ onto surface, deposition results at different temperature are represented in bar chart. .. 71

**Figure 20.** (a) Pt 4f, and (b) Ni 2p XPS spectra of single cycle $MeCpPtMe_3$ deposition on a clean Ni sample at 523 K, completed by three separated dosings. ... 79

**Figure 21.** Uptake curves for platinum and carbon during the adsorption of $MeCpPtMe_3$ on a Ni substrate at 573 K as a function of dose. ... 82

**Figure 22.** (a) Pt 4f, (b) Ni 2p XPS of single half cycle $MeCpPtMe_3$ deposition on Ni surface as a function of substrate temperature. ... 84

**Figure 23.** Chemical formulas of the inhibitor precursor molecules: Linear Formula: $C_6H_{19}NSi_2$, Synonym: HMDS [26]. ... 89

**Figure 24.** Schematic showing the deactivation of surface hydroxyls after treatment of HMDS........................................................................ 90

**Figure 25.** Chemical formulas of the hafnium precursor molecules: Linear Formula: $[(CH_3)_2N]_4Hf$, Synonym: TDMAHf [31]. ................................ 91

**Figure 26.** C 1s, N 1s, Si 2p, and O 1s XPS of 72-hr dose of HMDS/300 nm $SiO_2$, $T_s$ set at 25ºC, ion gauge was deactivated. ..................................... 96

**Figure 27.** Macrographs of the selected samples: (a) 300 nm $SiO_2$/Si(100), (b) SC1 pretreated - 300 nm $SiO_2$/Si(100), (c) SC1 pretreated - 300 nm $SiO_2$/Si(100), followed by 96 hrs of HMDS dosing @ 25°C, showing various degree of hydrophobicity/ hydrophilicity with contact angles measured 46.2°, 22.6°, and 77.3°, respectively. .................................... 100

**Figure 28.** Hf 4f, C 1s, Si 2p and O 1s XPS of $HfO_2$/ $SiO_2$, dosing process completed at $T_s$ of 100ºC. ...................................................................... 104

**Figure 29**. Estimated thickness of $HfO_2$ film calculated via attenuations of Si signals versus the number of deposition cycle....................................... 106

## List of Tables

**Table 1.** Atomic ratios estimated from curve fitted C 1s, Pt 4f, Si 2p XPS peaks of single dose of $MeCpPtMe_3$ on Si(100) @ $T_s$ = 400˚C.......................... 28

**Table 2.** Summary of Pt 4f XPS peak position. ............................................... 49

**Table 3.** Data from water contact angle measurements on the 300 nm $SiO_2$/Si(100) surface after different cleaning and silylation steps. ......... 100

# CHAPTER ONE

## Introduction and Overview

### 1.1 Thin film scaling and nanostructured materials resizing

For more than three decades microelectronics has been the most important driving force for almost all kinds of technology evolutions [1]. The metal-oxide-semiconductor (MOS) transistor, has been downscaled with an impressive rate. In order to meet up industry's needs, the resizing technology is expected to continue according to Moore's law despite there are already many constraints ahead.

One of the majors is, the silicon gate oxide has reached close to its physical limit to keep the proper functioning of the transistors in the sub-10 nm technology node [2]. The atomic scale gate dielectric has become the most critical constraint for further downscaling of the MOS transistors as the thinner the gate dielectric layer the higher possibility to cause high leakage current. Introducing physically thicker high-k materials, while maintaining the similar value of the capacitance required for controlling the current flow in the channel, could be an alternative.

Despite comparing the conventional $SiO_2$, the high-k materials commonly have much poorer properties, such as thermal stability and poor interface quality with the silicon

substrate, higher dielectric constant insulators such as transition metal oxides are becoming a popular topic in the field of study due to their capabilities to reduce overall power dissipation and leakage currents [3-6]. To achieve desired electrical characteristics, the deposited dielectric must have excellent interfacial and bulk properties in addition to good uniformity, which requires appropriate processing reactors with matching chemical precursors.

On the other hand, there's also a need for development of further synthesis of uniform bimetallic nanoparticles; the high activity of under-coordinated surface atoms has motivated efforts to synthesize supported precious metal nanoparticles in the size range of a few nanometers. In addition, the high price of precious metals dictates that the catalyst should be finely dispersed to have a very high ratio of surface atoms to bulk atoms. And such goal of improvements has proved to be challenging for traditional catalyst synthesis methods such as wet impregnation [7, 8], and colloidal chemistry [9-13].

To date, a number of methods have been used to synthesize such types of films, and one of the majors is chemical vapor deposition (CVD) [14-22]. Comparing with a standard CVD process which is limited by the uniformity, thickness, and continuity of the starting surface, atomic layer deposition (ALD) is regarded as an optimum deposition technique as it offers a number of potential advantages [14, 23, 24]. For example, extremely large

area, complete films, as well as conformal monolayer coatings and abrupt vertical heterostructures may be comparatively easy to achieve.

### 1.2 Atomic Layer Deposition (ALD)

Atomic layer deposition (ALD) is a promising technique for producing uniform precious metal nanoparticles on high surface area supports because of its unique feature of sequential, self-limiting surface reactions [25, 26], ALD allows the nanoparticle size and composition to be controlled precisely by adjusting the number and sequence of ALD cycles of each component. In addition, by combining ALD processes for metal oxides and noble metals, it is possible to engineer nanocatalysts with unique structure and properties by depositing a series of discrete layers, which each performs a specific function such as serving as the catalyst support, providing or promoting catalytic activity [27, 28].

ALD is a chemical gas phase thin film deposition method [29], which is modified from Chemical Vapor Deposition (CVD). Instead of relying physical material transport like PVD methods, CVD type films are formed via chemical reactions. In the ALD process, thin films are grown by dosing two precursors onto a substrate in sequential pulses rather than together as would occur in chemical vapor deposition (CVD). Separating the precursors in time allows each precursor sufficient time to coat the entire surface, reducing diffusion-limited deposition that can lead to non-uniform growth on high-aspect-ratio materials. One important feature brought by ALD is the self-limiting surface

reactions. This means that the during film deposition, once the absorption sites on the surface are all occupied, the reactions stop, regardless of the continuity of precursor exposure. Thus, in theory each ALD cycle results in precisely the amount of material deposited once the saturation threshold is exceeded.

A typical ALD process can be divide into four consecutive processes: 1) exposure of substrate to precursor; 2) purging for removal of excess reactant; 3) exposure of substrate to counter reactant; and 4) purging for removal of excess reactant and by-product [26].

The concept of the ALD window can be used to describe the temperature dependent processes which may or may not lead to film growth in the ALD mode. Processes leading to non-saturative growth, with either too high or low growth rates, occur outside the ALD window. An increased growth rate may either result from precursor condensation at too low temperatures, or from precursor decomposition at too high temperatures. Alternatively, a decreased growth rate may be a result of incomplete reactions at the low temperature regime, or of precursor desorption at too high temperatures. In the ALD window, the growth rate may or may not be dependent on temperature, depending on the particular process. The growth in the ALD window in theory is always saturative.

While ALD has been reported promising in film deposition, the growth process is still poorly understood relative to other common techniques such as physical vapor deposition (PVD). During the recent years, many research groups have been studying growth

characteristics during the early stages of growth in order to understand the growth mechanism and to better control the growth process. In many cases, poor nucleation has been observed that can lead to a discontinuous film when the thickness is only couple of nanometers. For several nm nanostructures devices, the surface roughness generally decreases with an increasing thickness, and thereby the effects of nucleation delay from the initial stage are usually underestimated; however, from the aspect of either further scaling down the gate structured layers in MOSFET or maximizing the catalytic activity in the energy harvesting devices, the understanding of the first few reactions which lead to deposition is becoming an important topic to study.

## 1.3 Dissertation Works

Platinum (Pt) nanoparticles or films have been attracting attentions due to their various potential applications. As a catalyst, Pt nanodots have been extensively used in fuel cells because of their excellent catalytic activity [30-32].

When Pt is used as the catalytic material/cathode, the oxygen reduction reaction is dominated by the electrode surface path and bulk diffusion of oxygen is negligible. Hence, maintaining catalytic activity while minimizing the loading of the noble metal Pt could be beneficial.

Meanwhile, Pt is also applicable as a gate metal in the metal-oxide-semiconductor field effect transistors (MOSFETs) because of its high work function (5.6 eV) [33].

Thermal stability, low resistivity, as well as a low reactivity with other materials involved in CMOS technology are additional advantages for a possible application in dynamical random access memories (DRAMs) [34]. The major challenge nowadays is, the trend of device miniaturization requires efficient techniques enabling Pt fabrication at nano-scale range, for such purposes, ALD, may prove to be a promising technique.

The most commonly applied ALD process for platinum uses trimethyl(methylcyclopentadienyl)platinum ($MeCpPtMe_3$) and $O_2$ as precursors as shown in Fig. 1 [34-36]. The reaction mechanism of this process has been researched intensively in recent literature and relies on combustion-like reactions that occur during both ALD half cycles [37-41]. During the reactant pulse, $O_2$ is dissociatively chemisorbed on the platinum surface, inducing combustion of the remaining ligands of the adsorbed $MeCpPtMe_3$ molecules and the formation of a layer of adsorbed O atoms on the surface. These O atoms then react with the precursor ligands during the subsequent $MeCpPtMe_3$ pulse. However, in a typical thermal ALD process, the oxidative decomposition becomes extremely difficult in the initial stage for spots where no platinum particles formed yet, and leading to a nucleation delay.

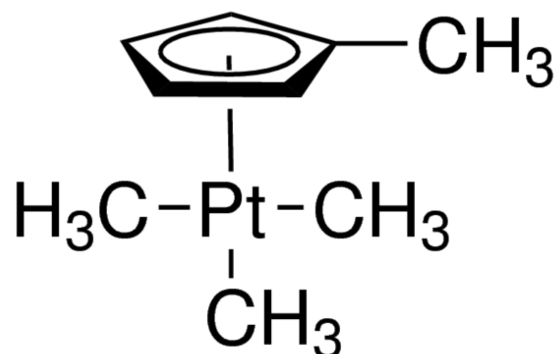


**Figure 1.** Chemical formulas of the platinum precursor molecules: Linear Formula: $C_9H_{16}Pt$, Synonym: $MeCpPtMe_3$ [42].

Such issue motivates many studies performed to understand and improve the surface reactions involved in metal ALD deposition [43-45]. For instance, the use of more reactive counter reactants than $O_2$ may enhances the chemisorption and oxidation of $MeCpPtMe_3$, results in faster growth rate, shorter nucleation delay, higher crystallinity, and wider range of deposition temperatures [38]. However, it still requires several tens of cycles of nucleation delay at the onset of deposition as Baker et al. presented in their investigations [46].

Despite improved deposition results shown from some reports, the ALD process lacks a detailed atomic-scale understanding of the formed interface structure and the effect of substrate used on the Pt growth, this is in part because the surface science involved in the first few layer is not easy to be identified, hence limiting the applicability of this technique for ultimate commercial fabrications. Considering the cost of Pt element, one

of the main goals for this study is detailed exploring, tailoring, and optimizing the selected metal precursor for specific surfaces.

It is commonly accepted that processes on the initial surface and within a metal nanoparticle on top of the substrate determine the subsequent growth and structure. Very few analytical tools can be utilized when the subject is in atomic scale, benefit from the built in-situ XPS unit and various surface sensitive techniques, herein, the dissertation works aimed on the investigation of surface reactions taking place at the initial stage of film formation. In addition, various tunable dosing parameters and substrates were detailed studied to map out a steady growth regime for ALD deposited platinum. In this work, platinum films were grown on Si(100), $SiO_2$, and metal substrates by both thermal and electron impact activated ALD, using trimethyl-(methylcyclopentadienyl)platinum and $O_2$ as precursors.

## 1.4 References

[1] Iwai, H. CMOS Downsizing Toward Sub-100 nm. Solid-State Electron. 2003, 48, 497.

[2] Wong, H. and Gritsenko, V. A. Defects in Silicon Oxynitride Gate Dielectric Films. Microelectron. Reliab. 2002, 42, 597.

[3] Roy Chowdhuri, A.; Jin, D.-U.; Rosado, J.; Takoudis, C. G. Strain and Substoichiometry at the Si(100)/Silicon Dioxide Interface. Phys. Rev. B 2003, 67(24).

[4] Roy Chowdhuri, A. and Takoudis, C.G. Investigation of the Aluminum oxide/Si(100) Interface Formed by Chemical Vapor Deposition, Thin Solid Films 2004, 446, 155.

[5] Katamreddy R.; Inman, R.; Jursich, G.; Soulet, A.; Nicholls, A.; Takoudis, C.G. Post Deposition Annealing of Aluminum Oxide Deposited by Atomic Layer Deposition Using Novel Tris(diethylamino)aluminum and Water Vapor on Si(100). Thin Solid Films 2007, 515, 6931-6937.

[6] Song, X.; Takoudis, C.G. Cyclic Chemical Vapor Deposited $TiO_2/Al_2O_3$ films Using Trimethyl Aluminum, Tetrakis(diethylamino)titanium and $O_2$. Journal of the Electrochemical Society 2007, G177-182, 154.

[7] Castillo, N.; Perez, R.; Martinez-Ortiz, M.J.; Diaz-Barriga, L.; Garcia, L.; Conde-Gallardo, A. Structural Analysis of Platinum–Palladium Nanoparticles Dispersed on Titanium Dioxide to Evaluate Cyclo-olefines Reactivity. J. Alloys Compd. 2010, 495 (2), 453−457.

[8] Adams, B.D.; Ostrom, C.K.; Chen, A.C. Highly Active Pd-Pt Catalysts for the Electrochemical Reduction of $H_2O_2$. J. Electrochem. Soc. 2011, 158 (4), B434−B439.

[9] Liu, Y.; Chi, M.F.; Mazumder, V.; More, K.L.; Soled, S.; Henao, J.D.; Sun, S.H. Composition-controlled Synthesis of Bimetallic Pd-Pt Nanoparticles and Their Electro-oxidation of Methanol. Chem. Mater. 2011, 23 (18), 4199−4203.

[10] Lim, B.; Wang, J.G.; Camargo, P. H.C.; Cobley, C.M.; Kim, M.J.; Xia, Y.N. Twin-induced Growth of Palladium-Platinum Alloy Nanocrystals. Angew. Chem., Int. Ed. 2009, 48 (34), 6304−6308.

[11] Zhang, H.; Jin, M. S.; Wang, J.G.; Kim, M.J.; Yang, D.R.; Xia, Y.N. Nanocrystals composed of alternating shells of Pd and Pt can be obtained by sequentially adding different precursors. J. Am. Chem. Soc. 2011, 133 (27), 10422−10425.

[12] Wang, L.; Nemoto, Y.; Yamauchi, Y. Direct Synthesis of Spatially-controlled Pt-on-Pd Bimetallic Nanodendrites with Superior Electrocatalytic Activity. J. Am. Chem. Soc. 2011, 133 (25), 9674−9677.

[13] Yin, A.X.; Min, X.Q.; Zhang, Y.W.; Yan, C.H. Shape-selective Synthesis and Facet-dependent Enhanced Electrocatalytic Activity and Durability of Monodisperse Sub-10 nm Pt-Pd Tetrahedrons and Cubes. J. Am. Chem. Soc. 2011, 133 (11), 3816−3819.

[14] Shi, Y.; Li, H.; Li, L.-J. Recent Advances in Controlled Synthesis of Two-Dimensional Transition Metal Dichalcogenides via Vapour Deposition Techniques. Chem. Soc. Rev. 2015, 44, 2744.

[15] Lee, Y.-H.; Yu, L.; Wang, H.; Fang, W.; Ling, X.; Shi, Y.; Lin, C.-T.; Huang, J.-K.; Chang, M.-T.; Chang, C.-S.; Dresselhaus, M.S.; Palacios, T.; Li, L.-J.; Kong, J. Synthesis and Transfer of Single Layer Transition Metal Disulfides on Diverse Surfaces. Nano Lett. 2013, 13, 1852.

[16] Lee, Y.-H.; Zhang, X.-Q.; Zhang, W.; Chang, M.-T.; Lin, C.-T.; Chang, K.-D.; Yu, Y.-C.; Wang, J. T.-W.; Chang, C.-S.; Li, L.-J.; Lin, T.-W. Synthesis of Large-Area $MoS_2$ Atomic Layers with Chemical Vapor Deposition. Adv. Mater. 2012, 24, 2320−2325.

[17] Cong, C.; Shang, J.; Wu, X.; Cao, B.; Peimyoo, N.; Qiu, C.; Sun, L.; Yu, T. Synthesis and Optical Properties of Large-Area Single- Crystalline 2D Semiconductor $WS_2$ Monolayer from Chemical Vapor Deposition. Adv. Opt. Mater. 2014, 2, 131−136.

[18] Huang, J.-K.; Pu, J.; Hsu, C.-L.; Chiu, M.-H.; Juang, Z.-Y.; Chang, Y.-H.; Chang, W.-H.; Iwasa, Y.; Takenobu, T.; Li, L.-J. Large-Area Synthesis of Highly Crystalline $WSe_2$ Monolayers and Device Applications. ACS Nano 2014, 8, 923−930.

[19] Dumcenco, D.; Ovchinnikov, D.; Marinov, K.; Lazić, P.; Gibertini, M.; Marzari, N.; Sanchez, O. L.; Kung, Y.; Krasnozhon, D.; Chen, M.; Bertolazzi, S.; Gillet, P.; Fontcuberta i Morral, A.; Radenovic, A.; Kis, A. Large-Area Epitaxial Monolayer $MoS_2$. ACS Nano 2015, 9, 4611−4620.

[20] Kang, K.; Xie, S.; Huang, L.; Han, Y.; Huang, P. Y.; Mak, K. F.; Kim, C.-J.; Muller, D.; Park, J. High-Mobility Three-Atom-Thick Semiconducting Films with Wafer-Scale Homogeneity. Nature 2015, 520, 656−660.

[21] Bilgin, I.; Liu, F.; Vargas, A.; Winchester, A.; Man, M. K. L.; Upmanyu, M.; Dani, K.; Gupta, G.; Talapatra, S.; Mohite, A. D.; Kar, S. Chemical Vapor Deposition Synthesized Atomically-Thin Molybdenum Disulfide with Optoelectronic-Grade Crystalline Quality. ACS Nano 2015, 9, 8822.

[22] Yu, Y.; Li, C.; Liu, Y.; Su, L.; Zhang, Y.; Cao, L. Controlled Scalable Synthesis of Uniform, High-Quality Monolayer and Few-Layer $MoS_2$ Films. Sci. Rep. 2013, 3, 1866.

[23] M. Leskela, M. Ritala. Atomic Layer Deposition Chemistry: Recent Developments and Future Challenges. Angew. Chem. Int. Ed. 2003, 42 (45), pp. 5548-5554.

[24] R.L. Puurunen. Surface chemistry of atomic layer deposition: A case study for the trimethylaluminum/water process. J. Appl. Phys. 2005, 97 (12), 121301-121352.

[25] Puurunen, R.L. Surface Chemistry of Atomic Layer Deposition: A Case Study for the Trimethylaluminum/Water Process. J. Appl. Phys. 2005, 97 (12), 121301−121352.

[26] Leskela, M.; Ritala, M. Atomic layer deposition (ALD): from precursors to thin film structures. Thin Solid Films 2002, 409 (1), 138−146.

[27] Lu, J.L.; Lei, Y.; Elam, J.W. Atomic Layer Deposition of Noble Metals–New Developments in Nanostructured Catalysts. In Noble Metals; Su, Y.-H., Ed.; INTECH: Janeza Trdine, Slovenia, 2012, 159−178.

[28] Lei, Y.; Mehmood, F.; Lee, S.; Greeley, J.; Lee, B.; Seifert, S.; Winans, R. E.; Elam, J. W.; Meyer, R. J.; Redfern, P. C.; Teschner, D.; Schlogl, R.; Pellin, M. J.; Curtiss, L. A.; Vajda, S. Increased Silver Activity for Direct Propylene Epoxidation via Subnanometer Size Effects. Science 2010, 328 (5975), 224−228.

[29] Ritala, M. ; and Leskelä, M. in Handbook of Thin Films Materials, edited by Nalwa, Academic Press, 2002, San Diego, CA, U.S.A., p. 103.

[30] Gu, D.F.; Baumgart, H.; Tapily, K.; Shrestha, P.; Namkoon1, G.; Ao, X.Y.; Muller, F. Precise Control of Highly Ordered Arrays of Nested Semiconductor/Metal Nanotubes. Nano Res. 2011, 4:164–170.

[31] Jiang, X.R.; Huang, H.; Prinz, F.B.; Bent, S.F. Application of Atomic Layer Deposition of Platinum to Solid Oxide Fuel Cells. Chem Mater. 2008, 20:3897–3905.

[32] Yang, D.Q.; Zhang, G.X.; Sacher, E. Evidence of the Interaction of Evaporated Pt Nanoparticles with Variously Treated Surfaces of Highly Oriented Pyrolytic Graphite. J. Phys Chem B 2006, 110:8348–8356.

[33] Wilk, G. D.; Wallace, R. M.; Anthony, J. M. J. High-κ gate Dielectrics: Current Status and Materials Properties Considerations. Appl. Phys. 2001, 89, 5243.

[34] Aaltonen, T.; Ritala, M.; Sajavaara,T.; Keinonen, J.; and Leskelä, Atomic Layer Deposition of Platinum Thin Films. M. Chem. Mater. 2003, 15 (9), 1924–1928.

[35] Zhu,Y.; Dunn, K. A.; and Kaloyeros, A.E. Properties of Ultrathin Platinum Deposited by Atomic Layer Deposition for Nanoscale Copper-Metallization Schemes. J. Mater. Res. 2007, 22(5), 1292-1298.

[36] Jiang, X.; and Bent, S.F. Area-Selective Atomic Layer Deposition of Platinum on YSZ Substrates Using Microcontact Printed SAMs. J. Electrochem. Soc. 2007, 154, D648.

[37] Aaltonen, T.; Rahtu, A.; Ritala, M.; and Leskelä, M. Reaction Mechanism Studies on Atomic Layer Deposition of Ruthenium and Platinum. Electrochem. Solid-State Lett. 2004, 6, C130.

[38] Kessels, W. M. M.; Knoops, H. C. M.; Dielissen, S. A. F.; Mackus, A. J. M.; van de Sanden, M. C. M. Surface Reactions During Atomic Layer Deposition of Pt Derived From Gas Phase Infrared Spectroscopy. Appl. Phys. Lett. 2009, 95, 013114. Surface Reactions During Atomic Layer Deposition of Pt Derived From Gas Phase Infrared Spectroscopy.

[39] Mackus, A. J. M.; Leick, N.; Baker, L.; Kessels, W. M. M. Catalytic Combustion and Dehydrogenation Reactions During Atomic Layer Deposition of Platinum. Chem. Mater. 2012, 24, 1752-1761.

[40] Longrie, D.; Devloo-Casier, K.; Deduytsche, D.; Van den Berghe, S.; Driesen, K.; Detavernier, C. Plasma-Enhanced ALD of Platinum with $O_2$, $N_2$ and $NH_3$ Plasmas. ECS J. Solid State Sci. Technol. 2012, 1, Q123−Q129.

[41] Erkens, J. M.; Mackus, A. J. M.; Knoops, H. C. M.; Smits, P.; van de Ven, T. H. M.; Roozeboom, F.; Kessels, W. M. M. Mass Spectrometry Study of the Temperature Dependence of Pt Film Growth by Atomic Layer Deposition. ECS J. Solid State Sci. Technol. 2012, 1, P255−P262.

[42] Merck KGaA, Inc.
https://www.sigmaaldrich.com/catalog/product/aldrich/645605?lang=en®ion=US.
Retrieved July, 2018.

[43] Setthapun, W.; Williams, W. D.; Kim, S. M.; Feng, H.; Elam, J. W.; Rabuffetti, F. A.; Poeppelmeier, K. R.; Stair, P. C.; Stach, E. A.; Ribeiro, F. H.; Miller, J. T.; and Marshall, C. L. Genesis and Evolution of Surface Species During Pt Atomic Layer Deposition on Oxide Supports Characterized by in-situ XAFS Analysis and Water-Gas Shift Reaction. J. Phys. Chem. C 2010, 114, 9758.

[44] Sun, H.; Qin, X.; and Zaera, F. Chemical Nature of the Thin Films that Form on $SiO_2$/Si(100) Surfaces Upon Manganese Deposition. J. Phys. Chem. Lett. 2011, 2 (20), pp 2525–2530. DOI: 10.1021/jz201177w.

[45] Sun, H.; Qin, X.; and Zaera, F. Activation of Metal–Organic Precursors by Electron Bombardment in the Gas Phase for Enhanced Deposition of Solid Films. J. Phys. Chem. Lett. 2012, 3 (17), 2523–2527. DOI: 10.1021/jz3011332.

[46] Baker, L.; Cavanagh, A. S.; Seghete, D.; George, S.M.; Mackus, A.J.M.; Kessels, V.M.M.; Liu, Z. Y.; and Wagner, F.T. Nucleation and Growth of Pt Atomic Layer Deposition on $Al_2O_3$ Substrates Using (methylcyclopentadienyl)-trimethyl Platinum and $O_2$ plasma. J. Appl. Phys. 2001, 109, 084333.

# CHAPTER TWO

## Experimental

### 2.1 Introduction

All the film growing processes and the XPS-related analysis discussed in this dissertation were performed in a commercialized UHV duo-chamber system (Leybold) as shown in Fig. 2. Briefly, while the deposition processes were carried out in an auxiliary chamber, which is kept at a vacuum pressure on the order of 1 x $10^{-8}$ Torr by using a turbomolecular pump backing with mechanical pump, whereas analytical tasks including XPS data are acquired inside the main chamber equipped with an in situ energy spectrometer (EA11 MCD), base pressure of it is evacuated down to ~ 4 x $10^{-9}$ Torr. Sample can be freely transferred within chambers without the need of vacuum break and the exposure to the outside air.

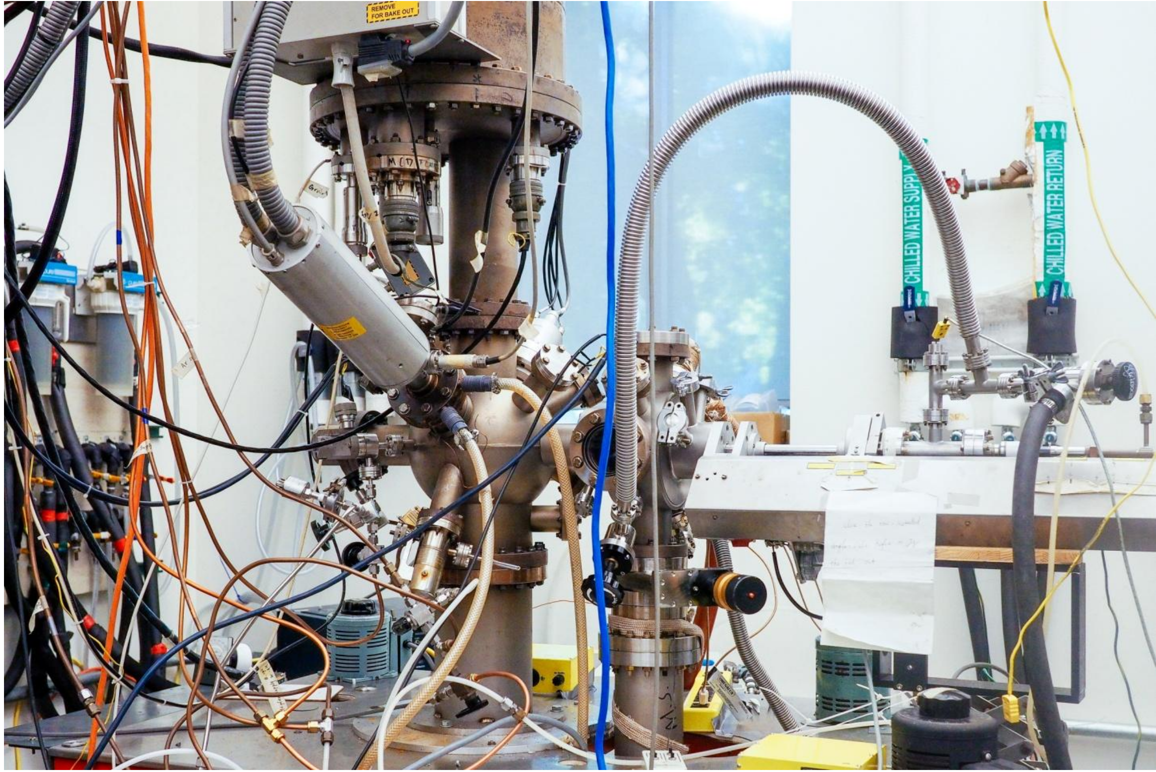


**Figure 2.** Picture of the UHV system used in this dissertation.

**2.2 Film Depositions**

The standard procedures preparing for samples are conducted as follows: Immerse a ~1 cm x 1 cm-size substrate in a beaker filled with acetone, ultrasonic cleaned for 10 minutes, followed by deionized water rinsing for 2 minutes, and blow air dried. The sample is then mounted on a tantalum bridge which poses excellent thermal conductivity. The thermal deposition is achieved by heating the bridge structure, and hence the substrate clipped on top is thermally heated. The temperature of the substrate is monitored with a K-type thermocouple inserted between the sample and the metallic clip that holds the substrate in place. The ionization gauge as shown in Fig. 3 is coupled to the

UHV system not only for pressure monitoring purpose, but utilized as a gas-activating source and plays an important role in electron impact activated deposition. Detailed mechanism will be described later in Ch 3.2.

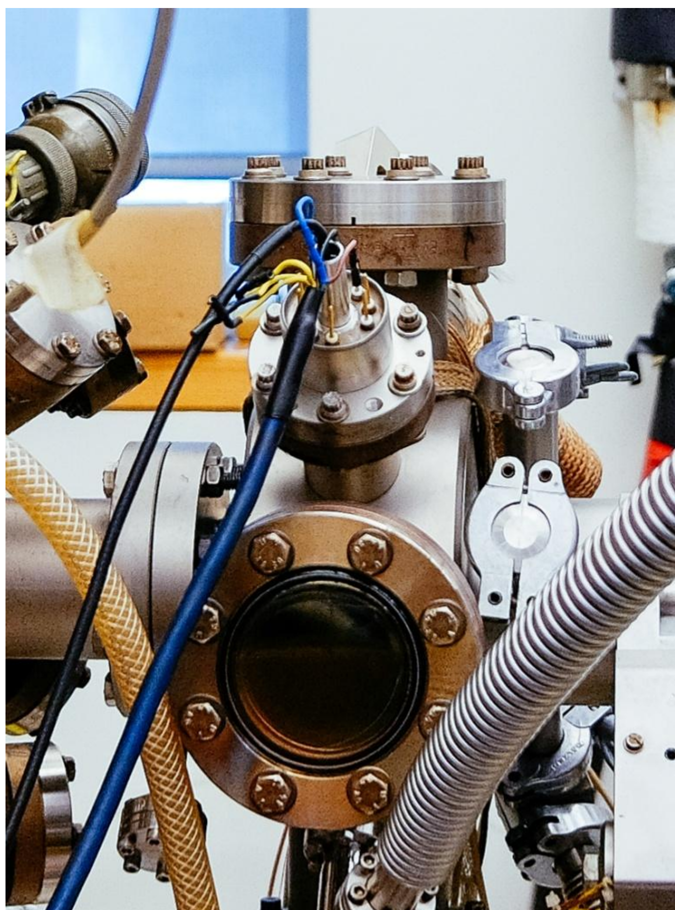

**Figure 3.** Pictures of the ionization gauge used in this study.

The sample was loaded into the center of the reactor. The surface was cleaned before each experiment by a combination of chemical treatments, and high-temperature annealing. Metal type surfaces are additionally pretreated with ion sputtering. Prior to any dosing process, the starting surface was first scanned by XPS, which used as a reference

group for later experiments. The substrates were then heated by resistively heating the sample bridge to the desired growing temperature. The growth temperature in this study was varied between 293 K and 673 K. The feed gas, vaporized precursor, was introduced after reaching the desired growth temperature.

The trimethyl(methylcyclopentadienyl)platinum(IV) ($MeCpPtMe_3$) precursor used in this study was purchased from Sigma Aldrich (98% purity), which has a melting point of 29.5-30.0°C and its vapor pressure at 23°C is 0.053 Torr, high enough for the delivery and deposition without heating the manifold. The precursor was purified in situ in the gas manifold via repeated freeze-pumpthaw cycles, and dosed via a leak valve. Oxygen gas was purchased from liquid carbonic (research purity, >99.995%) and used as a co-reactant. Gas doses were set by fixing the gas pressure and dosing times, and are reported in units of Langmuirs ($1 \text{ L} = 1 \times 10^{-6}$ Torr • s). The precursor container was slightly heated during dosing to 305 K to increase its vapor pressure, and the dosing line was maintained at 330 K to minimize condensation. The source gases were delivered into the chamber using leak valve, and subsequently deposited on the substrate at a typical pressure of $5E^{-5}$ Torr. Once the dosing process is completed, it is returned back to the main chamber for XPS collection.

### 2.3 Characterizations

The XPS data were acquired using the aluminum anode (hν=1486.6 eV) of a non-monochromatized dual-Mg-Kα/Al-Kα X-ray excitation source and a Leybold EA11

semispherical electron energy analyzer equipped with multi-channel detection. The (fixed) pass energy used led to a total resolution of the instrument of approximately 1.0 eV, and to an accuracy in the determination of peak positions of approximately 0.1 eV.

XPS works by irradiating the sample surface, hitting the core e- of the atoms with X-Ray photons, and causing the ejection of electrons. The kinetic energy (KE) of the emitted electrons is then being measured. The “binding energy” (BE), is the energy required to remove an electron from its orbital, and hence is characteristic of the core electrons for each element, can be calculated. The binding energy of the core electron ($E_b$) is give by the Einstein relationship:

$$hv = E_b + E_k + \varphi$$

where $hv$ is the X-ray photon energy; $E_k$ is the kinetic energy of photoelectron, which can be measured by the energy analyzer; and $\varphi$ is the work function induced by the analyzer, about 4~5eV [1].

XPS counts electrons ejected from a sample surface when irradiated by x-rays. A spectrum representing the number of electrons recorded at a sequence of energies includes both a contribution from a background signal and also resonance peaks characteristic of the bound states of the electrons in the surface atoms. XPS spectra are, for the most part, quantified in terms of peak intensities and peak positions. Raw data was

acquired using the SPECS software, XPS peak analysis including deconvolution was performed using MS Excel and XPS Peak 4.1 with Shirley backgrounds subtracted and Gaussian-Lorentzian product line shapes [2, 3]. The intensities of the signals are corrected by the XPS atomic sensitivity factors for referencing data of the other elements. All XPS peak positions are reported in binding energies (BE), in Si-based surface studies, peaks are calibrated against values for the Si 2p XPS peaks, and were corrected for sample charging using the reported values for the Ni 2p(3/2) XPS peak (852.6 eV) as an internal reference for Ni studies [4]. Surface coverages for the different elements were calculated via integration of the intensity of the XPS peaks after Shirley background subtraction and correction by the appropriate XPS atomic sensitivity factors.

## 2.4 References

[1] Lau, W. M.; Wu, X. W. Surf. Sci. 1991, 245, 345.

[2] Ma, Q.; Guo, H.; Gordon, R. G.; Zaera, F. Surface Chemistry of Copper(I) Acetamidinates in Connection with Atomic Layer Deposition (ALD) Processes. Chem. Mater. 2011, 23, 3325-3334.

[3] Ma, Q.; Zaera, F.; Gordon, R.G. Thermal chemistry of copper(I)-N,N'-di-sec-butylacetamidinate on Cu(110) Single-crystal Surfaces. J. Vac. Sci. Technol., A 2012, 30, 01A114.

[4] Wagner, C. D.; Riggs, W.M.; Davis, L.E.; Moulder, J.F.; Muilenberg, G.E.; G.E. Eds. Handbook of X-Ray Photoelectron Spectroscopy, Perkin-Elmer Corporation: Eden Prairie, MN, 1978.

# CHAPTER THREE

## Gas Phase Electron Impact Activation of $MeCpPtMe_3$

### 3.1 Introduction

To achieve ALD's unique characteristics and to be suitable as a practical vapor deposition process, ALD precursors must have specific properties, for instance, be sufficiently volatile, thermally stable in the gas phase but reactive enough towards both the target surface [1]. Furthermore, the byproducts are best to be as well volatile to be easily purged in order to prepare for the subsequent half cycle. The fulfillment of these properties ensures fast kinetics and thus lower ALD temperatures and cycle times.

Selecting precursors with all of the desired properties is not always straightforward, especially for late transition metals, partly because among limited available options are either have proven quite versatile but also fairly reactive, easily decomposing on the surface once adsorption has taken place [2-11] or in sturdy forms which are difficult to activate and/or remove from the surface. [12-17], and partly due to detailed ALD chemistry has not been well understood.

In the case of platinum precursors, $CpPtMe_3$, [18, 19] $MeCpPtMe_3$, [19, 20] $Pt(acac)_2$, [21, 22] and $Pt(hfa)_2$ [23, 24] are commonly available for CVD of Pt thin films.

$MeCpPtMe_3$ is a widely studied CVD precursor because of its low melting point of 30°C [25]. Platinum film deposition by ALD has been studied by using $Pt(acac)_2$ and hydrogen as precursors [26]. However, $Pt(acac)_2$ was found to be an unsuitable precursor due to its thermal decomposition at low temperatures. Sufficient thermal stability is required for the ALD precursors since thermal decomposition of the precursors destroys the self-limiting growth mechanism. The most commonly applied ALD process for Pt uses $MeCpPtMe_3$ and $O_2$ as precursors, such combination is as well adapted into this study.

Standard ALD depositions utilize thermal energy to activate the surface reactions and thereby facilitate the film growth. Such thermally driven processes taken place on substrates, though, are often limited to a specific range of elevated temperatures, while at lower temperature the nucleation would often either being hindered or experiencing lengthy built up rate. Another option to facilitate the deposition rate is to activate the complex externally, via electron excitation, for instance. Such approach functions similarly as plasma, which simultaneously generates high momentum ions, while these highly reactive species induce the surface reactions, they may result in unexpected ligand decomposition and further leads to non self-limiting film growth scheme. Thereby detailed studies involved with assistance of the electron excitation require careful inspections to ensure clean chemistry employed during film deposition.

In this study, an approach was advanced for depositing Pt on Si-based surfaces benefited from the activation of the ionization source. Discussions in terms of crack pattern of the

utilized precursor, $MeCpPtMe_3$, the impacts of the resultant species on deposition results, and explanations from aspect of gas phase chemistry are presented in this chapter.

### 3.2 Experimental

The reactor used in the experiments is described in Ch.2.1. The substrates involved in the experiments are Si with ~ 1 nm native oxide, and Si with 300 nm thick $SiO_2$. The depositions of Pt on Si-based substrates were achieved via assistance of ionization source as shown in Fig. 4. which functions similarly as plasma, but also served for pressure monitoring; the negative electrons are emitted at a constant rate from a heated filament (cathode) and are accelerated toward a positively-charged wire grid (anode). Electrons pass into the space enclosed by the grid. In this space the electrons collide with the gas molecules that are in the vacuum system, and produce positive ions. The positive ions are thereby collected by the ion collector. At a constant filament-to-grid voltage and electron emission current, the rate that positive ions are formed is directly proportional to the density of molecules in the gauge. The strength of the ion current is then indicated on an electrometer that is calibrated in the units of pressure.

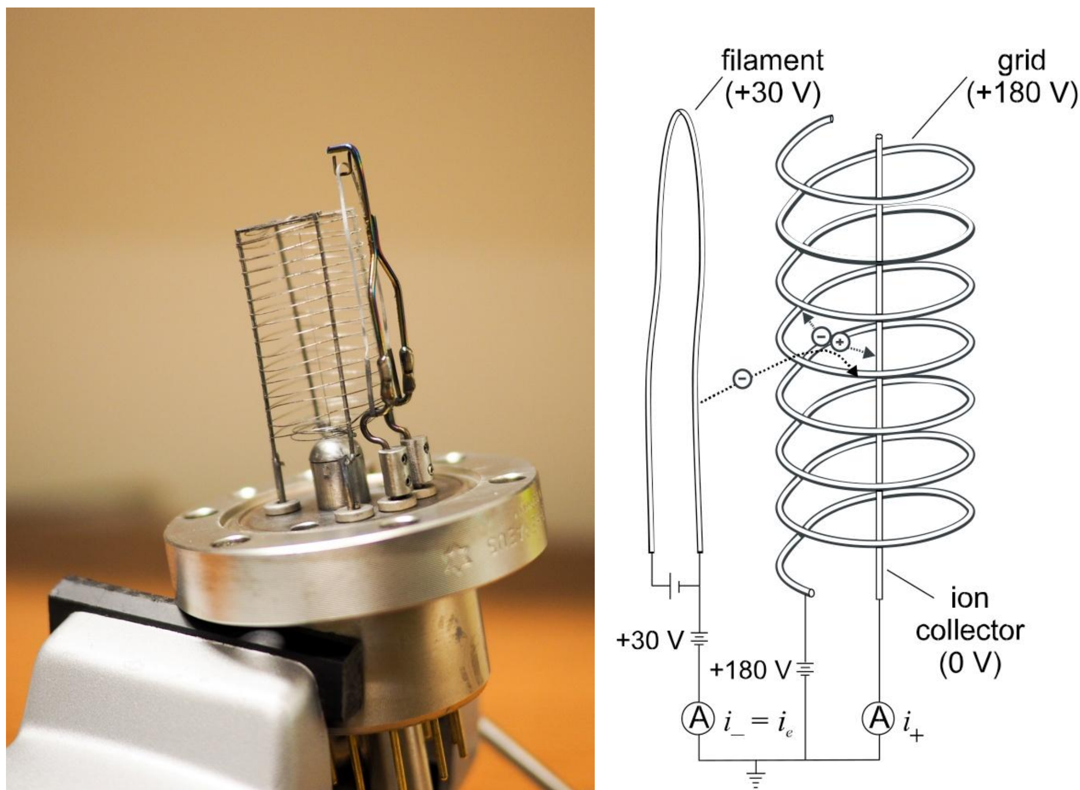


**Figure 4.** (Left) Image and (Right) schematic of a Bayard-Alpert ionization gauge [27].

### 3.3 Results and Discussions

Fig. 5 displays the Pt 4f XPS results of experiments related to the deposition of $MeCpPtMe_3$ on Si with 1 nm native oxide. The surface was exposed to a total of 300 min dose of precursor with 5 x $10^{-5}$ Torr (9 x $10^{5}$ L equiv.) The bottom (blue) traces correspond to the sample set conduct without the activation of ionization source, while the top (red) traces represent the activated case.

In the case of pure thermal driven ALD process, the $MeCpPtMe_3$ posed as stable compound; the activation of the ionization source during exposure significantly induced

the surface reaction towards the silicon surface, and led to higher yield of Pt. From the curve fitting results, the integrated area reveals an enhancement in Pt signal with a factor of ~ 17 when ionization source was implemented into the deposition process.

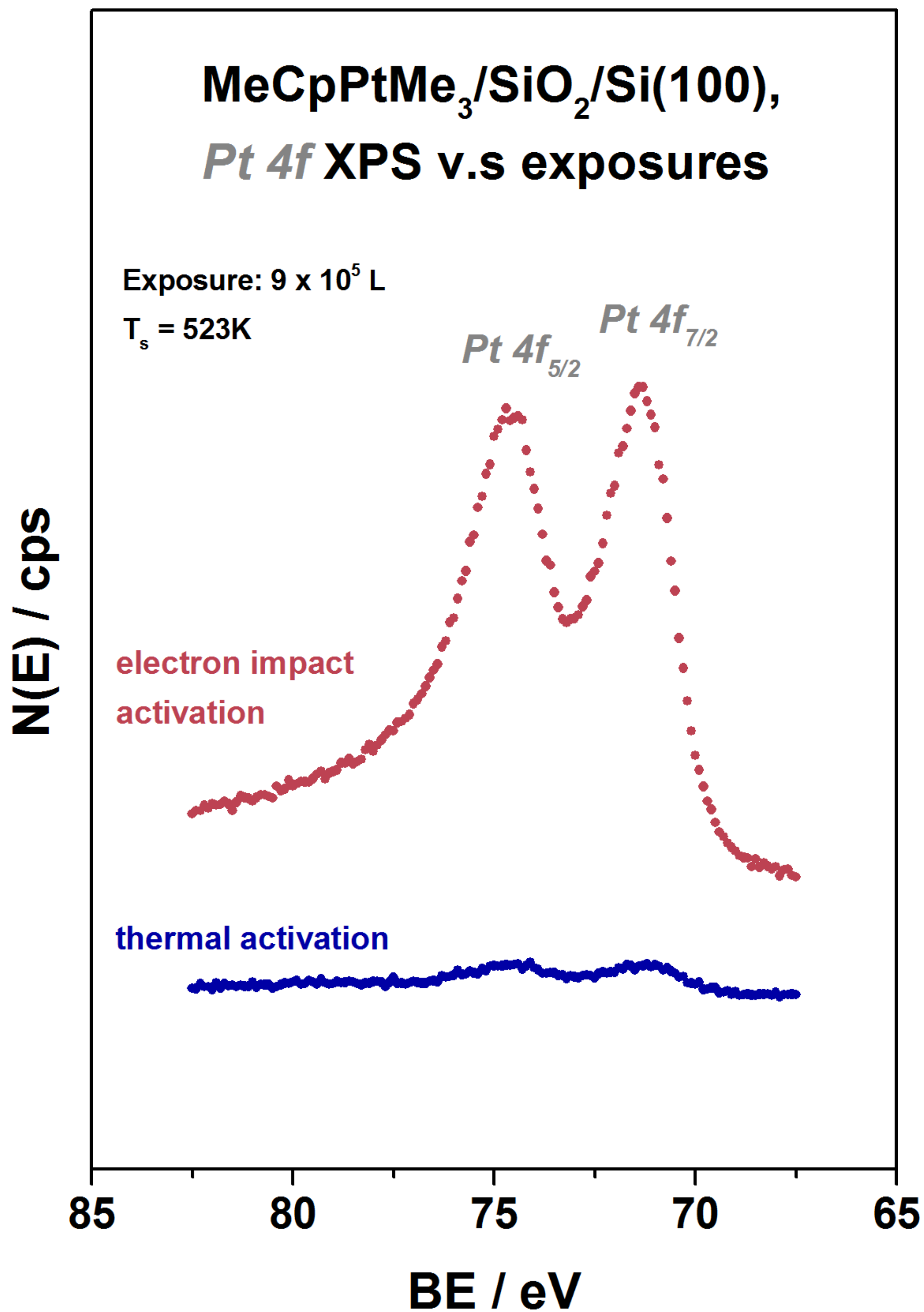


**Figure 5.** Pt 4f XPS spectras from Si(100) film exposed to defined first half cycle dose of $MeCpPtMe_3$ with $T_s$ set at 673K.

With the underlying assumption when quantifying XPS spectra is that the number of electrons recorded is proportional to the number of atoms in a given state, the peak intensities are commonly used to measure how much of a material is at the surface. However, not all the emitted electrons from the sample are recorded by the instrument, and hence a direct comparison of peak areas from different elements is not accurate. The efficiency of recording these emitted electrons depends on the kinetic energy of the electrons, which in turn depends on the operating mode of the instrument. As a result, the best way to compare XPS intensities is via calculating percentage of atomic concentrations, in other words, the ratio of the intensity to the total intensity of electrons in the measurement. This ensures that despite the experimental conditions change in any way between measurements, the peak intensities would change in an absolute sense, but all else being equal, would remain constant in relative terms.

The atomic ratio of C:Pt ratio for thermal deposition was estimated to be 17.1:1, and such value is dramatically reduced down to a 6.5:1 in electron impact activated deposition; the closeness value versus a theoretical value of 6:1 indicates that the MeCpPt moiety remains coordinated to the Pt atom, and the direct Pt bonded methyl groups were successfully loosen, results in a clean Pt film yet still owns self-limiting property.

**Table 1**. Atomic ratios estimated from curve fitted C 1s, Pt 4f, Si 2p XPS peaks of single dose of $MeCpPtMe_3$ on Si(100) @ $T_s$ = 400˚C.

| Dose condition | Atomic Ratio |
|---|---|
| Thermal | C:Pt = 17.7:1<br>Pt:Si = 1:129 |
| Electron Impact | C:Pt = 6.48:1<br>Pt:Si = 1:3.88 |

The difference in outcome may be explained by the change in reactivity of the precursor molecules. The design of the ionization gauge functions as a plasma source, which the emitted electrons collide with the dosed gas molecules. With sufficient energy to break chemical bonds, ions, fragmentations, chemically active species are thereby generated.

From such electron impact approach introduced in the first half cycle, the surface is catalyzed by the kinetic energy of the accelerated electrons from the electric field, converting them into gaseous breakdown products. Such taken approach worth further investigations as similar studies has reported the potential non-selective conversion of the ALD precursor, which could lead to ligand decomposition and to the deposition of impurities. This has been seen, for instance, in some electron-induced activation processes of adsorbed species [28, 29].

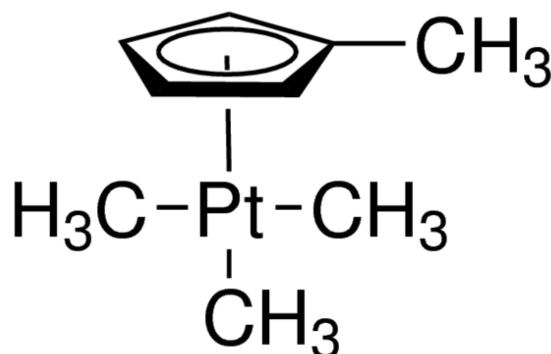


**Figure 6.** Chemical formulas of the platinum precursor molecules: Linear Formula: $C_9H_{16}Pt$, Synonym: $MeCpPtMe_3$.

To achieve self-limiting growth, the ideal desorption process in this case undergoes by releasing one or more Pt-bonded methyl groups but leaving the cyclopentadienyl ligand remained attached with the metal element. The pattern and decompose level of electron impact ionization can be reproduced by conducting quadrupole mass spectrometry which commonly used for the purpose of residual gas analysis; The integrated mass filter differentiates the produced ions and selects species for detection. Due to its similarity in operating mechanism as a typical ionization gauge, the function rely on the conversion of gas molecules into charged particles, and is achieved by electron impact ionization via thermoionic emission from a hot filament. Cracking arises during ionization when high energy electrons used not only ionize species but fragment them. Fig. 7 shows the mass spectra obtained for $MeCpPtMe_3$, taken with 100 eV electron energy excitation. Multiple fragment peaks are shown apart from the base peaks, under normal conditions the cracking pattern is characteristic of a species, a series of peaks for lower m/z values,

corresponding to sequential loss of $CH_3$ moieties, and spectra in Fig. 7 clearly illustrates the accessibility of such approach.

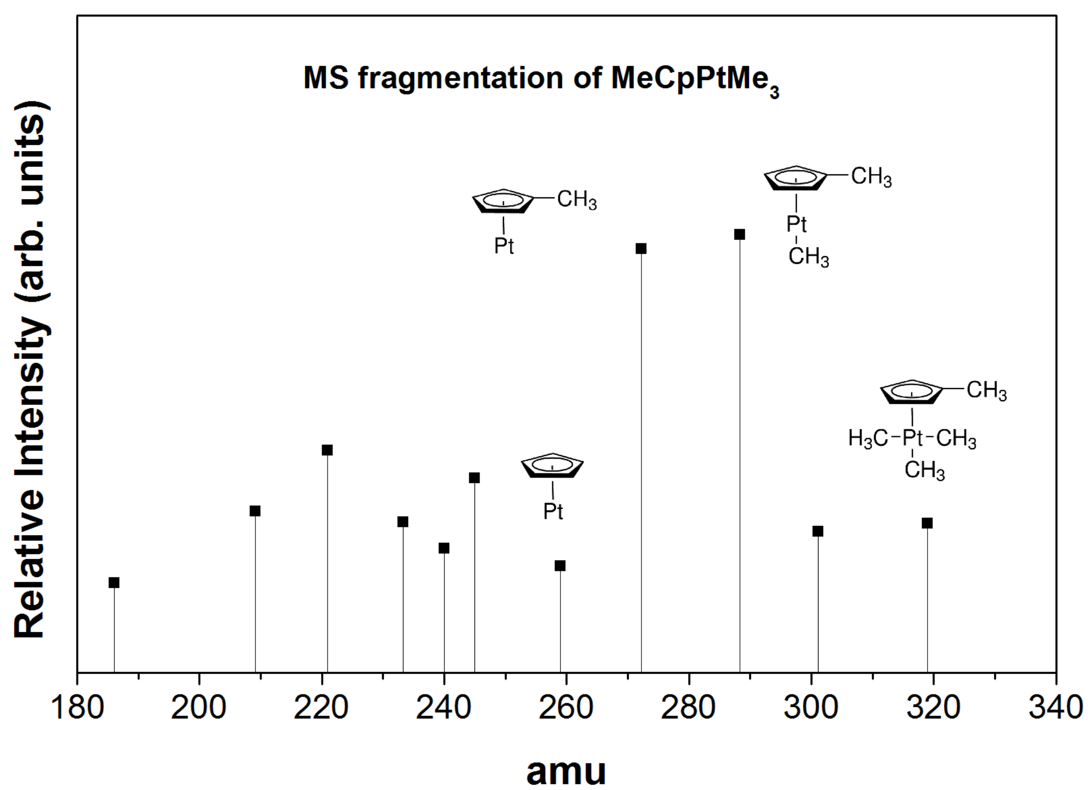


**Figure 7.** Electron-impact mass spectrum of $MeCpPtMe_3$ recorded with a quadrupole mass spectrometer.

In the spectra above the two fragment peaks account for the greatest portion of entire ions, which located at ~270 & 290 amu, correspond to the MeCpPt and identical structure with addition of methyl group. Hence, the cracking pattern undergoes to a path favored for the subsequent film deposition, which that, as the main structure turning to active species upon adsorption by losing three methyl groups which bond directly with Pt atom, the MeCp moiety remained intact, for controlled removal in the second half of the ALD cycle.

This approach is ideal for the relatively stable reactant which the structure is unlikely to be activated only by thermal energy. From the XPS spectras it is clear to observe the limited platinum deposition on both types of silicon starting surface even large exposure has applied. With assistance of electron impact ionization, the nucleation rate has significantly improved; in the mean time it is also important to verify if the excitation towards the precursor is selective by examining the cracking pattern, which the blocking ligand should remained bonded with the target element while other undesired carbonaceous species are best to be decomposed to fulfill a complete reaction. The intact of the blocking ligand prevents acceptance of further exposures of gas molecules once the surface has saturated, such scheme ensures that in each half cycle the thickness of the film will be limited within monolayer. Since the availability of the types of platinum precursor is very limited, thereby the proposed approach is exceptional ideal as an alternative to enhance the nucleation of platinum particles.

The approach in this study utilizes electron impact to dissociate gas molecules and thereby produce the desired fragments, which then functions as the non-metal precursor. The metal precursor cannot be dissociated as this would lead to CVD growth. It suggests that for other cases it may not be easy to design processes to partially catalyze the stable metal precursor while retaining self-limiting character. How the electron impact environment are mainly attributed to the following factors, e.g., i) ion bombardment and plasma etching affects the dosing processes and translates into higher growth rates, and ii) lower activation energies for platinum growth, essentially remains unclear [30-35]. The distinctive feature of this approach is that the substrate is located close to and is exposed to the charged species originating from the ionization source. The proximity of the discharge to the substrate may results in a large flux of radicals which is a major advantage of radical enhanced deposition. Also, in theory the particle bombardment may provide additional energy to the adsorbed species and increase their surface mobility and the rate of the film forming reactions [36]. This chapter shows the possibilities to obtain a self-limiting scheme with the cyclopentadienyl ligand remained intact and attached to the platinum metal upon adsorption, which is ready for the second half cycle of ALD process.

### 3.4 Conclusions

It is shown that within the targeted temperatures range, the thermal energy is insufficient for effective catalytic precursor decomposition; the use of highly reactive species plays a key role in the promotion of platinum growth, which eliminates the regime of incomplete reactions, and partially induces the adsorption of the metal precursor on the Si(100)

surface. In addition, with this approach it is possible to deposit the films at lower temperature, a series of experiments were setup to map out the ALD windows of $MeCpPtMe_3$ on Si-based surfaces, to be noted all the Pt/Si experiments discussed later in this dissertation are conducted with ionization source activated.

### 3.5 References

[1] Koponen, S. E.; Gordon, P. G.; Barry, S. T. Principles of Precursor Design for Vapour Deposition Methods. Polyhedron 2016, 108, 59-66.

[2] Kwon, J.; Dai, M.; Halls, M. D.; Langereis, E.; Chabal, Y. J.; Gordon, R. G. In Situ Infrared Characterization During Atomic Layer Deposition of Lanthanum Oxide. J. Phys. Chem. C 2009, 113, 654-660.

[3] Ma, Q.; Guo, H.; Gordon, R. G.; Zaera, F. Surface Chemistry of Copper(I) Acetamidinates in Connection with Atomic Layer Deposition (ALD) Processes. Chem. Mater. 2011, 23, 3325-3334.

[4] Ma, Q.; Zaera, F. Chemistry of $Cu(acac)_2$ on Ni(110) and Cu(110) Surfaces: Implications for Atomic Layer Deposition Processes. J. Vac. Sci. Technol., A 2013, 31, 01A112.

[5] Kim, T.; Yao, Y.; Coyle, J. P.; Barry, S. T.; Zaera, F. Thermal Chemistry of Cu(I)-Iminopyrrolidinate and Cu(I)-Guanidinate Atomic Layer Deposition (ALD) Precursors on Ni(110) Single-Crystal Surfaces. Chem. Mater. 2013, 25, 3630-3639.

[6] Duan, Y.; Gao, F.; Teplyakov, A. V. Role of the Deposition Precursor Molecules in Defining Oxidation State of Deposited Copper in Surface Reduction Reactions on HTerminated Si(111) Surface. J. Phys. Chem. C 2015, 119, 27018-27027.

[7] Gordon, P. G.; Kurek, A.; Barry, S. T. Trends in Copper Precursor Development for CVD and ALD Applications. ECS J. Solid State Sci. Technol. 2015, 4, N3188-N3197.

[8] Yao, Y.; Zaera, F. Thermal Chemistry of Copper Acetamidinate Atomic Layer Deposition Precursors on Silicon Oxide Surfaces Studied by XPS. J. Vac. Sci. Technol., A 2016, 34, 01A101.

[9] Yao, Y.; Coyle, J. P.; Barry, S. T.; Zaera, F. Thermal Decomposition of Copper Iminopyrrolidinate Atomic Layer Deposition (ALD) Precursors on Silicon Oxide Surfaces. J. Phys. Chem. C 2016, 120, 14149–14156.

[10] Duan, Y.; Teplyakov, A. V. Deposition of Copper from Cu(I) and Cu(II) Precursors onto HOPG Surface: Role of Surface Defects and Choice of a Precursor. J. Chem. Phys. 2017, 146, 052814.

[11] Qin, X.; Zaera, F. Chemistry of Ruthenium Diketonate Atomic Layer Deposition (ALD) Precursors on Metal Surfaces. J. Phys. Chem. C 2018, DOI: 10.1021/acs.jpcc.1027b11960.

[12] Aaltonen, T.; Rahtu, A.; Ritala, M.; Leskelä, M. Reaction Mechanism Studies on Atomic Layer Deposition of Ruthenium and Platinum. Electrochem. Solid State Lett. 2003, 6, C130-C133.

[13] Elam, J. W.; Pellin, M. J.; Elliott, S. D.; Zydor, A.; Faia, M. C.; Hupp, J. T. Mechanism for Zirconium Oxide Atomic Layer Deposition Using bis(Methylcyclopentadienyl)Methoxymethyl Zirconium. Appl. Phys. Lett. 2007, 91, 253123.

[14] Diskus, M.; Balasundaram, M.; Nilsen, O.; Fjellvåg, H. Influence of Precursors Chemistry on ALD Growth of Cobalt-Molybdenum Oxide Films. Dalton Trans. 2012, 41, 2439-2444.

[15] Bouman, M.; Qin, X.; Doan, V.; Groven, B. L. D.; Zaera, F. Reaction of Methylcyclopentadienyl Manganese Tricarbonyl on Silicon Oxide Surfaces: Implications for Thin Film Atomic Layer Depositions. Organometallics 2014, 33, 5308-5315.

[16] Lubers, A. M.; Muhich, C. L.; Anderson, K. M.; Weimer, A. W. Mechanistic Studies for Depositing Highly Dispersed Pt Nanoparticles on Carbon by Use of trimethyl(Methylcyclopentadienyl)Platinum(IV) Reactions with $O_2$ and $H_2$. J. Nanopart. Res. 2015, 17, 179.

[17] Bouman, M.; Zaera, F. Kinetics of Adsorption of Methylcyclopentadienyl Manganese Tricarbonyl on Copper Surfaces and Implications for the Atomic Layer Deposition of Thin Solid Films. J. Phys. Chem. C 2016, 120, 8232–8239.

[18] Chen, Y.-J.; Kaesz, H. D.; Thridandam, H.; Hicks, R. F. Low - temperature Organometallic Chemical Vapor Deposition of Platinum. Appl. Phys. Lett. 1988, 53, 1591.

[19] Xue, Z.; Thridandam, H.; Kaesz, H. D.; Hicks, R. F. Organometallic Chemical Vapor Deposition of Platinum. Reaction Kinetics and Vapor Pressures of Precursors. Chem. Mater. 1992, 4, 162.

[20] Goswami, J.; Majhi, P.; Wang, C. G.; Dey, S. K. Properties of Platinum Films by Liquid-Source MOCVD in H2 and $O_2$. Integr. Ferroelectr. 2002, 42, 13.

[21] Rand, M. J. Chemical Vapor Deposition of Thin-Film Platinum. J. Electrochem. Soc. 1973, 120, 686.

[22] Kwak, B. S.; First, P. N.; Erbil, A.; Wilkens, B. J.; Budai, J. D.; Chisholm, M. F.; Boatner, L. A. Study of Epitaxial Platinum Thin Films Grown by Metalorganic Chemical Vapor Deposition. J. Appl. Phys. 1992, 72, 3735.

[23] Lecohier, B.; Philippoz, J.-M.; van den Bergh, H. Selective Low Pressure Chemical Vapor Deposition of Copper and Platinum. J. Vac. Sci. Technol. B 1992, 10, 262.

[24] Lee, J. M.; Hwang, C. S.; Cho, H.-J.; Suk, C.-G.; Kim, H.J. Effect of $O_2$ Addition on the Deposition of Pt Thin Films by Metallorganic Chemical Vapor Deposition. J. Electrochem. Soc. 1998, 145, 1066.

[25] Xue, Z.; Strouse, M. J.; Shuh, D. K.; Knobler, C. B.; Kaesz, H. D.; Hicks, R. F.; Williams, R. S. Characterization of (methylcyclopentadienyl)trimethylplatinum and Low-temperature Organometallic Chemical Vapor Deposition of Platinum Metal. J. Am. Chem. Soc. 1989, 111, 8779.

[26] Utriainen, M.; Kroger-Laukkanen, M.; Johansson, L.-S.; Niinisto, L. Studies of Metallic Thin Film Growth in an Atomic Layer Epitaxy Reactor using $M(acac)_2$ (M=Ni, Cu, Pt) Precursors. Appl. Surf. Sci. 2000, 157, 151.

[27] Brooks, Inc. Introduction to Bayard-Alpert Ionization Gauges.

[28] Wnuk, J. D.; Rosenberg, S. G.; Gorham, J. M.; van Dorp, W. F.; Hagen, C. W.; Fairbrother, D. H. Electron Beam Deposition for Nanofabrication: Insights from Surface Science. Surf. Sci. 2011, 605, 257-266.

[29] Thorman, R. M.; Kumar T. P, R.; Fairbrother, D. H.; Ingólfsson, O. The Role of Low-Energy Electrons in Focused Electron Beam Induced Deposition: Four Case Studies of Representative Precursors. Beilstein J. Nanotechnol. 2015, 6, 1904-1926.

[30] Grobert, N. Carbon Nanotubes – becoming Clean. Mater. Today 10, 28(2007).

[31] Keidar, M.; Monteiro, O. R.; and Brown, I. G. Plasma Drift and Nonuniformity Effects in Plasma Immersion Ion Implantation. Appl. Phys. Lett. 76, 3002 (2000).

[32] Teo, K. B. K.; Hash, D. B.; Lacerda, R. G.; Rupesinghe, N. L.; Bell, M. S.; Dalal, S. H.; D. Bose,; Govindan, T. R.; Cruden, B. A.; Chhowalla, M.; Amaratunga, G. A. J.; Meyyappan, M.; and Milne, W. I. The Significance of Plasma Heating in Carbon Nanotube and Nanofiber Growth. Nano Lett. 4, 921 (2004).

[33] Okita, A.; Suda, Y.; Ozeki, A.; Sugawara, H.; Sakai, Oda, Y.; A.; and Nakamura, J. Predicting the Amount of Carbon in Carbon Nanotubes Grown by $CH_4$ rf Plasmas. J. Appl. Phys. 99, 014302 (2006).

[34] Lim, S. H.; Yoon, H. S.; Moon, J. H.; Park, K. C.; and Jang, J. Optical Emission Spectroscopy Study for Optimization of Carbon Nanotubes Growth by A Triode Plasma Chemical Vapor Deposition. Appl. Phys. Lett. 88, 033114 (2006).

[35] Anders, A. Atomic Scale Heating in Cathodic Arc Plasma Deposition. Appl. Phys. Lett. 80, 1100 (2002).

[36] Messier, R.; Yehoda; J. E. and Pilione , L. J. in Handbook of plasma processing technology, edited by Rossnagel, Cuomo and Westwood, Noyes, 1990, Park Ridge, New Jersey, U.S.A., p. 448

# CHAPTER FOUR

## Thermal/Electron Impact Activated CVD/ALD process of Pt on Si-based substrates

### 4.1 Introductions

Films grew by atomic layer deposition in theory undergoes one monolayer per cycle, in real world the growth per cycle is usually deviate from such expectation due to steric hindrance, which prevents certain chemical reactions to happen, and thereby the deposition rate in ALD is rather low compared to a typical chemical vapor deposition technique. In modern technology the required film thickness is often from a couple of nanometers up to few tens of nanometers, thus the low growth rate is not seen as severe problem anymore. In addition, large batch processing is a rather straightforward way to increase throughput [1]. However, to further scale down the thickness of the film or to maximize the catalytic activity of the platinum particles used in energy harvesting devices, such issue is becoming more prominent.

Thereby understanding the initial growth of target materials during the nucleation stage is essential to develop ALD process for the thinnest of films. In this chapter, we report results from in-situ X-ray photoelectron spectroscopy (XPS) analysis on the nature of films prepared by chemical means using $MeCpPtMe_3$ as the precursor on Si(100) with native oxide films. Since it is common that the chemical type vapor depositions are

temperature sensitive and only within specific range which terminated surface reactions shown would fit to ALD scheme, the study began by first investigating the temperature dependence of $MeCpPtMe_3$ on Si-based surfaces, thereby uptake of half cycle $MeCpPtMe_3$ deposition conducted with various temperature sets was acquired to map out the ALD temperature regime. Ideal exposure conditions for saturating the Si(100) surfaces were defined, Peak positions, intensities, surface species, and coverage, etc, were quantitatively reported and discussed in this chapter. The goal is to develop a molecular-level understanding of the surface chemistry in ALD of Pt on Si-based surfaces.

Experimentally, two types of Si surfaces were utilized, the Si(100) with ~1 nm native oxide, and the 300 nm thick $SiO_2$/Si(100). The dosing pressure was maintained at 5 x $10^{-5}$ Torr. As addressed in previous section, it is unlikely to have the platinum particles nucleid on the surface with pure thermal energy, and hence all the experiments conducted later were preceded with the ionization gauge being activated to ensure effective surface reaction.

## 4.2 Half Cycle Depositions of $MeCpPtMe_3$ on $SiO_2$ Surfaces

### 4.2.1 ALD temperature window

To locate the saturate region for deposition of $MeCpPtMe_3$, multiple substrate temperature sets ranged from 100˚C to 400˚C, with increment of 50˚C were applied in the experiments. Fig. 8 shows Pt 4f XPS results of the half cycle $MeCpPtMe_3$ deposition

processed at $T_s$ of 423 K and 573 K, it is clear to be seen at lower temperature the addition of the deposits is very limited, the intensity reached to its plateau condition by the 1st dose of 2.7 x $10^5$ L exposure, beyond this point no significant increase of accumulation was observed, suggesting that the surface reaction has terminated. In contrast, with the deposition of $MeCpPtMe_3$ conducted at 573 K, the film was significantly built up faster.

**(a)** **(b)**

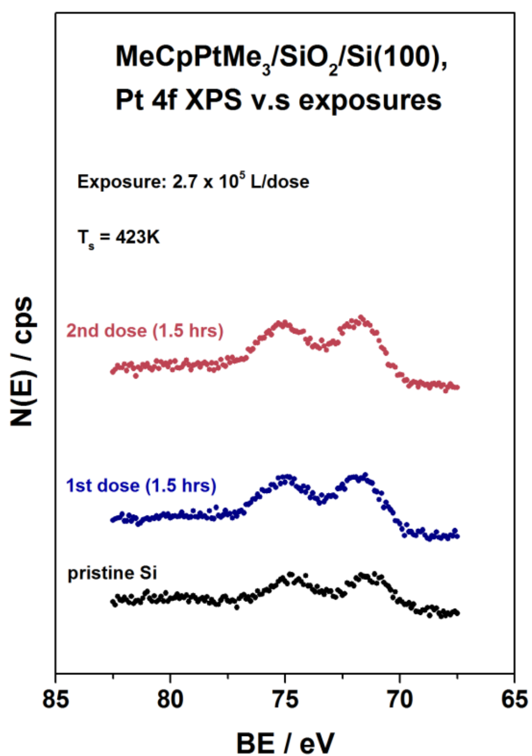


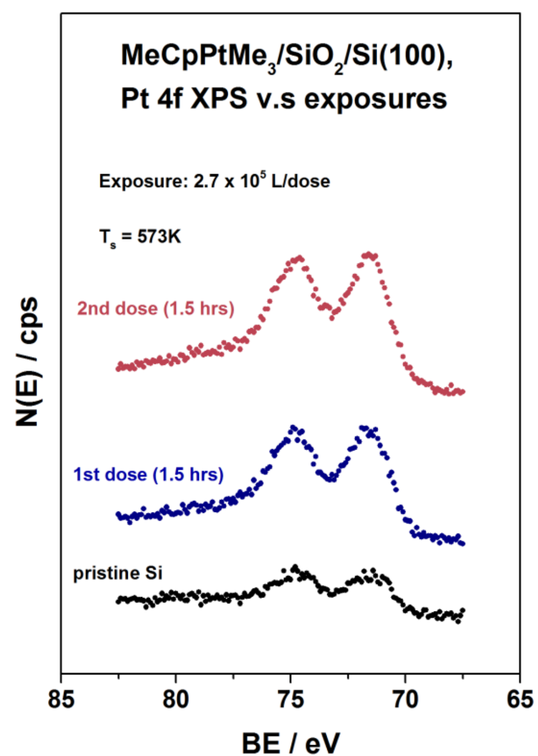


**Figure 8.** Pt 4f XPS spectra of single cycle $MeCpPtMe_3$ deposition on a Si(100) sample at (a) 423 K, and (b) 573 K completed by two separated dosings.

The temperature range for this series of experiments was targeted within 373 K and 673K to locate the proper temperature for deposition of $MeCpPtMe_3$ on Si surfaces. Fig. 9 displays the Pt 4f XPS peaks after a $MeCpPtMe_3$ exposure of 5.4 x $10^5$ L posed onto native oxide at different temperatures. It clearly shows more dominated results on higher $T_s$, and depositions were visibly hindered at lower temperature. Despite higher $T_s$ yields more amount of metal deposits, such conditions does not always favored for ALD process as self-limiting feature is its advantage compared with other typical chemical type vapor depositions. A higher temperature would result in larger chance of chemical decompositions.

A clearer overview of $T_s$ uptake versus exposures is presented in Fig. 10. Based on the observations it can be concluded the growth of $MeCpPtMe_3$ on native oxide is substrate temperature dependant; ineffective deposition takes place at lower temperature of 373 K – 473 K suggesting low reactivity of the precursor mainly due to lacks of thermal energy to initiate the surface reaction. Saturating growth behavior is observed at temperature of 523, 573 K, with no significant additional growth after greater exposure. The ideal region for deposition of $MeCpPtMe_3$ on the target substrate with self-limiting growth regime falls within 523 K – 573 K, which is best classified as the ALD window. Above 623 K, conventional CVD starts and the deposition process is no longer self-limited by saturating surface reactions, suggesting the precursor has partially decomposed while reaching the surface, which most likely due to the loss of cyclopentadienyl ligand leads to continuous accepting of further dosed gas molecules.

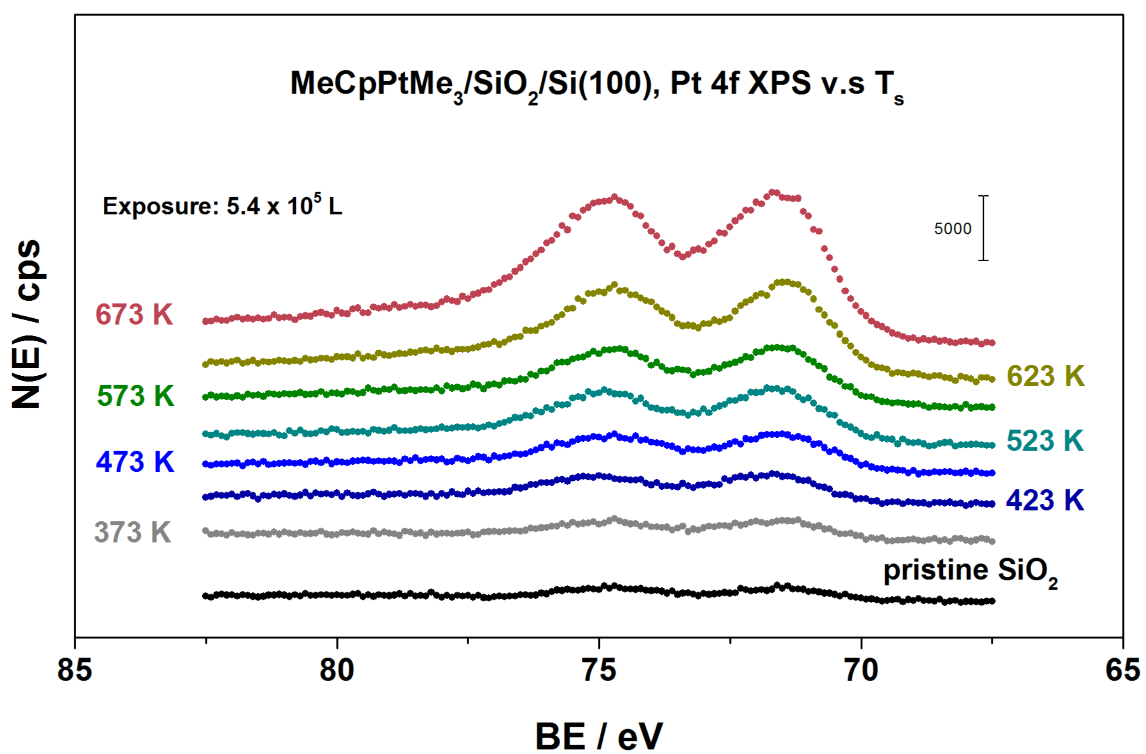


**Figure 9.** Pt 4f XPS of single half cycle saturated $MeCpPtMe_3$ deposition on Si(100) samples as a function of substrate temperature.

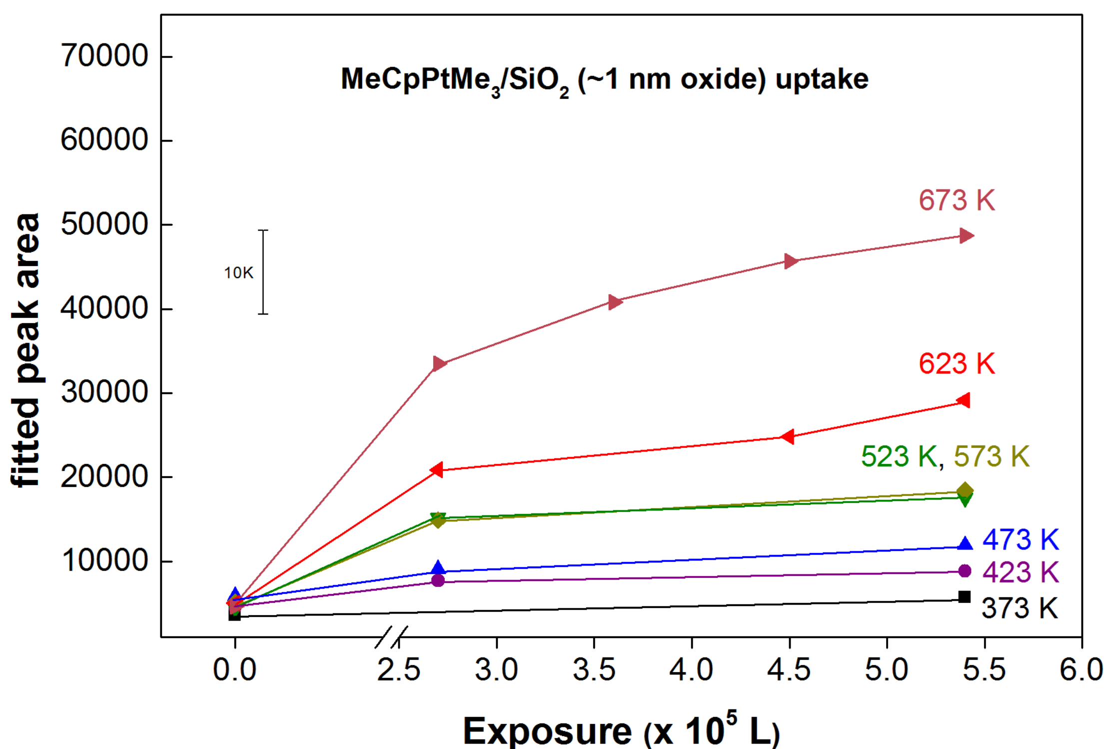


**Figure 10.** Uptake curves of given exposure (5.4 x $10^5$ L) of $MeCpPtMe_3$ on Si(100) samples, in form of quantified Pt 4f peak area versus exposure, deposition taking place at various substrate temperatures between 373 and 673 K. The half-reaction displays a near-saturating reaction between 523-573 K.

### 4.2.2 Surface Species Identifications

While the peak intensities measure how much of a material is at the surface, the peak positions in terms of binding energy provide information about the chemical state for a material. Other values, such as the full width at half maximum (FWHM) are useful indicators of chemical state changes and physical influences. That is, broadening of a peak may indicate: a change in the number of chemical bonds contributing to a peak shape, a change in the sample condition or differential charging of the surface (localized differences in the charge-state of the surface).

X-ray photoelectron spectra was acquired after each dose to determine the change in composition and the bonding states of the prepared sample. In the case of Pt XPS spectra, the most intense doublet (71.4 and 74.7 eV) most likely corresponds to metallic platinum [2], and if exists, the commonly observed second doublet (72.0 and 76.0 eV) ascribed to the $Pt^{2+}$ ($Pt^{II}O$) will be shown here; the slight higher binding energy of metallic Pt than the reported value (70.9 eV) may due to the formation of incomplete film mainly composed by discrete nanoclusters. Fig. 11 shows a total of 5.4 x $10^5$ L of $MeCpPtMe_3$ exposure on 1 nm $SiO_2$/Si at $T_s$ of 523 K, given that the presented Pt 4f XPS peaks are displaying similar binding energies with maximum of 0.2 eV difference in peak position, and no appearance of additional satellite peaks formed nearby the main Pt 4f peaks, which is evident from similar FWHM values of this series of experiments, results here show little evidences of newly generated Pt oxidation states, and hence strongly suggests the presence of platinum in +0 oxidation state, also known as pure platinum metal in form

of $Pt^0$. This is also evident from the limited chemical shifting and newly formed peak of C 1s, Si 2p, and O 1s peaks. The BE of C 1s XPS peak is 284.6 eV, consistent with it corresponding to the MeCp ligand. Similar observations in terms of chemical shifting apply to other temperature sets as summarized in Table 2.

(a) (b)

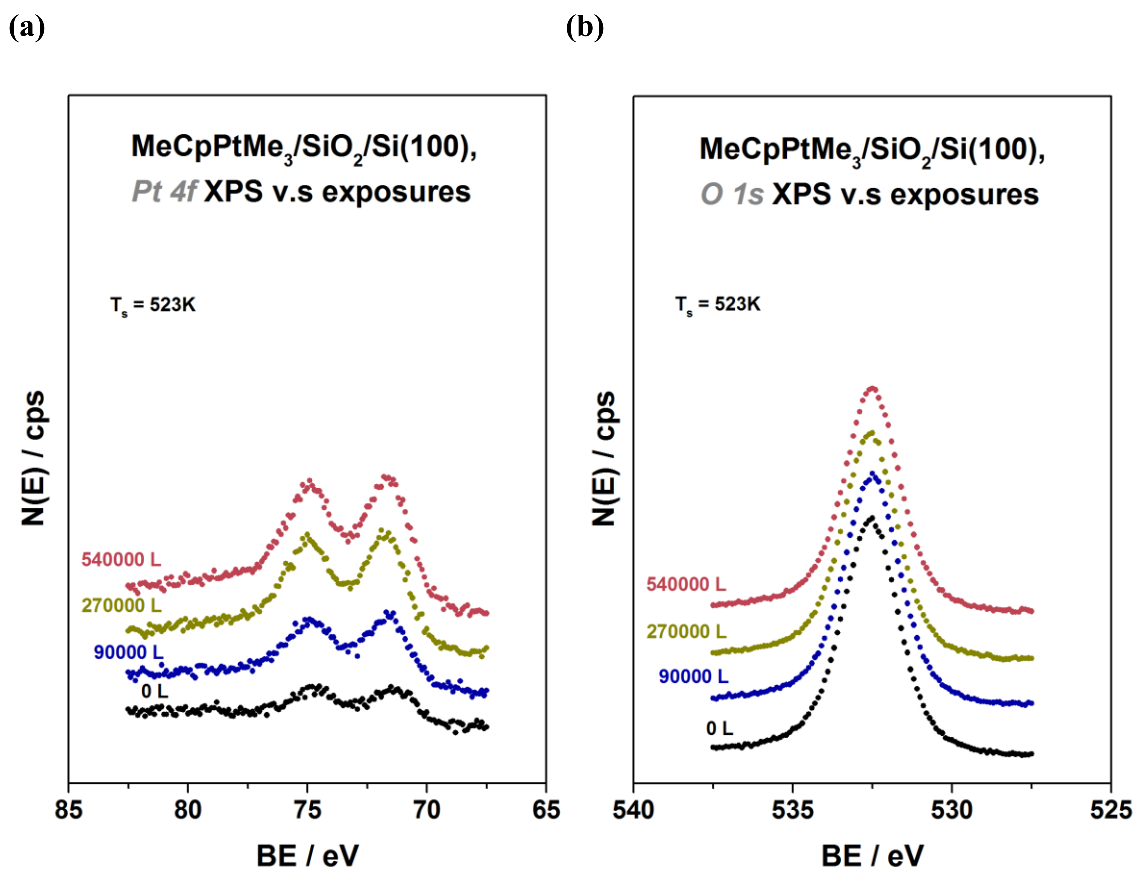


**Figure 11**. (a) Pt 4f, and (b) O 1s XPS spectra of single cycle $MeCpPtMe_3$ deposition on a Si(100) sample at 523 K, completed by three separated dosings.

**Table 2**. Summary of Pt 4f XPS peak position.

| $T_s$ | Exposures | Peak positions (Pt $4f_{5/2, 7/2}$) |
|---|---|---|
| 200°C | 0 L | 74.6, 71.3 eV |
| | $2.7 \times 10^5$ L | 74.8, 71.5 eV |
| | $5.4 \times 10^5$ L | 74.8, 71.5 eV |
| 300°C | 0 L | 74.9, 71.6 eV |
| | $2.7 \times 10^5$ L | 74.9, 71.6 eV |
| | $5.4 \times 10^5$ L | 74.9, 71.6 eV |
| 400°C | 0 L | 74.8, 71.5 eV |
| | $2.7 \times 10^5$ L | 75.0, 71.7 eV |
| | $5.4 \times 10^5$ L | 74.8, 71.5 eV |

### 4.2.3 Surface Coverage

Though one key characteristic of the ALD half cycle is the self-limiting feature, such feature in XPS analysis will not be presented straightforward. In this case, Fig. 12 presents an increased Pt intensities with limited leveling off of Si & O signals, the plateau in intensity of platinum 4f spectra does not necessarily correspond to a fully saturated surface but more likely, a nucleation delay leading to low step coverage in first half cycle. Thereby the XPS not only detect the platinum deposits but also simultaneously picks up signals from exposed underlying Si surface.

(a) (b)

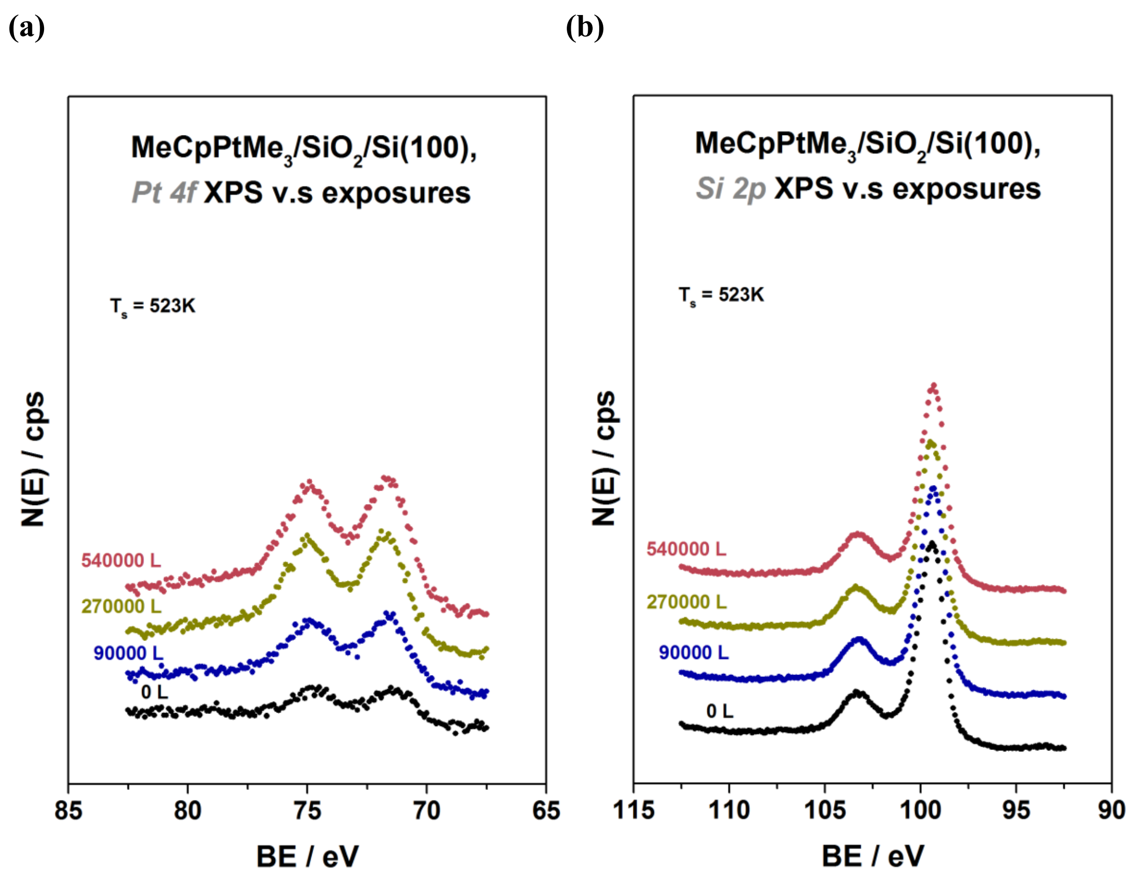


**Figure 12.** (a) Pt 4f, and (b) Si 2p XPS spectra of single cycle $MeCpPtMe_3$ deposition on a Si(100) sample at 523 K, completed by three separated dosings.

In real world many ALD processes begin with a nucleation stage, leading to less than a monolayer per cycle, and is usually referred as nucleation delay or steric hindrance [3]. Nucleation delay prevents certain chemical reactions to happen as a result of the molecule structure and size, this phenomenon is usually observed in molecules with large groups. Though, the actual factors governing the nucleation involved in ALD is not yet fully understood.

The typical steps in making thin films proceed by: emission of particles from source, transport of particles to substrate, condensation of particles on substrate. And there are some contradictories ongoing here; in terms of thermal accommodation and surface energy, the substrate should be maintained cold, and the impinging materials should have low energy to lower the bouncing back kinetics; however in terms of the surface reactions, the higher substrate temperature usually increase the reaction rate. Regardless which adsorption mechanism the precursor bound onto the surface, the local energy barrier which causes desorption has to be counterbalanced. Once an atom bonds with the surface, it creates a tension due to the surface atoms stretching their bonds in response to the adsorption of the atom.

Fig. 13 (a) shows the 3-D or island growth mode, the atoms have a strong affinity with each other and build 3-D islands that grow in all directions, including the direction normal to the surface. The growing islands eventually coalesce and form a continuous film. Fig. 13 (b) displays the 2-D layer-by-layer growth expected for ideal ALD scheme;

the condensing particles have a strong affinity for the substrate atoms: they bond to the substrate rather than to each other. And Fig. 13 (c) shows another common thin film pattern, which is a mixed mode that could either starts from either any of the top methods then undergoes to another type after one or more layers. For most electronic devices, the non-uniformity caused by nucleation negatively affects film performance, and thereby continuous films are generally required [1, 4].

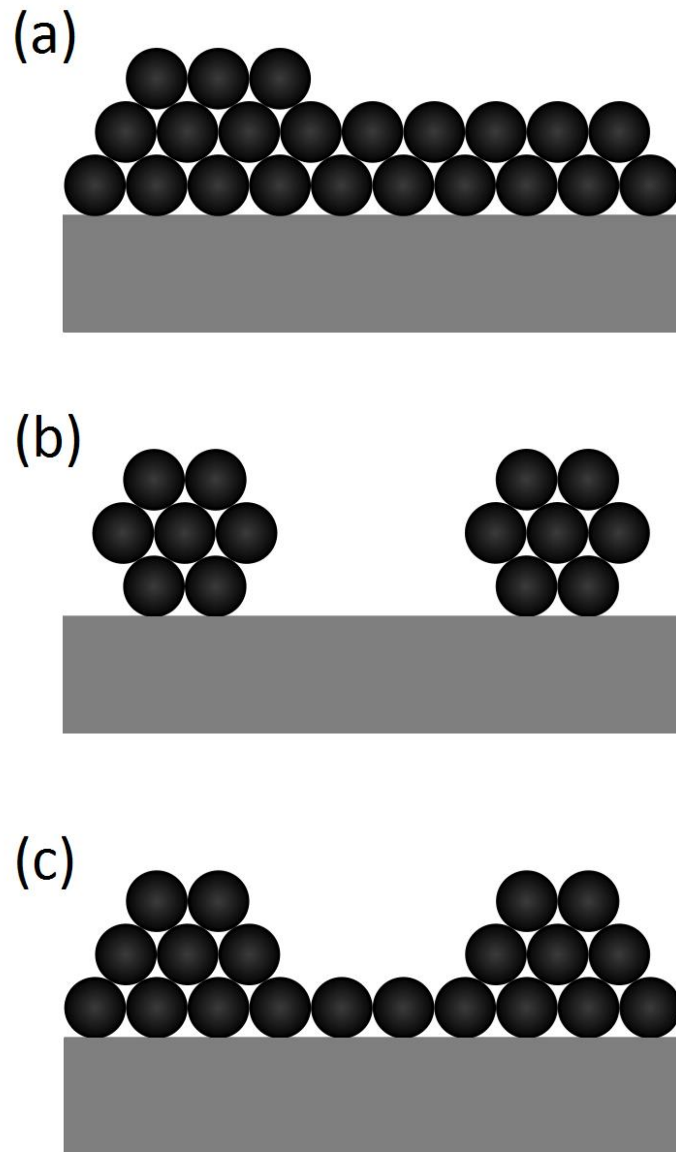


**Figure 13.** Schemes of different phase growth mechanisms, (a) layer-by-layer growth, (b) island growth, and (c) mixed growth.

In general, the nucleation and film growth are favored on adsorption sites with higher bonding energy such as step edges and defects, etc; due to high comformlity of Si benefited from its mature manufacturing development, without any surface pretreatment the adsorption sites on it are very limited for incoming molecules, in addition, the bonding is usually more favored between molecules than molecule to substrate. As a result the metal particles ball up to minimize interface with the substrate, such homogenous kinetics leads to the nucleation in the first layer in form of 3-D islands (Volmer-Weber growth) as shown in Fig. 13(b), and is commonly observed in most types of CVD/ALD on oxide substrates. After a variable number of cycles which is governed by the precursor-surface chemistry, the islands coalesce into a continuous film.

One of the possible methods to achieve high positional uniformity is to minimize the surface energy, from the aspect of surface chemistry is to create sufficient and effective adsorption sites, such approaches avoids the localized deposition on typical favored spots such as defects, trenches, etc. This can be completed by additive of proper adsorption sites, for instance, hydroxyl groups, which are commonly proposed as the nucleation sites for proper ligand exchange mechanism of $MeCpPtMe_3$, or simply by extending the exposure allowing the molecules having sufficient time to diffuse through the entire surface.

### 4.3 Cyclewise and Alternate Exposures

Fig. 14 shows an example set of XPS spectra of a single completed cycle in which 1 dose of $MeCpPtMe_3$ followed by 1 dose of oxygen. An increased O 1s intensity is clearly to be observed after the oxygen dose indicates that the surface was effectively exposed to gas source; the proper removal of excess reactant is also evident from the C 1s spectrums, where the amount of carbonaceous materials was significantly reduced, in the mean time new side shoulder is observable on C 1s peak after oxygen dose revealing the newly formed C-O-C bonding, and indicating the second half cycle properly employed.

(a) (b)

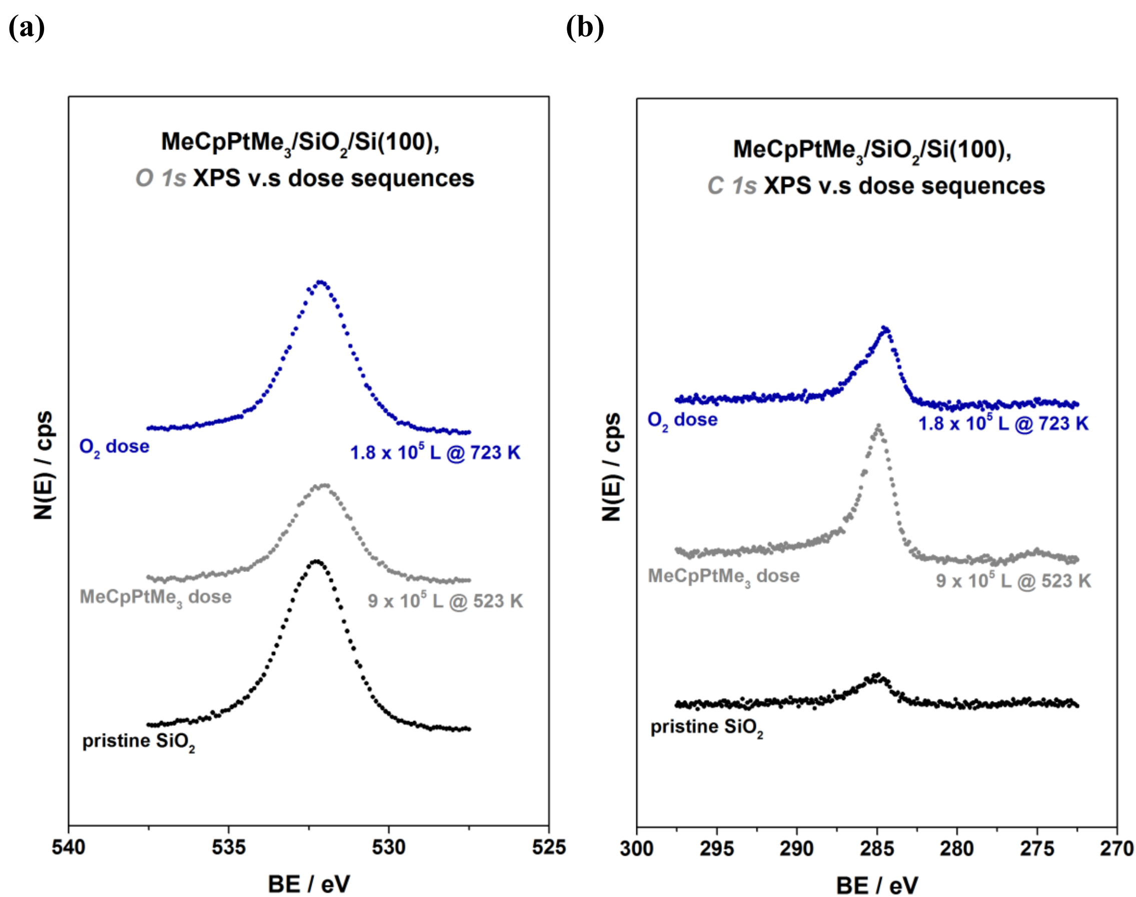


**Figure 14.** (a) O 1s, and (b) C 1s XPS spectra of single cycle $MeCpPtMe_3$ deposition on a Si(100) sample at 523 K.

To grow multiple layered thick films, experiments in this section involved consecutively dosing of platinum precursor and oxygen served as purging and counter reactant. The total exposures for one half cycle is set to be $5.4 \times 10^5$ L. The Pt 4f XPS versus number of the cycle is plotted as shown in Fig. 15.

A notable increase in Pt growth can be observed from 2nd cycle, in later cycles the peak intensities not only grow but also shift, such minimal shift in peak position may suggests possibility of changes in charging, in other words, the platinum particles accumulates in cluster form result in multiple 3-D island with large interstitial spacing within each other. Such presumption may explain the absence of monolayer formation while a visible increase in Pt deposit has already taken place within the $1^{st}$ cycle.

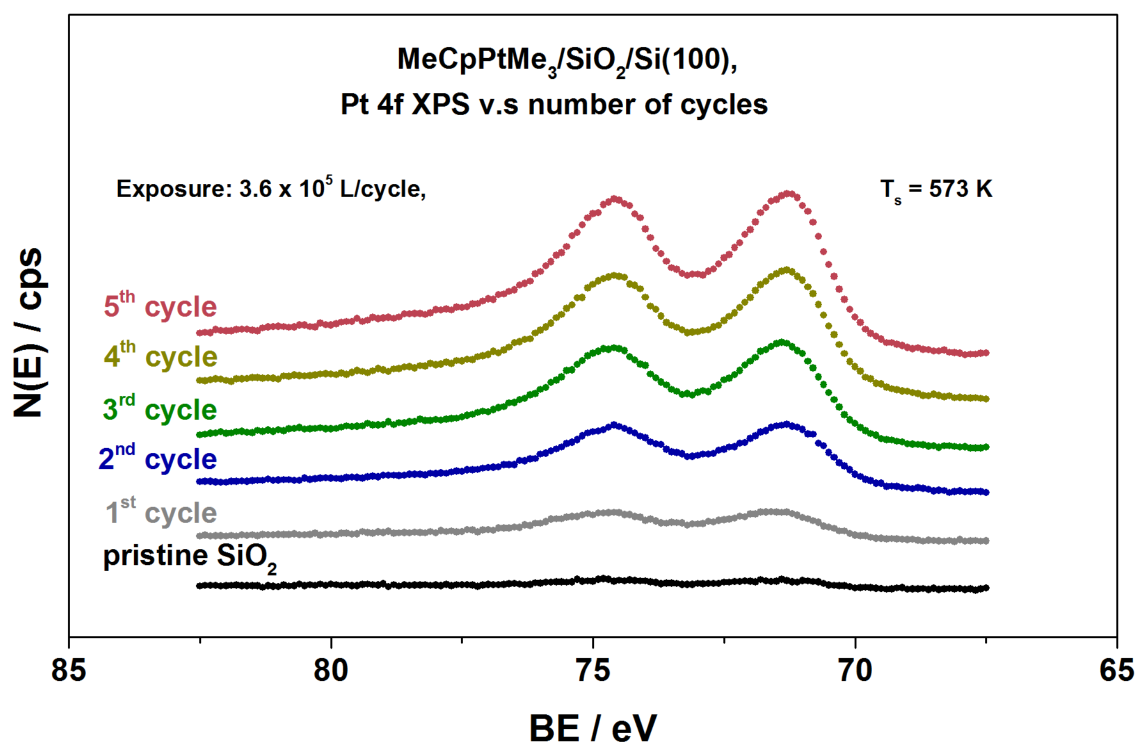


**Figure 15.** Pt 4f XPS of $MeCpPtMe_3$ deposition on Si(100) samples as a function of the number of cycles.

On the basis of the attenuation of the measured Si 2p XPS signals, the surface coverage after each cycle is calculated by quantifying the intensities of the XPS peaks, and converting results into monolayer equivalents by assuming growth proceeded in layer-by-layer model and using reported values for the electron inelastic mean free path lengths [5]. Relative sensitivity factors were also applied into the calculation of ratio between each element for adjustment of instrument transmission and escape depth corrections. Converted results are plotted as average thickness versus number of ALD cycle as shown in Fig. 16.

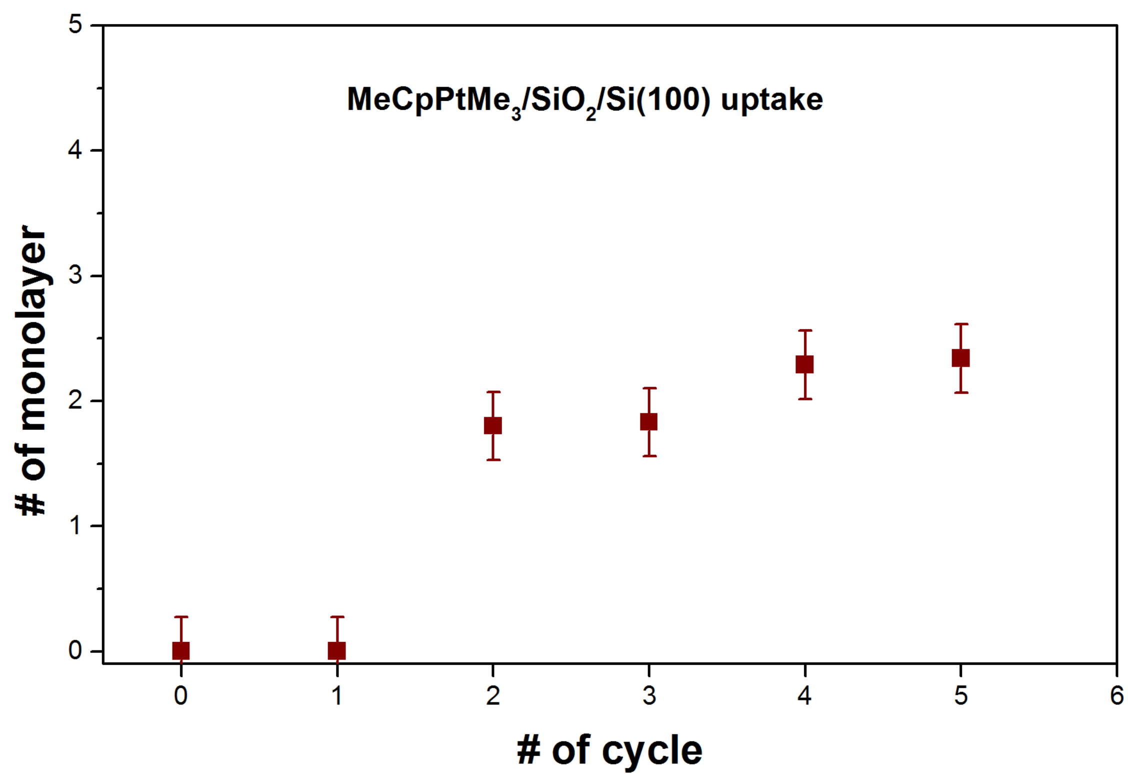


**Figure 16.** Estimated thickness of platinum film in monolayer equivalent calculated via attenuations of Si signals versus the number of deposition cycle.

From the plot of growth per cycle shown above, it is clear to observe an inhibition period taking place during the 1$^{st}$ cycle, noted that the extremely low thickness value of it is mainly due to insignificant attenuation of Si 2p XPS signals, which doesn't necessarily completely correspond to the actual amount of Pt deposits.

The inhibited growth can occur due to a relative lack of surface sites, or attributed to the difficulties to thoroughly remove the cyclopentadienyl ligands and prepare for the next cycle, direct evidences have been reported from related studies of ALD with sequential $H_2O$ and $O_2$ exposure [6].

Noble metal ALD processes typically consist of alternating exposure to an organometallic precursor and oxygen gas, separated by purge steps [7]. During the $O_2$ pulse, oxygen dissociatively chemisorbs on the catalytic metal surface [8]. These O atoms subsequently participate in catalytic combustion of the precursor ligands during the next half-reaction [9]. In addition, dehydrogenation of the precursor ligands occurs on the catalytic Pt surface [9-11]. In contrast, the surface reactions during film nucleation on nonmetallic substrates such as oxides in this case are more complex; One of the mains is the initial surface does not have the ability to catalyze the surface reactions; Secondly, the cyclopentadienyl ligand serves as the blocking functional group to reject the excess exposure once surface has already saturated; on the other hand, if these carbonaceous layers aren't properly removed, they will slow or even inhibit the growth rate of the following cycles. Each reaction cycle progressively populates the surface with additional

surface sites until a monolayer of ALD material is grown upon which the linear growth regime is reached. The growth afterwards then becomes enhanced and eventually settling to the steady-state growth rate.

### 4.4 Surface Types

In this section, silicon wafer with thick thermally grown oxide (300 nm $SiO_2$) is employed. The top panel of Fig. 17 shows the Pt 4f XPS spectra obtained at 573 K on: Si(100) wafer covered with a 300 nm thick $SiO_2$ layer, and Si(100) wafer with ~1 nm thick native oxide.  It is found that in initial low exposure condition, there is a significant faster Pt nucleation rate (factor of ~3.5) on thick $SiO_2$ film versus the native oxide, with ionization source turned on.

**(a)**

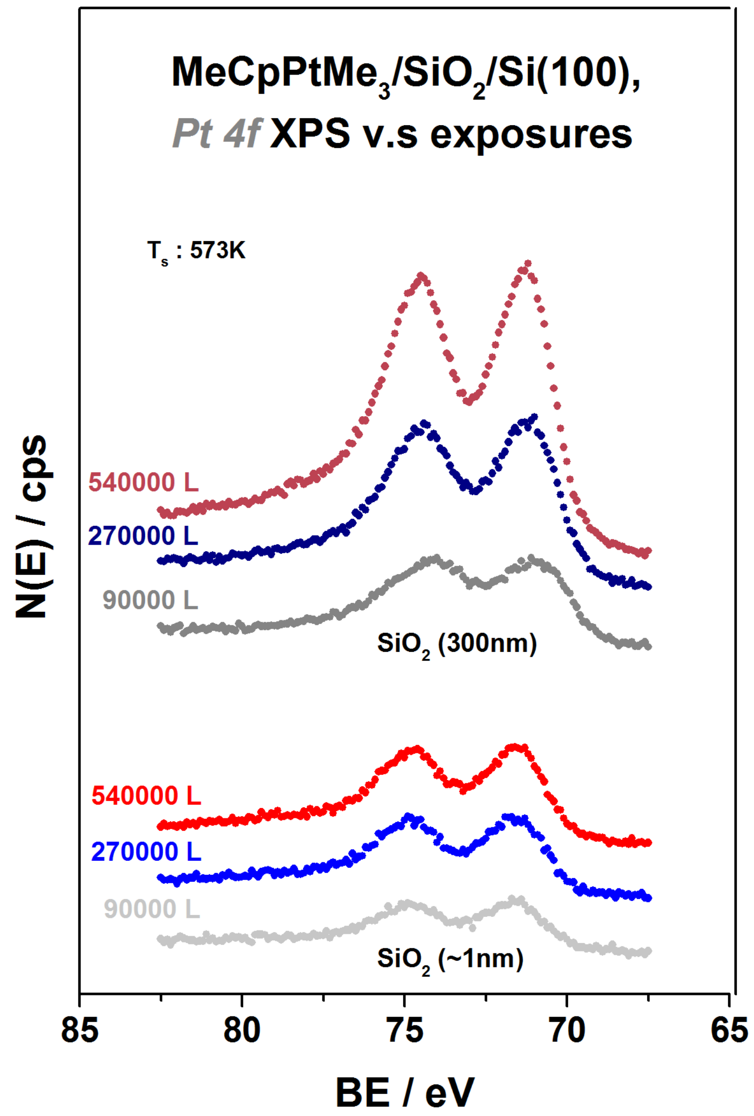

(b)

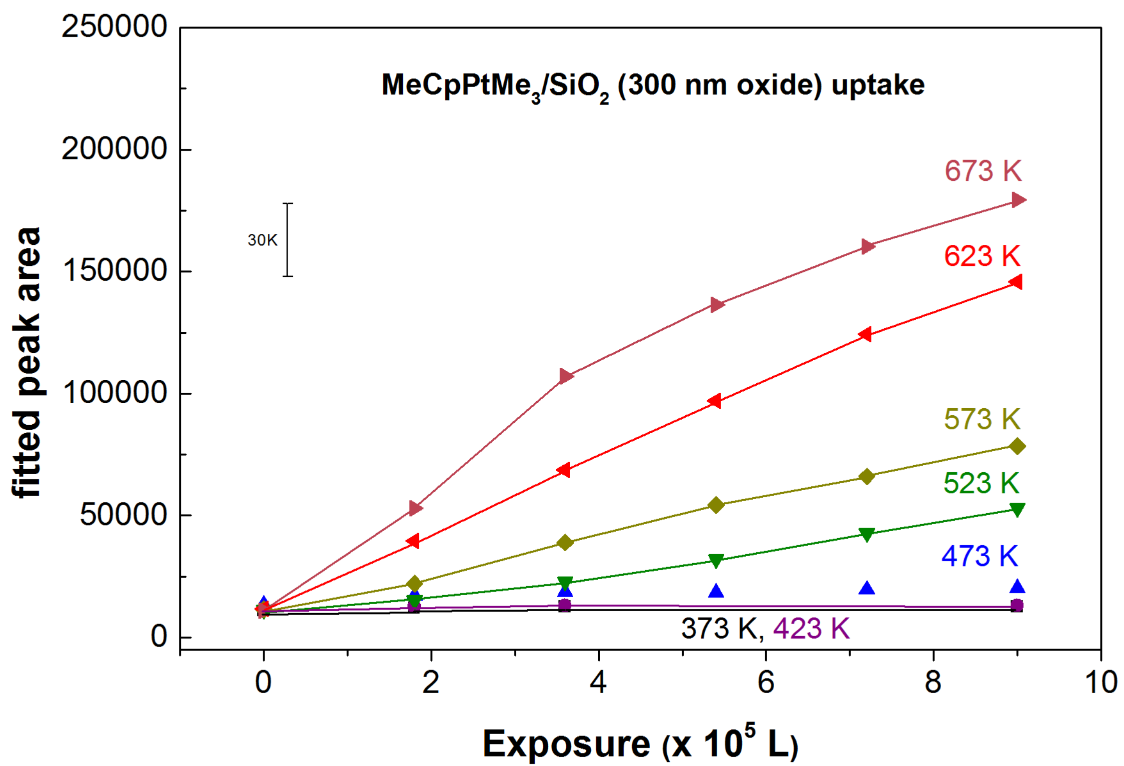

**(c)**

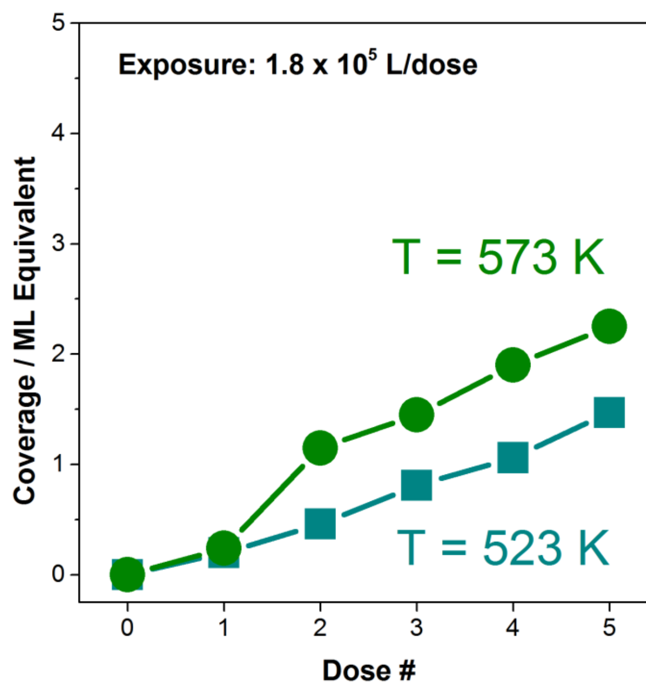


**Figure 17.** (a) Pt 4f XPS of single cycle $MeCpPtMe_3$ deposition on different thickness of $SiO_2$ covered on Si(100) at 673 K. (b) Uptake curves of given exposure of $MeCpPtMe_3$ on 300 nm $SiO_2$/Si(100) samples, in form of quantified Pt 4f peak area versus exposure, deposition taking place at various substrate temperatures between 373 and 673 K. The half-reaction displays a near-saturating reaction between 523-573 K. (c) Growth rate of half cycle exposure of $MeCpPtMe_3$ on 300 nm $SiO_2$/Si(100) conducted at 523 and 573 K.

Despite a notably higher yielded metal deposits were found on thick $SiO_2$ samples compared with native oxides under similar experimental conditions, it was not primarily used as the starting surface in this study mainly due to the difficulties in locating self-limiting regime with sufficient deposits in all tested temperature sets, this is also evident from the calculated low C:Pt ratio of  3.4 when the surface is exposed to a single dose (540000 L) of $MeCpPtMe_3$ @ $T_s$ = 400˚C, suggesting missing of MeCp ligand from the main structure, and lead to a faster CVD uptake. On the other hand, taking T of 523 K for example, the growth rate as shown in Fig. 17(c) has a linear relationship with dosing time, suggesting that the thickness of the film can still be reasonably controlled by the dosing time.

It is commonly accepted that in ALD reaction the nucleation occurs favorably on hydrophilic substrates that contain OH-terminated groups, which promotes chemical reaction with the precursors [12]. The schematic in Figure X illustrates the ideal surface reaction taking place on a hydroxyl group containing surface; during the adsorption step, one of the Pt-bonded methyl groups is released and exchange with the surface group, producing byproducts, and the Pt loading should be increased linearly as it is absorbed on the surface in form of $MeCpPtMe_2$.

Once all the adsorption sites on the surface are occupied, the attached molecules will reject the excess precursors prohibiting them reacting with each other, after purging the saturating surface and applying $O_2$ treatment, the surface is oxidized, turning into PtO.

During the 2nd cycle of Pt addition, there was again a linear increase in the amount of adsorbed $MeCpPtMe_2$ and the absorbed PtO began to reduce to metallic Pt. $O_2$ is dissociatively chemisorbed on the platinum surface, inducing combustion of the remaining ligands of the adsorbed $MeCpPtMe_3$ molecules and the formation of a layer of adsorbed O atoms on the surface. These O atoms then react with the precursor ligands during the subsequent $MeCpPtMe_3$ dose.

Based on the commonly proposed scheme, the followed up experiment was aimed on enhancing the surface hydroxyl groups; due to that the oxide on Si(100) is natively grown and may be less even compared to thermally grown oxide, thereby the 300 nm $SiO_2$ was selected as the starting surface.

Two types of surfaces put into comparisons in this section are 300nm $SiO_2$, and piranha cleaned 300nm $SiO_2$; piranha solution is a powerful oxidizing agent, which is able to hydroxylate many organic compounds; wafers pretreated with such solution is believed that highly reactive atomic oxygen is formed. Piranha solution was prepared via protocol as follows: 1) 3 parts sulfuric acid ($H_2SO_4$ – 98%) - heat to 100°C; 2) add 1 part hydrogen peroxide ($H_2O_2$ – 30%); 3) place wafer into solution for 10 min, and finally 4) rinse with DI water, blow dried. 300nm $SiO_2$ substrates were cleaned by piranha solution and used as a standard OH-terminated $SiO_2$ surface. The nonpiranha-treated sample was cleaned by standard procedures addressed in Section 2.2.

Fig. 18 shows the measured water contact angles were 41° and 18° on $SiO_2$ surfaces without and with piranha cleaning, respectively. The lower water contact angle achieved after piranha cleaning reflects an even more hydrophilic surface related to the higher number of surface hydroxyl groups. Once all the samples were prepared, Pt ALD was carried out in the same reactor using the identical dosing conditions described earlier in this chapter.

The XPS analysis shows no significant difference in chemical state between two types of surfaces. Fig. 19(a) displays the temperature uptake curve versus exposure for both types of surfaces, in which the solid sphere and star signs correspond to piranha cleaned and unmodified $SiO_2$ surface, respectively; On the SiO2 surface pretreated with piranha solution, a faster growth rate with is shown and applies to majority of the exposure cases. Fig. 19(b) converts the curve fitting results of 9 x $10^5$ L exposure of $MeCpPt_3$ onto the targeted surfaces to bar chart. Here it clear shows the promotion in metal deposits is much more significant at lower temperature, which suggests that the addition of the surface hydroxyl groups may gradually thermal decomposed with elevated substrate temperature. The enhancement in metal deposits may be attributed to an increase in the number of hydroxyl groups serves as the chemisorptions sites for Pt precursor molecules, resulting in a higher nucleation rate.

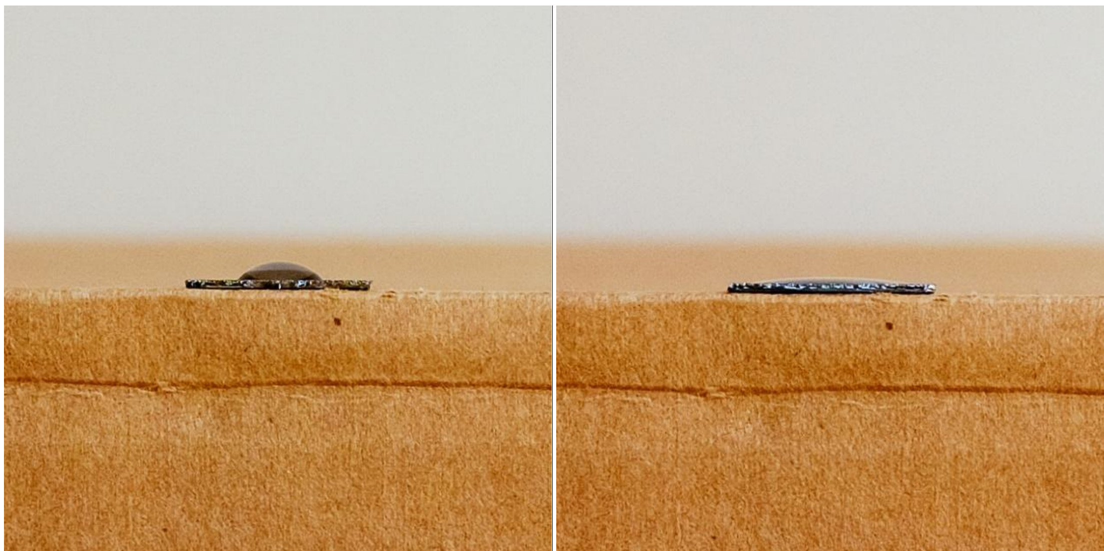

**Figure 18.** Macrographs of the selected samples: (left) pristine, and (right) piranha cleaned 300 nm $SiO_2$/Si(100), showing various degree of hydrophobicity/ hydrophilicity with contact angles measured 41°, and 18°, respectively.

(a)

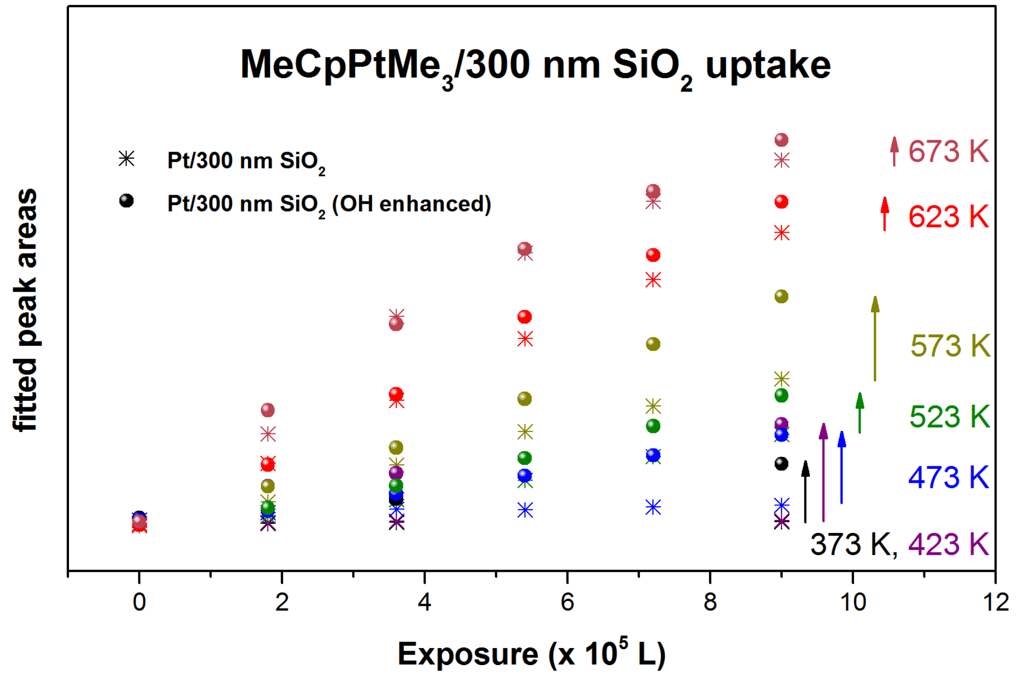


(b)

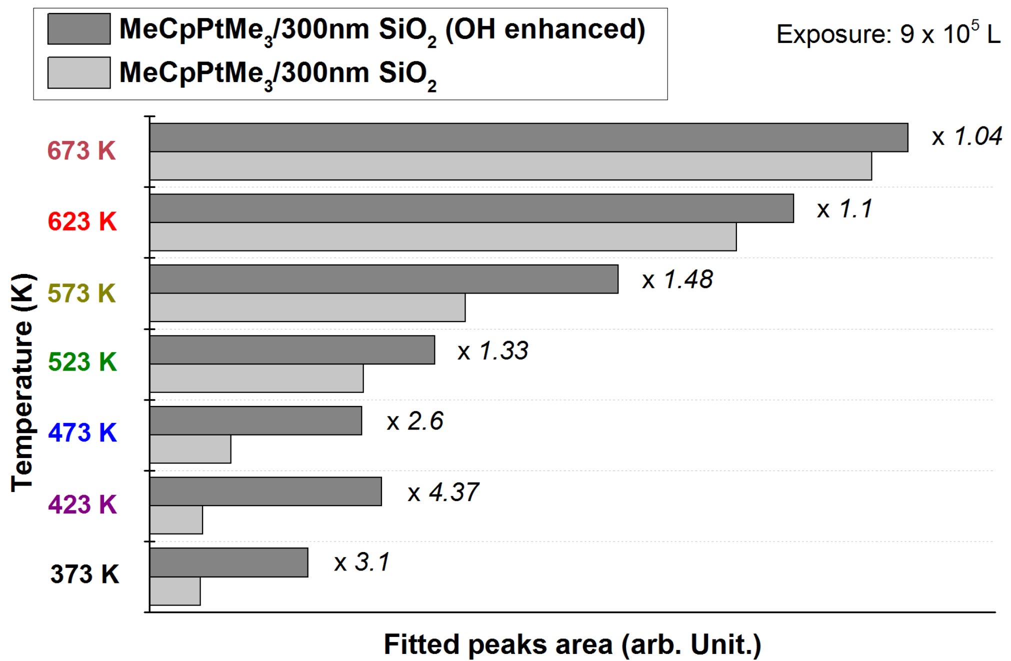

**Figure 19.** (a) Uptake curves of given exposure of $MeCpPtMe_3$ on pristine, and piranha cleaned 300 nm $SiO_2$/Si(100) samples, in form of quantified Pt 4f peak area versus exposure, deposition taking place at various substrate temperatures between 373 and 673 K. (b) Side by side comparisons on curve fitted area between two types of starting surface, with deposition underwent by introducing 9 x $10^5$ L of $MeCpPtMe_3$ onto surface, deposition results at different temperature are represented in bar chart.

### 4.5 Conclusions

In this chapter, the experients were aimed on the growth mechanisms of $MeCpPtMe_3$ on SiO2. The deposition of Pt-based films was tested and characterized using XPS, and the optimum dosing conditions for obtaining saturative growth were detailed investigated on two types Si(100) surfaces with different thickness of oxide. Oxygen treatment was conducted for further multi-layering growth.

The results suggest that saturation of $MeCpPtMe_3$ occurs by exposure of 2.7 x$10^5$ L, and such self-limiting growth applies to temperature range as low from 523 K up to 573 K, deposition conducted below this temperature may result in very thin films due to the factor that lower thermal energy cannot effectively initiate the surface reaction. $MeCpPtMe_3$ was deposited on surface as pure platinum metal in form of $Pt^0$.

In situ XPS analyses have been carried out to examine the surface reactions of each deposited layer including post-annealed films for reference.

In situ x-ray photoelectron spectroscopy was used to obtain chemical information on the reaction products during atomic layer deposition of Pt from (methylcyclopentadienyl)trimethylplatinum $MeCpPtMe_3$ and $O_2$.

## 4.6 References

[1] Dasgupta, N. P.; Jung, H. J.; Trejo, O.; McDowell, M. T.; Hryciw, A.; Brongersma, M.; Sinclair, R.; Prinz, F. B. Atomic Layer Deposition of Lead Sulfide Quantum Dots on Nanowire Surface. Nano Lett. 2011, 11, 934−940.

[2] Handbook of X-Ray Photoelectron Spectroscopy; Wagner, C. D.; Riggs, W. M.; Davis, L. E.; Moulder, J. F.; Muilenberg, G. E., Eds.; Perkin-Elmer Corporation: Eden Prairie, MN, 1978.

[3] Puurunen, R. L.; Vandervorst, W. Island Growth as a Growth Mode in Atomic Layer Deposition: A Phenomenological Model. J. Appl. Phys. 2004, 96, 7686−7695.

[4] King, J. S.; Wittstock, A.; Biener, J.; Kucheyev, S. O.; Wang, Y. M.; Baumann, T. F.; Giri, S. K.; Hamza, A. V.; Baeumer, M.; Bent, S. F. Ultralow Loading Pt Nanocatalysts Prepared by Atomic Layer Deposition on Carbon Aerogels. Nano Lett. 2008, 8, 2405−2409.

[5] Seah, M.P.; Dench, W.A. Quantitative Electron Spectroscopy of Surfaces: A standard Data Base for Electron Inelastic Mean Free Paths in Solids. Surf. Interface Anal. 1, 1979, 2–11.

[6] Libera, J. A.; Hryn, J. N.; Elam, J. W. Indium Oxide Atomic Layer Deposition Facilitated by the Synergy between Oxygen and Water. Chem. Mater. 2011, 23, 2150−2158.

[7] George, S. M. Atomic Layer Deposition: An Overview. Chem. Rev. 2010, 110(1), 111-131.

[8] Aaltonen, T.; Rahtu, A.; Ritala, M.; Leskelä, M. Reaction Mechanism Studies on Atomic Layer Deposition of Ruthenium and Platinum. Electrochem. Solid State Lett. 2003, 6, C130-C133.

[9] Mackus, A. J. M.; Leick, N.; Baker, L.; Kessels, W. M. M. Catalytic Combustion and Dehydrogenation Reactions during Atomic Layer Deposition of Platinum. Chem. Mater. 2012, 24, 1752−1761.

[10] Leick, N.; Agarwal, S.; Mackus, A. J. M.; Kessels, W. M. M. Dehydrogenation Reactions during Atomic Layer Deposition of Ru Using $O_2$. Chem. Mater. 2012, 24(19), 3696.

[11] Erkens, J. M.; Mackus, A. J. M.; Knoops, H. C. M.; Smits, P.; van de Ven, T. H. M.; Roozeboom, F.; Kessels, W. M. M. Mass Spectrometry Study of the Temperature

Dependence of Pt Film Growth by Atomic Layer Deposition. ECS J. Solid State Sci. Technol. 2012, 1, P255−P262.

[12] Kobayashi, N.P.; Donley, C.L.; Wang, S.-Y.; Williams, R.S. Atomic Layer Deposition of Aluminum Oxide on Hydrophobic and Hydrophilic Surfaces. J. Cryst. Growth 2007, 299 (1), 218−222.

# CHAPTER FIVE

## Platinum Atomic Layer Deposition on Metal Substrates

### 5.1 Introduction

In previous chapter, results clearly shows difficulties to naturally deposit platinum films on oxide films by only relying thermal process, which agrees with the nucleation issue spotted on most type of metal ALD process. From the aspect of thin film deposition, the Pt growth in form of nanoclusters on an oxide surface during the nucleation stage of ALD may not be highly desired; on the other hand, such phenomenon resembles the structure of oxide supported Pt catalysts, which has been intensively studied in the field of surface science for the purpose of maximizing the reactivity to increase its utilize efficiency in catalytic converter.

In terms of Pt-based catalyst, by applying concept that, the precursor ligands are similarly eliminated in combustion-like reactions that are catalyzed by the Pt nanoparticles, several works reported an enhancement of the oxygen reduction reaction activity for Pt-alloys in comparison to pure Pt; since the deposition of Pt on Pt is difficult to characterize experimentally, and one of the most promising and studied formulations is Pt-Ni, which has been shown to exhibit a greatly enhanced mass activity for the oxygen reduction reaction [1-9], thereby nickel has been chosen here as the substrate instead.

In terms of nucleation sites on thin films, metals do not possess OH nucleation sites, yet they tend to show much higher reactivity toward the activation of CVD/ALD precursors, facilitating film growth at much lower temperatures than on other solids [10-13].

In the meantime, though electron impact activated atomic layer deposition (ALD) has been demonstrated a clean chemistry on Si-based surfaces via electron impact process, such approach isn't always favored for other type of precursor/substrate combination due to the complexity and uncertainty of the cracking pattern, thereby the examination of the intact of the molecule structure is critical as an important index lead to success self-limiting film growth. In contrast, the reaction mechanism including ligand exchange involved in thermal ALD is more straightforward as in most cases reactant loss does not occur when operating within the ALD-window. Hence in this chapter, the growth of platinum was tested on Ni surface via thermal deposition using the same recipe, MeCpPtMe3 and O2 as reactants.

## 5.2 Experimental

The depositions of platinum on Ni surface were performed in an ultrahigh vacuum (UHV) apparatus described in Section 2.2. The procedures of precursor handling, substrate loading, heating, gas feeding path, and XPS data acquisitions, remained identical to the previous studies, except the replacement of starting surface from Si-based substrates to Ni. The nickel foil used as the substrate was purchased from Sigma-Aldrich (99.995% purity), and was cleaned before each experiment by a combination of chemical treatments,

ion sputtering, and high-temperature annealing until least amount of carbon or oxygen contaminants were detected. A certain amount of carbons were always added to the surface during the transfer of the Ni sample to the reaction chamber. It is presumed these carbons do not affect the chemistry of the Pt ALD precursor reported here.

**5.3 Half cycle depositions of $MeCpPtMe_3$ on Ni surface**

The use of $MeCpPtMe_3$ as primary platinum precursor was demonstrated near-saturated regime within substrate temperature of 523-573 K when the reactions were taking place on top of the Si(100) with native oxide. Here in order to test the self-limiting character on Ni surface, the experiment was first carried out by applying three consecutive doses (6 x $10^5$ L/dose), and XPS data was acquired upon each dose completion. Fig. 20 presents the Pt 4f, C 1s, Ni 2p XPS spectra as a function of dose attempt, with surface temperature maintained at 300˚C. Additionally, a shoulder belongs to Ni 3p on low binding energy side of the Pt 4f (7/2) peak at binding energy of ~67 eV is spotted. Unlike Si-type surfaces, the entire deposition process was conducted thermally without the assistance of electron impact actiavtion, and yet a significant increased amount of Pt 4f, C 1s intensities can be observed after a single dose of Pt precursor, accompanying partially depleted Ni (3p:~67 eV, 2p: ~853, 870 eV) intensities. The following dosing with same amount of exposure does not result in significant change in peak intensities; the plateau in Pt growth and limited attenuation of Ni intensities suggests that the reaction with the $MeCpPtMe_3$ exposure saturates on Ni surface within a single dose (~5 x $10^5$ L) in a similar magnitude compared with the deposition of Pt/Si(100) surface. Such self-

terminated growth is characteristic for an ideal ALD scheme; this case clearly shows that once all the adsorption sites on the surface were occupied, any excess exposures of precursor molecules does not undergo further surface reaction prior to the purging process.

(a) (b)

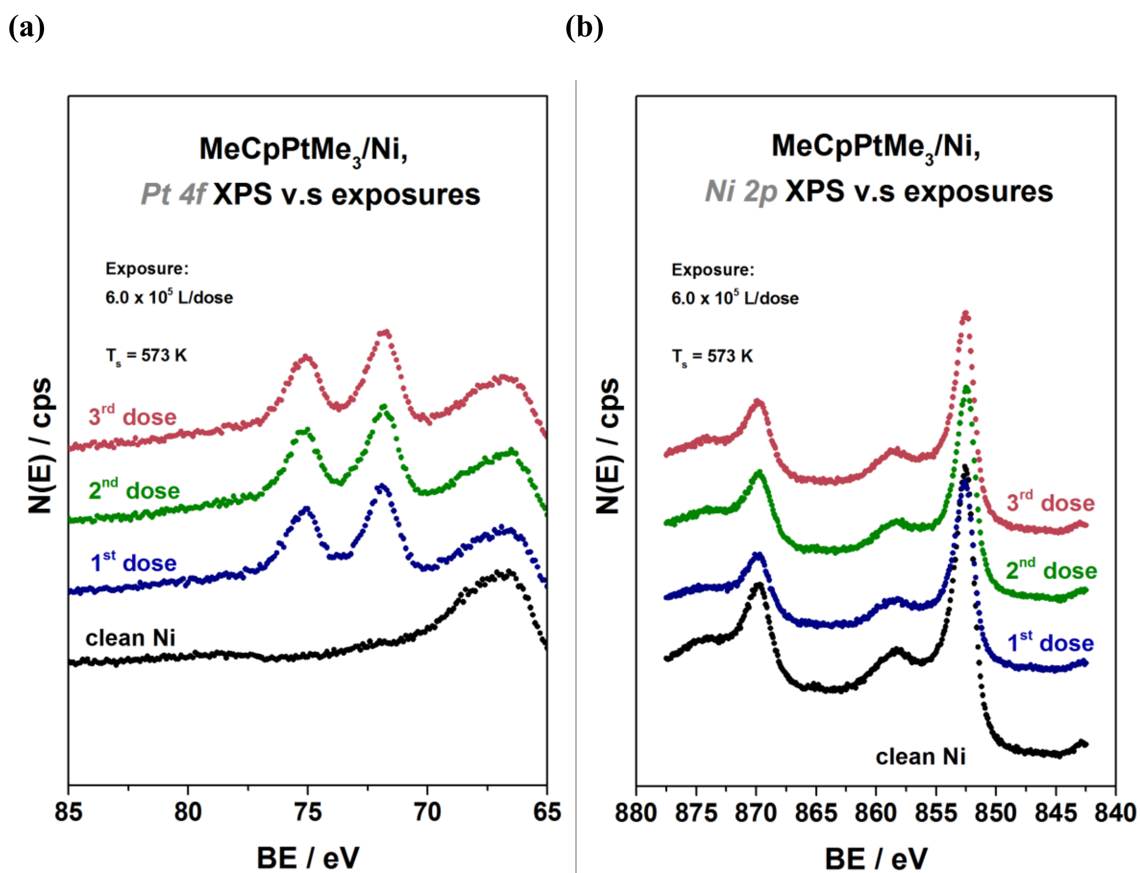


**Figure 20**. (a) Pt 4f, and (b) Ni 2p XPS spectra of single cycle $MeCpPtMe_3$ deposition on a clean Ni sample at 523 K, completed by three separated dosings.

To further investigate the possible adsorption process of a gaseous reactant molecule upon the surface, and the stoichiometry of the deposited layer, curve fitting of the obtained spectras was performed and quantified in terms of peak positions, the results were then further applied to estimate the coverage and atomic ratio. Similar to previous Pt/Si-based surface studies, peak positions in binding energy remained nearly identical between doses, thereby strongly suggests the presence of platinum in +0 oxidation state, also known as pure platinum metal in form of $Pt^0$.

The surface coverage after each dose is calculated by integrating the intensities of the XPS peaks, and converting results into monolayer equivalents (ML equivalent, defined as one adsorbed atom per Ni surface atom) by assuming growth proceeded in layer-by-layer model and using reported values for the electron inelastic mean free path lengths.
Relative sensitivity factors were also applied into the calculation of ratio between each element for adjustment of instrument transmission and escape depth corrections.

Fig. 21 shows the quantified results of platinum and carbon uptake, it clearly reveals for the case of experiment conducted at 573 K, the saturation has taken place after the first dose as further exposure didn’t lead to any significant changes but a slight drop in terms of surface coverage, which could be attributed to minor desorptions as the deposition continues. The estimated thickness suggests roughly a monolayer was forming within the first half cycle by the given amount of exposure, which meets to an ideal ALD profile,

the fulfillment of self-limiting growth and ~ 1 layer/cycle. Similar saturative behavior was observed on carbon deposits by the end of the 3rd dose.

The calculated stoichiometry of the deposited layer was estimated at approximately C:Pt = 7:1, slightly higher than what would be expected if adsorbed Pt atoms retain their methylcyclopentadienyl (MeCp) ring (6:1), which partial amount of it is attributed to the initial carbon residues nearing the sample mounting area. The converted results though, may suggest that at least two of the metal direct bonded methyl groups were removed upon adsorption on the surface.

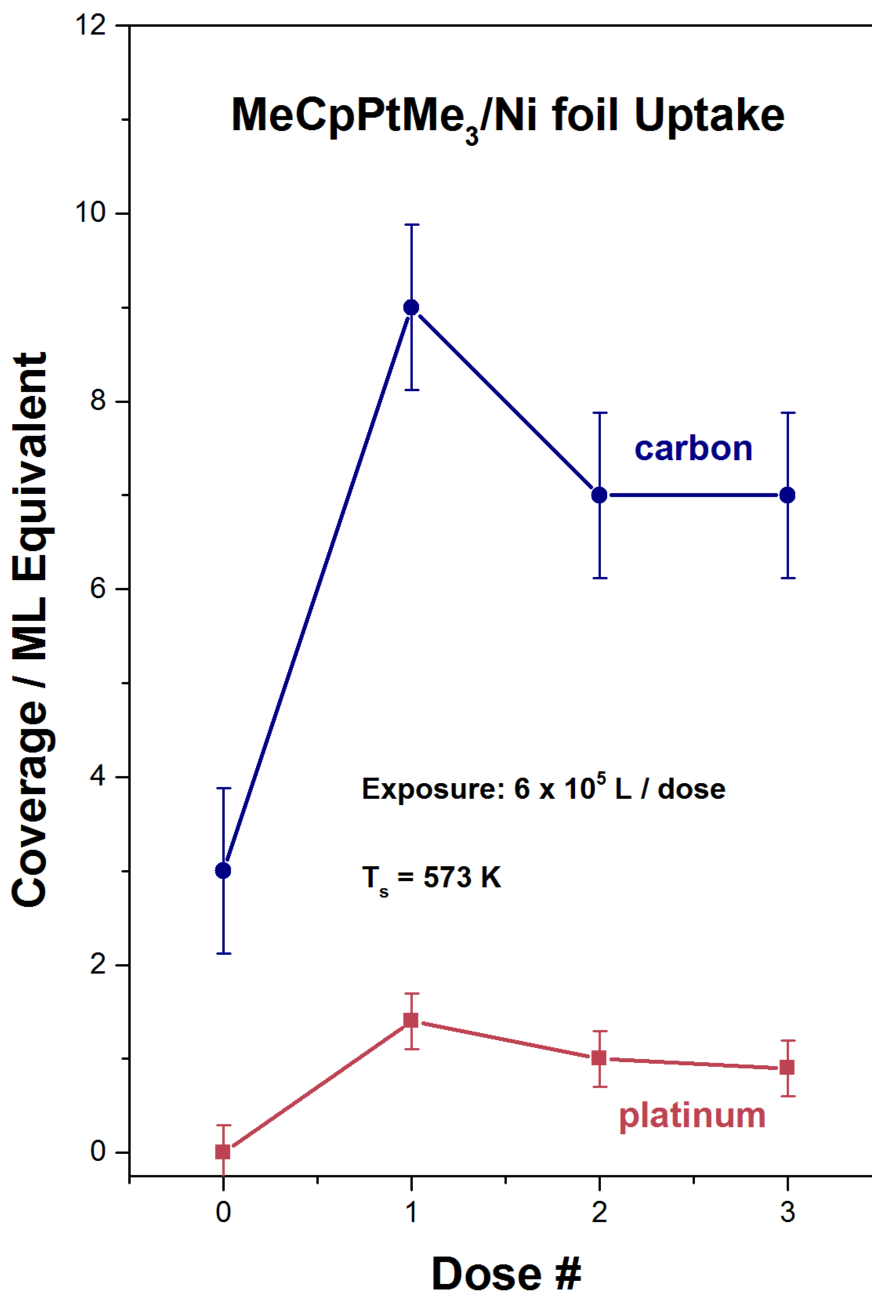


**Figure 21.** Uptake curves for platinum and carbon during the adsorption of $MeCpPtMe_3$ on a Ni substrate at 573 K as a function of dose.

The half cycle experiment was later then carried out by applying 3 x $10^5$ L exposures on different sets of substrate temperature ranging from 525 – 675 K to locate the ALD window. Fig. 22 summarizes the data corresponding to the uptake of MeCpPtMe3 on Ni as a function of substrate temperature. Platinum deposition is evidenced in all cases by the development of the Pt 4f peaks and the attenuated Ni 2p, 3p peaks features, the main difference from Si surface studies is that the growth of platinum within 523 – 623 K is not only self-limiting but also is temperature independent; on temperature equal/higher than 673 K, a significant larger deposit is built up. To avoid the possibilities of thermal decomposition, experiments discussed later were all conducted at 573 K.

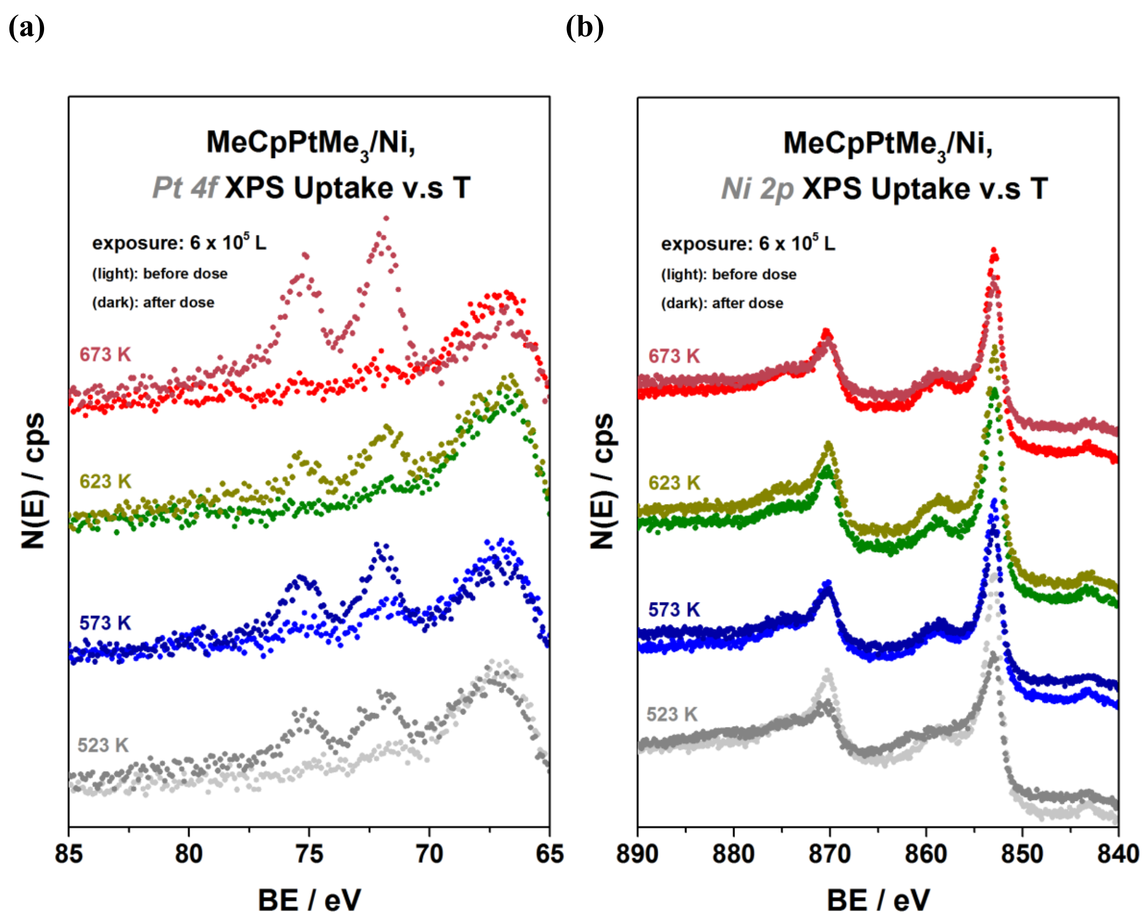


**Figure 22.** (a) Pt 4f, (b) Ni 2p XPS of single half cycle $MeCpPtMe_3$ deposition on Ni surface as a function of substrate temperature.

## 5.4 References

[1] Baldizzone, C.; Mezzavilla, S.; Carvalho, H.W.P.; Meier, J.C.; Schuppert, A.K.; Heggen, M.; Galeano, C.; Grunwaldt, J.-D.; Schuth, F.; Mayrhofer, K.J.J. Confined-Space Alloying of Nanoparticles for the Synthesis of Efficient PtNi Fuel-Cell Catalysts. Angew. Chem. Int. Ed. 2014, 53, 14250–14254.

[2] Du, S.; Lu, Y.; Malladi, S.K.; Xu, Q.; Steinberger-Wilckens, R. A simple approach for PtNi-MWCNT hybrid nanostructures as high performance electrocatalysts for the oxygen reduction reaction. J. Mater. Chem. A 2014, 2, 692–698.

[3] Choi, J.; Lee, Y.; Kim, J.; Lee, H. Enhancing stability of octahedral PtNi nanoparticles for oxygen reduction reaction by halide treatment. J. Power Source 2016, 307, 883–890.

[4] Tuaev, X.; Rudi, S.; Petkov, V.; Hoell, A.; Strasser, P. In situ study of atomic structure transformations of Pt–Ni nanoparticle catalysts during electrochemical potential cycling. ACS Nano 2013, 7, 5666–5674.

[5] Wu, J.B.; Yang, H. Synthesis and electrocatalytic oxygen reduction properties of truncated octahedral Pt3Ni nanoparticles. Nano Res. 2011, 4, 72–82.

[6] Huang, X.Q.; Zhu, E.B.; Chen, Y.; Li, Y.J.; Chiu, C.Y.; Xu, Y.X.; Lin, Z.Y.; Duan, X.F.; Huang, Y. A facile strategy to Pt3Ni nanocrystals with highly porous features as an enhanced oxygen reduction reaction catalyst. Adv. Mater. 2013, 25, 2974–2979.

[7] He, T.; Kreidler, E.; Xiong, L. F. J. Power Sources 2007, 165, 87–91.

[8] He, T.; Kreidler, E.; Xiong, L. F.; Luo, J.; Zhong, C. J. J. Electrochem. Soc. 2006, 153, A1637 A1643.

[9] M. F. Li, Z. P. Zhao, T. Cheng, A. Fortunelli, C. Y. Chen, R. Yu, Q. H. Zhang, L. Gu, B. V. Merinov, Z. Y. Lin, E. B. Zhu, T. Yu, Q. Y. Jia, J. H. Guo, L. Zhang, W. A. Goddard III, Y. Huang and X. F. Duan, Science, 2016, 354, 1414–1419.

[10] Zaera, F. The surface chemistry of thin film atomic layer deposition (ALD) processes for electronic device manufacturing. J. Mater. Chem. 2008, 30, 3521–3526.

[11] Bouman, M.; Qin, X.; Doan, V.; Groven, B.L.D.; and Zaera, F. Organometallics, 2014, 33, 5308–5315.

[12] Bouman, M. and Zaera, F. J. Phys. Chem. C 120 (2016) 8232–8239.

[13] Yao, Y.; Coyle, J. P.; Barry, S.T.; Zaera, F. The many-body expansion combined with neural networks. J. Chem. Phys., 2017, 146, 052806.

# CHAPTER SIX

## Selective ALD on silylated Silicon Surfaces

### 6.1 Introduction

From the aspect of commercial use, thin films are usually required to fabricate in 3-D forms [1-5]. The deposition of atoms at specific locations on a surface can boost advances in catalysis [6-8], energy harvesting [9], and semiconductor device fabrication [10].

Current semiconductor manufacturing primarily relies on many lithography and etching steps to fabricate multilayered 3D devices. However, the disadvantages of conventional methods include complicated processes, short-range of materials suitable for patterning, and expensive reagents [11, 12]. Further, as of today, chip scaling is becoming more challenging at each process node in terms of atomic-scale precision and reliable processing [13].

To prevent those occurrences, manufacturers are working on development of innovative bottom-up techniques that would produce good overlay between the various masks. One in particular attracts attention is selective deposition, in other words, a material is deposited on a predetermined area in a selective manner, has been suggested as a single

step patterning process with the various advantages of conventional ALD processes, such as large area uniformity, excellent conformality, and thickness control [14]. As patterned films can be obtained directly during selective deposition, without any subsequent processes, complicated etching processes are reduced and the use of expensive and poisonous reagents is minimized [5]. Thus, area selective ALD processes have been widely investigated in recent years [15-19].

The one step patterning process requires a predetermined surface which is commonly prepared in ex-situ condition. In this chapter, a versatile and simple approach was demonstrated to generate functionalized surface structures for selective deposition via dry process. Silylation based on addition of hydrophobicity [20, 21], is adapted for surface passivation [22-25]. The main objectives of the experiments in this chapter were to explore the possibility to perform the surface passivation in gas phase, and test with different exposures of silylation agent and temperatures to optimize the doses; the capping effect was then evaluated against the reference group by the surface coverage of the followed up regular ALD process. Quantifications based on in situ XPS analysis were performed to study the mechanistic aspects of the chemoselective inhibitor adsorption and the percentage rejection of precursor absorptions. With sample being prepared entirely in in-situ condition, thereby enables time, cost-effective options with better impurity control. One pronounced benefit of this approach is the avoidance of complicated photolithography and printing processes, additionally, the resulting modified surface provides reactive accessibility toward only specific reactions.

### 6.2 Surface Modification by Silanes

Many substrate surfaces ($SiO_2$ or Si, for example) have little selectivity toward most ALD precursors, hence the need to utilize modifiers such as silanes to achieve surface modification for selective deposition. The selective process in this study is based on depositing a capping layer on top of the targeted surfaces. Hexamethyldisilazane (HMDS) as a type of silanes was utilized as an inhibitor molecule, which provides the ability to tune the reactivity between ALD precursors and the surface by changing its key functional groups.

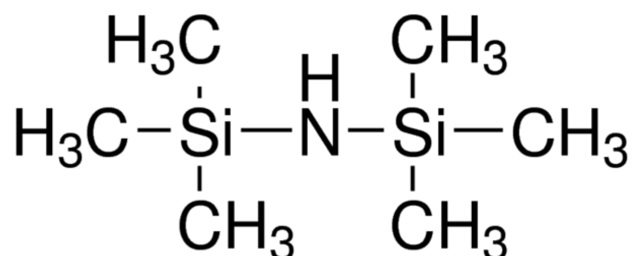


**Figure 23.** Chemical formulas of the inhibitor precursor molecules: Linear Formula: $C_6H_{19}NSi_2$, Synonym: HMDS [26].

For the case of $SiO_2$ surfaces, the HMDS chemically reacts with its Si atom to the oxygen of oxidized surfaces (silanol groups, -Si-OH), OH-groups which form hydrophilic surfaces are cracked, lead to strong Si-O-Si bonding, accompanied by the release of ammonia ($NH_3$) [16]. The methyl groups of the HMDS fragment hereby form a hydrophobic surface.

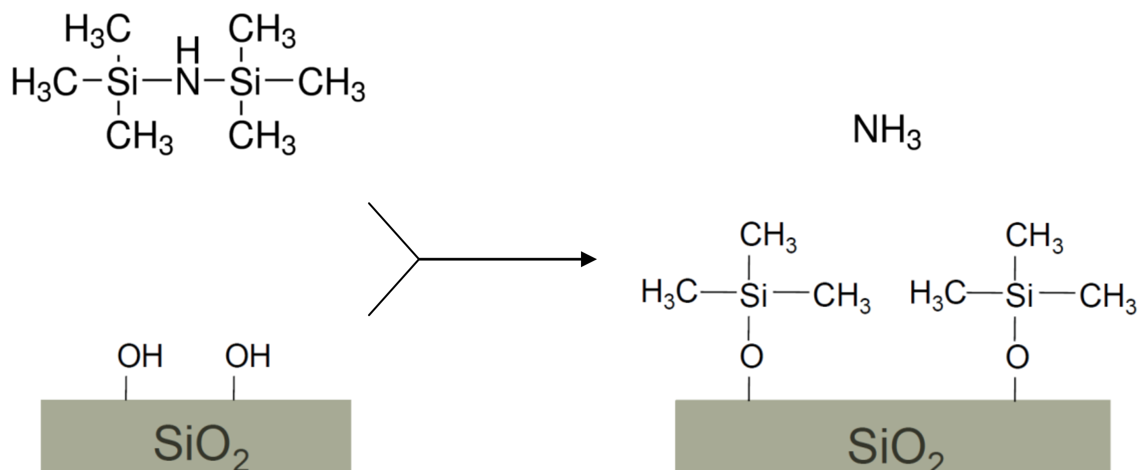


**Figure 24.** Schematic showing the deactivation of surface hydroxyls after treatment of HMDS.

### 6.3 Experimental

The film deposition procedure reported here was studied on ~1 × 1 $cm^2$ square pieces of Si(100) samples cut from commercial Si(100) wafers (Si-Tech), two thickness types of surface were utilized, which covered with native ~1 nm, and 300 nm thick silicon oxide films [27, 28]. The films were precleaned via a modified RCA protocol, which the SC-1 mixture was prepared by heating 5 parts deionized water to 80°C, adding 1 part sodium hydroxide (NaOH - 50%) and 1 part hydrogen peroxide ($H_2O_2$ - 30%) [29, 30]. Treatment of the wafers lasts 30 min at 70-75℃ followed by an overflow rinse in running DI water. Silylation of the surfaces was completed in gas phase inside the UHV chamber described in at T = 293 K, using hexamethyldisilazane (HMDS, Sigma-Aldrich, 99.9% purity) as the source gas, dosing duration varies. To test the capping effect of HMDS, besides the HMDS exposed samples, a comparison set of unmodified pristine Si (100) with 1 nm native oxide surfaces was made as a reference group. The followed up ALD process of

$HfO_2$, was carried out by using a commercial Savannah Ultratech/Cambridge Nanotech instrument, alternating exposing surface to tetrakis(dimethylamido) hafnium(IV) (TDMAHf, $[(CH_3)_2N]_4Hf$, Sigma-Aldrich, 99%) and deionized water with dry $N_2$ purging in between, using the following sequence: TDMAHf/$N_2$/ $H_2O$/$N_2$ = 0.25 s/45 s/0.025 s/35 s. The substrate temperature was kept at 373 K, and the estimated deposition rate was approximately 0.05 nm/cycle. The deposition processes involved in this chapter were preceded without the activation of ionization source; all the films are thermally grown.

**Figure 25.** Chemical formulas of the hafnium precursor molecules: Linear Formula: $[(CH_3)_2N]_4Hf$, Synonym: TDMAHf [31].

## 6.4 Characterization

### 6.4.1 X-Ray Photoelectron Spectroscopy (XPS)

The preliminary deposition of HMDS on Si(100) was analyzed by the X-ray photoelectron spectroscopy coupled to Leybold EA11 multichannel detection system, as details described in Section 2.3.

The deposition of $HfO_2$ was monitored by XPS using a Kratos analytical AXIS instrument equipped with a 165 mm mean radius semi-hemispherical electron energy analyzer and a 120-element delay line detector. A monochromatized Alanode x-ray source was used for the excitation, and an electron flood gun was employed as needed to compensate for sample charging. The Hf 4f, Si 2p, O 1s, C 1s data were acquired using a spectrometer constant pass energy of 20 eV, 0.1 eV energy steps, and a 200 ms dwell time. Film thicknesses were estimated by using an homogeneous layer model and exponential signal decay versus film thickness, using reported electron inelastic mean free paths.

### 6.4.2 Water Droplet Tests

The hydrophobicity/hydrophilicity of the surfaces was evaluated by imaging the deposited water droplets using Fujifilm X-E2 digital camera in manual focusing mode, and the contact angles were measured via ImageJ software. An overall measurement error of ±3° was estimated by averaging 6–12 measurements with different samples.

### 6.5 Half cycle ALD HMDS on $SiO_2$/Si

### 6.5.1 Introduction

The entire process consists of Hexamethyldisilazane (HMDS) as the inhibitor, Tetrakis(dimethylamino)hafnium, 98+% as the Hf precursor, and $H_2O$ as the co-reactant. To ensure a uniformly OH-groups distributed on starting surface, the samples were pretreated with SC-1 solution, such solution dissolves the thin native oxide layer on silicon at a very low rate and forms a new oxide on the silicon surface by oxidation at approximately the same rate, and thereby leaves the silicon surface with a thin hydrophilic oxide layer. The follow up HMDS process will tie up the molecular water of the hydrated wafer surface and increase liquid contact angle as the wafer surface turns more hydrophobic. The capping ability of the inhibitor highly relies on the integrity of the Si-$CH_3$ bonding, to ensure such functional groups remained intact and effective for the later selective deposition process, the temperature of the precursor (HMDS) is kept at 30ºC, and substrate is unheated during the dosing process. Instead of fabricating a pattered film to investigate the capping effect, another set of control sample was separately prepared by introducing regular ALD process without implementation of HMDS dosing for comparisons.

### 6.5.2 Results and Discussions

As shown from the C 1s XPS spectra in Fig. 26, a certain amount of carbonaceous materials is visible from the starting surface due to the lack of high temperature annealing procedures, on the other hand, which also rules out the possibilities the thermal energy

could partially remove the hydroxyl groups built up from RCA cleaning, or the capping features on silylated surface. It is clear to be seen that the carbon intensity is gradually increased by dose time, which highly suggests that the adsorption of methyl groups detached from HMDS compound on the oxide surface, this is also evident from the attenuated Si and O signals.

(a) (b)

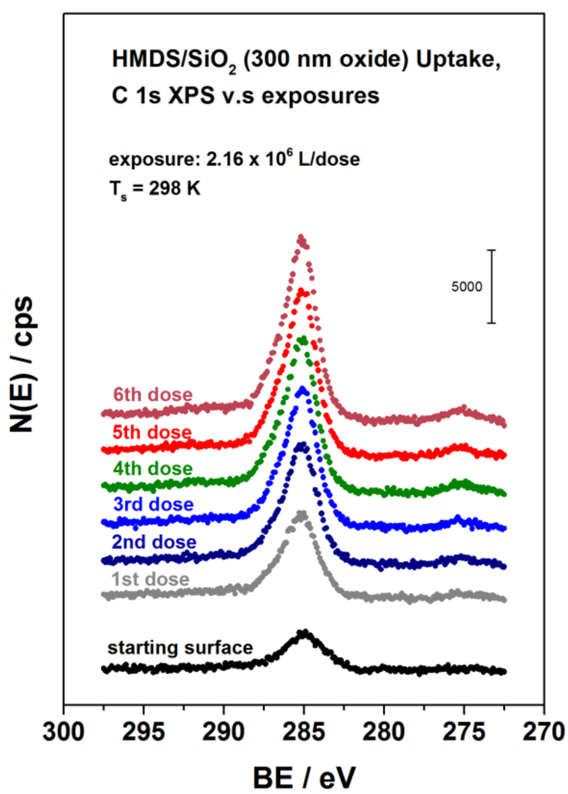


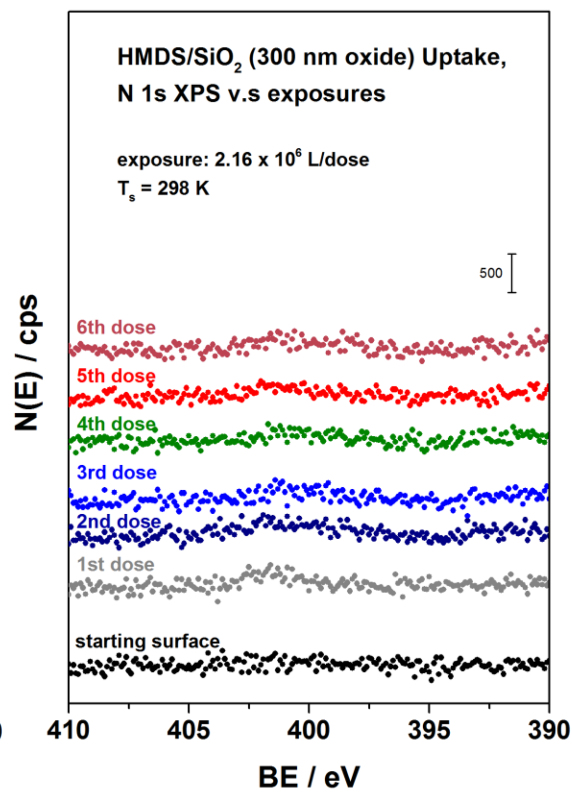

**(c)** **(d)**

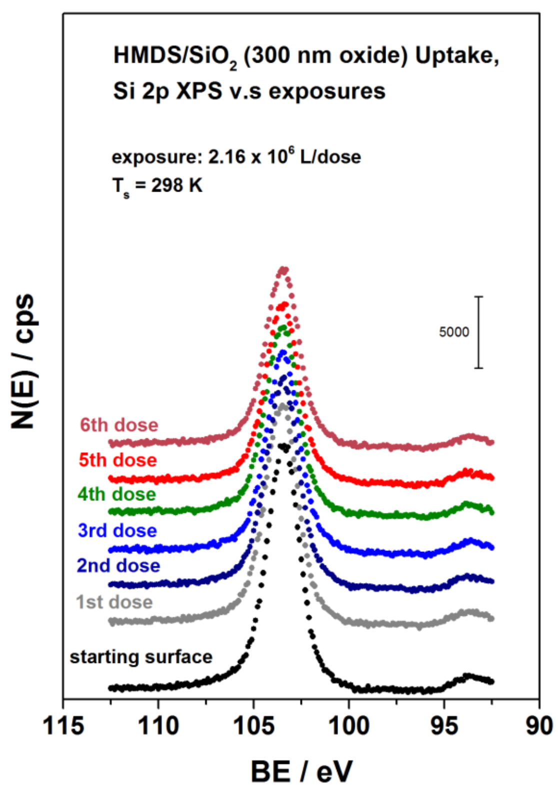


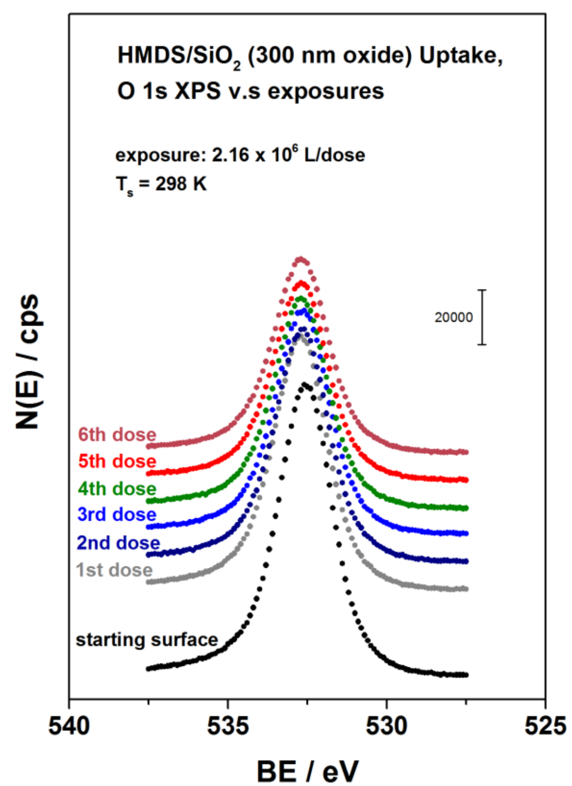


**Figure 26**. C 1s, N 1s, Si 2p, and O 1s XPS of 72-hr dose of HMDS/300 nm $SiO_2$, $T_s$ set at 25ºC, ion gauge was deactivated.

One qualitative method to verify the silylation process is measuring contact angles via water droplet test. The shape of a liquid droplet can be alternately explained by the surface tension of the liquid. In a pure liquid, each molecule in the bulk is pulled equally in every direction by neighboring liquid molecules, resulting in a net force of zero. The molecules exposed at the surface though, do not have neighboring molecules in all directions to provide a balanced net force. Instead, they are pulled inward by the neighboring molecules, creating an internal pressure. As a result, the liquid tends to contract its surface area to maintain the lowest surface free energy. The droplet in ideal condition should be maintained as spherical, which gives the minimum surface area for a fixed volume. This intermolecular force to contract the surface is called the surface tension, which is responsible for the shape of liquid droplets. In practice, there are various external factors that may deform the shape of the droplet such as gravity, properties of the surface, etc. Hence the contact angle in real world is determined by a combination of surface tension and external forces. [32]

It is though, commonly accepted that, a contact angle less than 90° indicates that wetting of the surface is favorable, and the fluid will spread over a large area on the surface; while contact angles greater than 90° generally means that wetting of the surface is unfavorable so the fluid will minimize its contact with the surface and form a compact liquid droplet. Macrographs shown in Fig. 27 displays the water droplet tests on different types of surfaces including the unmodified pristine 300 nm $SiO_2$, 300 nm $SiO_2$ precleaned

with SC-1 solution, and 300 nm $SiO_2$ precleaned with SC-1 solution followed by silylation.

It is clearly to observe an intermediate hydrophobicity exhibit on pristine 300 nm $SiO_2$ samples with contact angle approximately measured to be 46.2°. Cleaning the surface following a modified SC-1 solution significantly improves the wettability, yielding a reduced contact angle of 22.6°. A dramatic increase of contact angle is visible after silylation, strongly suggests successful addition of $Si\text{-}CH_3$, blocks the -OH groups on their surface. The absorption of inhibitors on both types of starting surface, not only restored but also further enhanced their hydrophobicity. Results shown here further solidify the observations from XPS analysis. Small differences in contact angle measurements are seen among different attempts of silylation process, the general trends though, are similar in all cases.

(a)

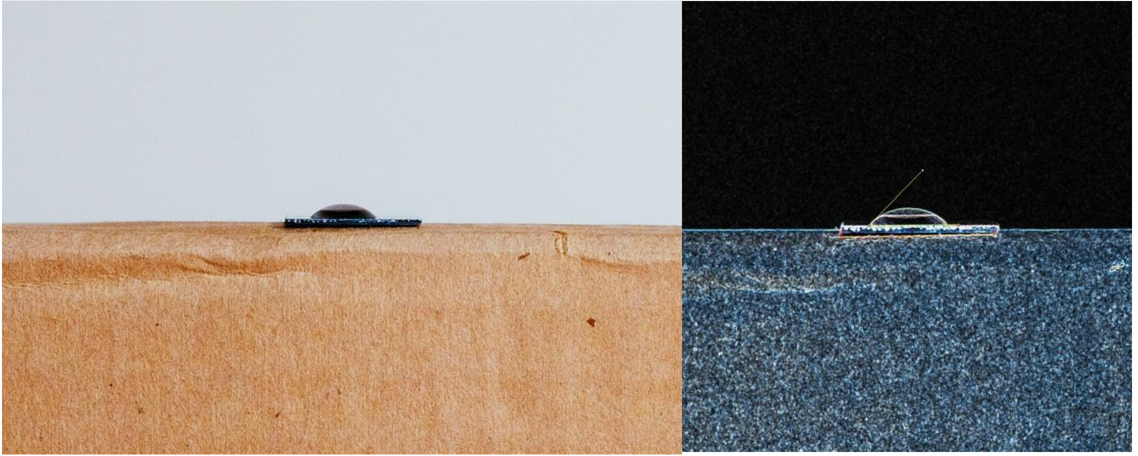

(b)

(c)

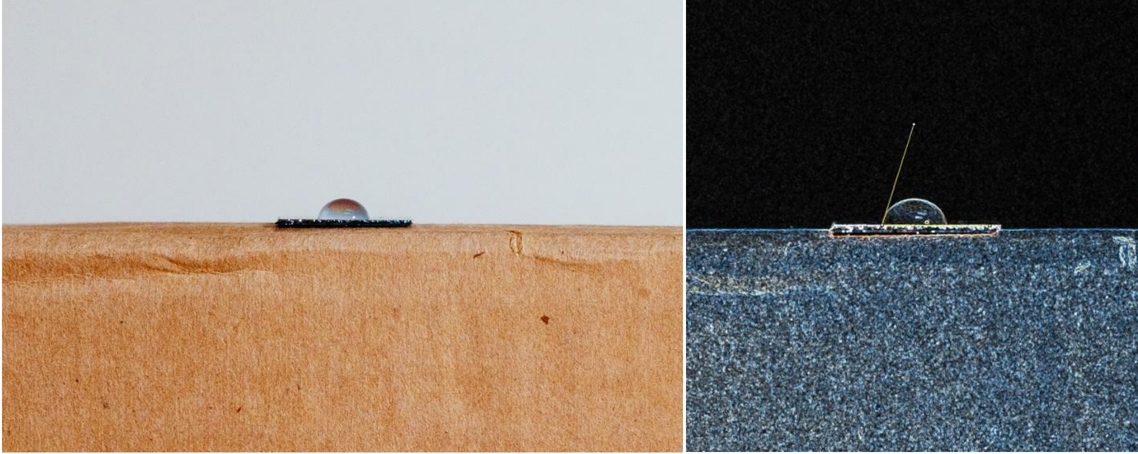

**Figure 27.** Macrographs of the selected samples: (a) 300 nm $SiO_2$/Si(100), (b) SC1 pretreated - 300 nm $SiO_2$/Si(100), (c) SC1 pretreated - 300 nm $SiO_2$/Si(100), followed by 96 hrs of HMDS dosing @ 25°C, showing various degree of hydrophobicity/ hydrophilicity with contact angles measured 46.2°, 22.6°, and 77.3°, respectively.

**Table 3**. Data from water contact angle measurements on the 300 nm $SiO_2$/Si(100) surface after different cleaning and silylation steps.

| Sample | Contact angle/° (±3°) |
|---|---|
| 300 nm $SiO_2$/Si(100), As Is | 46 |
| 300 nm $SiO_2$/Si(100), SC 1 | 23 |
| 300 nm $SiO_2$/Si(100), SC 1, HMDS | 77 |

### 6.6 Multicylces of Hf on HMDS/$SiO_2$/Si

To test the capping effect of HMDS, two groups of Si(100) with native oxide samples were utilized as starting surfaces; one of them was RCA cleaned, followed by an exposure of $3 \times 10^7$ L HMDS dose at room temperature, while the other group was

unmodified, unsilylated pristine Si(100) surfaces used as reference. A total of eight samples in group of 4 were prepared and processed with 1, 5, 10, 20 cycles of ALD $HfO_2$.

Fig. 28 presents the preliminary XPS data acquired as a function of ALD cycles at 110°C for both groups of Si(100) surfaces. Regardless the type of starting surface, the deposition of TDMAHf starts to take off at $5^{th}$ cycle, the signal intensities grow with increasing number of ALD cycles afterwards, indicating Hf depositions; $HfO_2$ were observed in form of doublets as expected due to Hf 4f spin splitting, peaks position at 17.8 eV and 19.5 eV corresponded to $4f_{(7/2)}$ and $4f_{(5/2)}$ photoelectrons, respectively; By contrast, lower Hf depositions can be observed on silylated samples in all cases. By $10^{th}$ cycle significant leveling off of Si 2p and O 1s intensities are shown, suggesting achievement of higher step coverage.

Si 2p peak has closely spaced spin-orbit components ($\Delta$=0.63eV), and thereby it is commonly observed as either two distinct, symmetric components or as single, asymmetric peak. Due to higher resolution of XPS analyzer, the $2p_{(1/2)}$ and $2p_{(3/2)}$ are split as two separated peaks and the position of later one (99.4 eV) was set as the reference for peak calibrations. As deposition continues with repeated precursor and $H_2O$ pulsing, additional C feature which peak centered at ~ 288.5 eV was shown suggesting the formation of carbonyl compounds (O-C=O bonding). When a $HfO_2$ layer was directly deposited on the Si substrate, peaks due to Hf silicide were commonly observed at 13.6 and 15.2 eV [F34-F36]; fortunately, this is not the case here, these results clearly

show that the thin SiO2 layers effectively prevent the Hf silicide formation. The formation of metal oxide is evident from shifting of O 1s towards lower B.E., too.

(a)

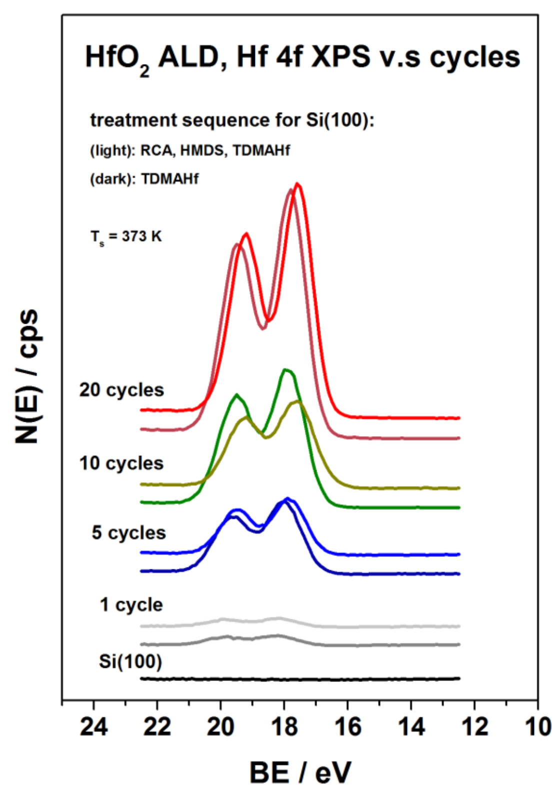


(b)

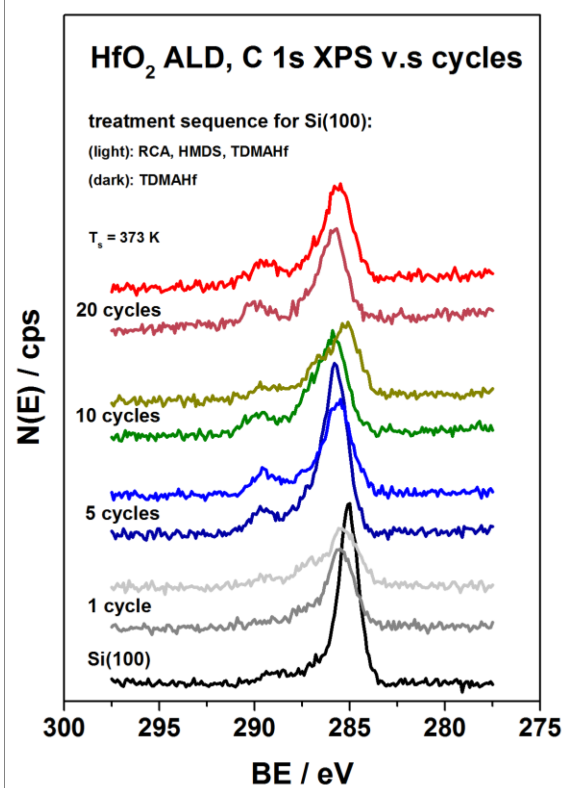

(c)

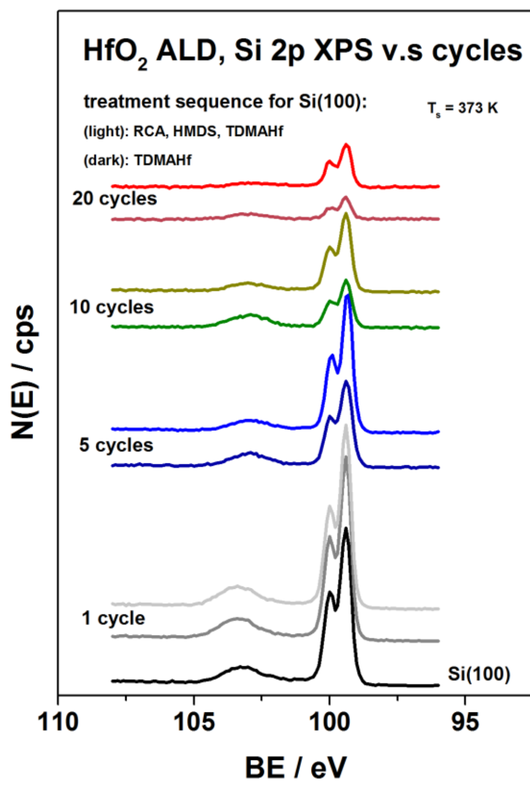


(d)

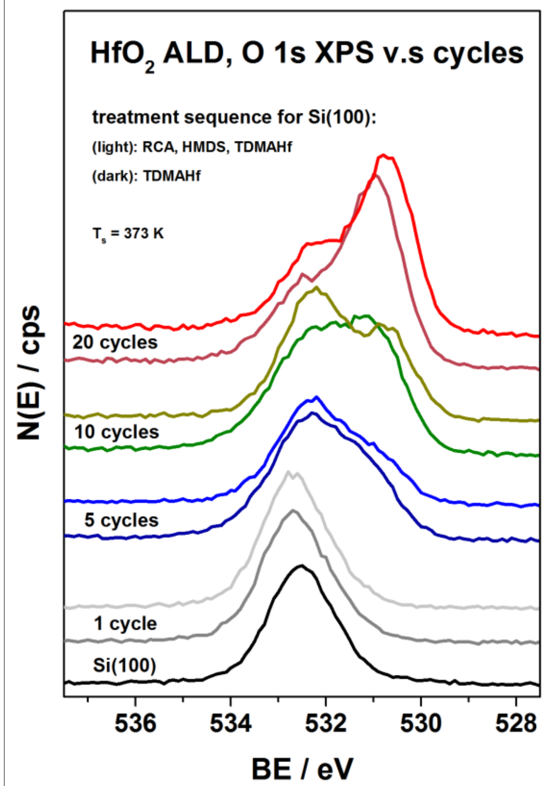


**Figure 28.** Hf 4f, C 1s, Si 2p and O 1s XPS of $HfO_2$/ $SiO_2$, dosing process completed at $T_s$ of 100ºC.

The ALD growth rates on both types of Si(100) surfaces, were quantified by processing the signal intensities from the Hf 4f and Si 2p XPS spectra. The $HfO_2$ film thickness was estimated by assuming layer-by- layer growth and using reported values for the electron inelastic mean free path lengths based on attenuation of the Si intensities (versus the intensities after HMDS dose); [33, 37] and relative sensitivities of the energy analyzer to the different elements. Fig. 29 shows the resulting $HfO_2$ uptake curves for the prepared samples including groups of unmodified and silylated Si(100). Less ideally, the surfaces exposed to HMDS were not entirely passivated and show HfO2 deposition on all silylated samples at 110 °C. Though, it is still clearly seen that the unmodified surfaces display significantly faster rates of $HfO_2$ deposition than those exposed to HMDS.

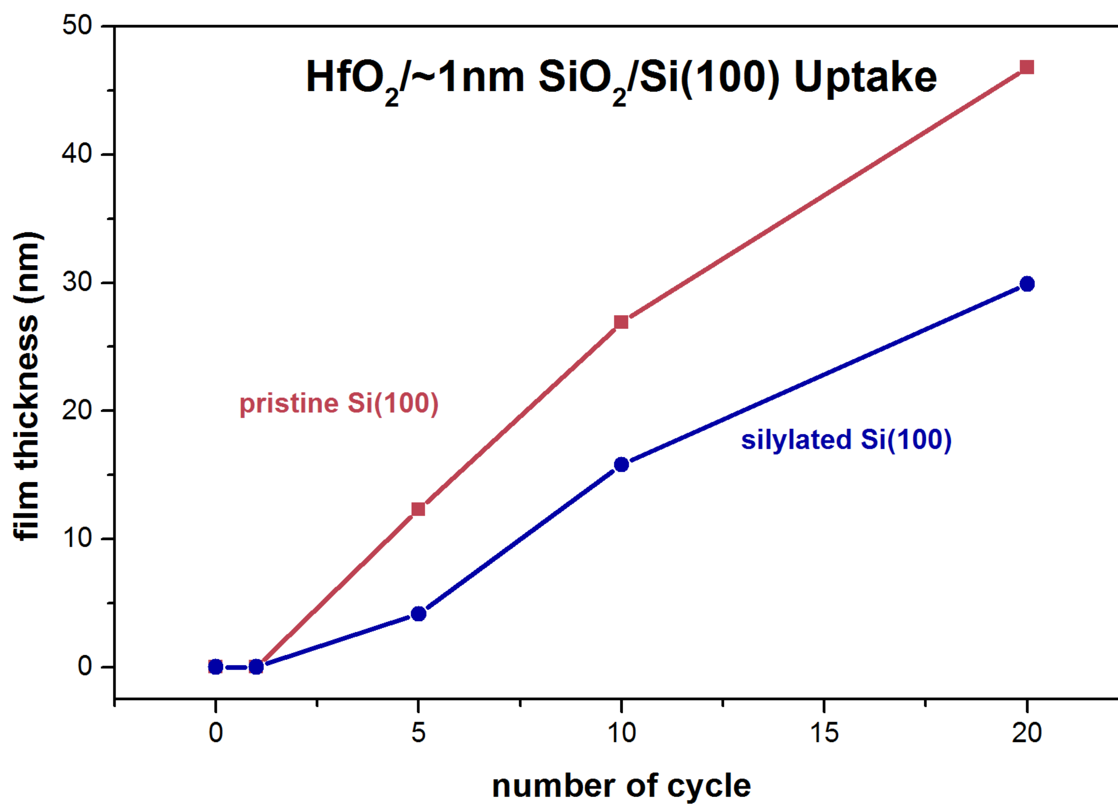


**Figure 29**. Estimated thickness of $HfO_2$ film calculated via attenuations of Si signals versus the number of deposition cycle.

The surface adsorptions were not completely blocked, though, which may attribute to 1) incomplete release of nitrogen atom from the HMDS molecule. The inhibited $HfO_2$ growth suggests the surface groups on starting substrate has deactivated, the relative degree of passivation still remained unclear due to the difficulties in quantifications; 2) improper ligand exchange of methyl groups from HMDS molecule with hydrogen on the surface, which could potentially lead to lower HMDS step coverage, in other words, only partial adsorption sites were blocked; 3) The HMDS molecules dissociate into covalently bonded methyl groups upon adsorption, and repeated heating processes may cause the decomposition of the methyl groups. Since the silylation was not implemented into the followed up cyclewised-doses as the first reactant except the very beginning, thereby the preexist capping sites were gradually desorbed, leading to loss of passivation.

## 6.7 Conclusions

A simple silylation approach has been developed and tested in gas phase to modify the chemistry of silicon surfaces. Emphasis has been placed on the surface reactivity toward the metalorganic precursors that are used in the atomic layer deposition of thin solid films. The study underwent by first increasing the nucleation sites for enhanced adsorptions of silylation agent, which is later used for blocking the initial adsorption sites and thereby inhibit the subsequent film growth; the promotion in adsorption sites was achieved by modifying the surface hydrophilic using reported SC-1 solution belonging to RCA cleaning steps. Such cleaning protocol is a treatment that presumably increases the surface concentration of hydroxyl moieties. Starting from such type of substrate, the

hydroxyl groups on those surfaces are capable of covalently reacting with a number of precursor molecules, facilitating their dissociative adsorption and initiating chemically based film deposition processes. A change in number of OH groups can be observed by the pose of hydrophilicity/hydrophobicity from the surface. Such property was here evaluated by measuring the contact angle between the surface and a droplet of water deposited on top. The water droplet test shows a significantly decreased of contact suggesting a promotion in number of OH groups on the starting surface. Conversely, the passivation of surface was achieved by increasing the surface hydrophobicity using any of many viable silanes, including HMDS. Due to the blocking of the OH groups by alkyl fragments, the contact angle increases after silylation.

The capping effect of the silylated species on the surface was tested by evaluating the rate of growth of $HfO_2$ films via atomic layer deposition using TDMAHf and water as precursors. It was found that the silylated layer does partially but not completely block the film growth at all cases except no difference was observed from the 1$^{st}$ cycle. This is in part because of the partial decomposition of the alkyl groups after repeated heat treatment during multilayer depositions, leading to loss of silylation layer and regained back their original hydrophobicity. Overall, the sequence of gas phase silylation treatments described in this chapter not only shows partial passivation on surface but also provides an insight of its viability served as blocking agent for the selective deposition of solid films.

## 6.8 References

[1] Long, J. W.; Dunn, B.; Rolison, D. R.; White, H. S. Three-Dimensional Battery Architectures. Chem. Rev. 2004, 104 (10), 4463− 4492.

[2] Cumpston, B. H.; Ananthavel, S. P.; Barlow, S.; Dyer, D. L.; Ehrlich, J. E.; Erskine, L. L.; Heikal, A. A.; Kuebler, S. M.; Lee, I.-Y. S.; McCord-Maughon, D.; Qin, J.; Röckel, H.; Rumi, M.; Wu, X.-L.; Marder, S. R.; Perry, J. W. Two-Photon Polymerization Initiators for Three-Dimensional Optical Data Storage and Microfabrication. Nature 1999, 398 (6722), 51−54.

[3] Holtz, J. H.; Asher, S. A. Polymerized Colloidal Crystal Hydrogel Films as Intelligent Chemical Sensing Materials. Nature 1997, 389 (6653), 829−832.

[4] Braun, P. V.; Rinne, S. A.; García-Santamaría, F. Introducing Defects in 3D Photonic Crystals: State of the Art. Adv. Mater. 2006, 18 (20), 2665−2678.

[5] Jiang, X.; Bent, S. F. Area-Selective ALD with Soft Lithographic Methods: Using Self-Assembled Monolayers to Direct Film Deposition. J. Phys. Chem. C 2009, 113 (41), 17613−17625.

[6] Cheng, N.; Banis, M. N.; Liu, J.; Riese, A.; Li, X.; Li, R.; Ye, S.; Knights, S.; Sun, X. Extremely Stable Platinum Nanoparticles Encapsulated in a Zirconia Nanocage by Area-Selective Atomic Layer Deposition for the Oxygen Reduction Reaction. Adv. Mater. 2015, 27, 277−281.

[7] Xie, J.; Yang, X.; Han, B.; Shao-Horn, Y.; Wang, D. Site-Selective Deposition of Twinned Pt Nanoparticles on $TiSi_2$ Nanonets by Atomic Layer Deposition and Their Oxygen Reduction Activities. ACS Nano 2013, 7, 6337−6345.

[8] Lee, H. B. R.; Baeck, S. H.; Jaramillo, T. F.; Bent, S. F. Growth of Pt Nanowires by Atomic Layer Deposition on Highly Ordered Pyrolytic Graphite. Nano Lett. 2013, 13, 457−463.

[9] Li, R.; Zhang, F.; Wang, D.; Yang, J.; Li, M.; Zhu, J.; Zhou, X.; Han, H.; Li, C. Spatial Separation of Photogenerated Electrons and Holes among {010} and {110} Crystal Facets of BiVO4. Nat. Commun. 2013, 4, 1432.

[10] Elko-Hansen, T. D.-M.; Dolocan, A.; Ekerdt, J. G. Atomic Interdiffusion and Diffusive Stabilization of Cobalt by Copper During Atomic Layer Deposition from Bis(N-Tert-Butyl-N'-Ethylpropionamidinato) Cobalt(II). J. Phys. Chem. Lett. 2014, 5, 1091−1095.

[11] Xia, Y.; Whitesides, G. M. Soft Lithography. Angew. Chem., Int. Ed. 1998, 37 (5), 550−575.

[12] Chen, R.; Kim, H.; McIntyre, P. C.; Bent, S. F. Self-Assembled Monolayer Resist for Atomic Layer Deposition of $HfO_2$ and $ZrO_2$ High-κ Gate Dielectrics. Appl. Phys. Lett. 2004, 84 (20), 4017−4019.

[13] Pan, D. Z.; Liebmann, L.; Yu, B.; Xu, X.; Lin, Y. Pushing Multiple Patterning in Sub-10nm. Proc. 52nd Annu. Des. Autom. Conf. - DAC ’15. 2015, 1−6.

[14] Kim, H.; Lee, H.-B.-R. B. R.; Maeng, W.-J. J. Applications of Atomic Layer Deposition to Nanofabrication and Emerging Nanodevices. Thin Solid Films 2009, 517 (8), 2563−2580.

[15] Fang, M.; Ho, J. C. Area-Selective Atomic Layer Deposition: Conformal Coating, Subnanometer Thickness Control, and Smart Positioning. ACS Nano 2015, 9 (9), 8651−8654.

[16] Guo, L.; Qin, X.; and Zaera, F. Chemical Treatment of Low-k Dielectric Surfaces for Patterning of Thin Solid Films in Microelectronic Applications. ACS Appl. Mater. Interfaces, 2016, 8 (9), pp 6293–6300. DOI: 10.1021/acsami.6b00495.

[17] Guo, L.; Lee, I.; and Zaera, F. Patterning of Solid Films via Selective Atomic Layer Deposition Based on Silylation and UV/Ozonolysis. ACS Appl. Mater. Interfaces, 2016, 8 (30), pp 19836–19841. DOI: 10.1021/acsami.6b07192.

[18] Guo, L.; and Zaera, F. Spatial resolution in thin film deposition on silicon surfaces by combining silylation and UV/ozonolysis. Nanotechnology, Volume 25(50), Nov. 2014.

[19] Slavov, S.V. ; Sanger, A.R.; and Chuang, K.T. Mechanism of Silation of Silica with Hexamethyldisilazane. J. Phys. Chem. B, 2000, 104 (5), pp 983–989. DOI: 10.1021/jp991715v.

[20] Flinn, D.H.; Guzonas, D.A.; and Yoon, R.H. Characterization of Silica Surfaces Hydrophobized by Octadecyltrichlorosilane. Colloids and Surfaces a-Physicochemical and Engineering Aspects, 1994. 87(3): p. 163-176.

[21] Schmohl, A.; Khan, A.; and Hess, P. Functionalization of oxidized silicon surfaces with methyl groups and their characterization. Superlattices and Microstructures, 2004. 36(1-3): p. 113-121.

[22] Sinha, A., ; Hess, D.W. ; and Henderson, C.L. Area-selective ALD of titanium dioxide using lithographically defined poly (methyl methacrylate) films. Journal of the Electrochemical Society, 2006. 153(5): p. G465-G469.

[23] Liu, J.R., et al., Generation of Oxide Nanopatterns by Combining Self –Assembly of Slayer Proteins and Area-Selective Atomic Layer Deposition. Journal of the American Chemical Society, 2008. 130(50): p. 16908-16913.

[24] Jiang, X.R. and Bent, S.F. Area-Selective ALD with Soft Lithographic Methods: Using Self-Assembled Monolayers to Direct Film Deposition. Journal of Physical Chemistry C, 2009. 113(41): p. 17613-17625.

[25] Deyhimi, F. and Coles, J.A. Rapid Silylation of a Glass-Surface - Choice of Reagent and Effect of Experimental Parameters on Hydrophobicity. Helvetica Chimica Acta, 1982. 65(6): p. 1752-1759.

[26] https://www.sigmaaldrich.com/catalog/product/sigma/h4875?lang=en®ion=US. Retrieved July, 2018.

[27] Chabal, Y. J.; Weldon, M. K.; Queeney, K. T.; Estève, A. Vibrational Studies of Ultra-Thin Oxides and Initial Silicon Oxidation. In Fundamental Aspects of Silicon Oxidation; Chabal, Y. J., Ed.; Springer-Verlag: Berlin, 2001; pp 143−159.

[28] Yao, Y.; Zaera, F. Thermal Chemistry of Copper Acetamidinate Atomic Layer Deposition Precursors on Silicon Oxide Surfaces Studied by XPS. J. Vac. Sci. Technol., A 2016, 34 (1), 01A101.

[29] Guo, L.; and Zaera, F. Spatial Resolution in Thin Film Deposition on Silicon Surfaces by Combining Silylation and UV/ozonolysis. Nanotechnology, 25(50), Nov.2014.

[30] Kern, W. The Evolution of Silicon Wafer Cleaning Technology. J. Electrochem. Soc. 1990, 137 (6), 1887−1892.

[31] Merck KGaA, Inc.
https://www.sigmaaldrich.com/catalog/product/aldrich/455199?lang=en®ion=US. Retrieved July, 2018.

[32] Snoeijer, J. H.; Andreotti, B. Phys. Fluids, 2008, 20, 057101.

[33] Seah, M.P. and Dench, W.A. Smoothing and the Signal-to-Noise Ratio of Peaks in Electron-Spectroscopy. J. of Electron Spectroscopy and Related Phenomena, 1989. 48(1-2): p. 43-54.

[34] Nagasato, Y. and Ueno, T., Jpn. J. Appl. Phys., Part 1, 2005, 44, 1665.

[35] Wang, L.; Xue, K.; Xu, J. B.; Huang, A. P.; and Chu, P. K. Appl. Phys. Lett., 2006, 88, 072903.

[36] Cho, D.-Y.; Park, K.-S.; Choi, B.-H.; Oh, S.-J.; Chang, Y. J.; Kim, D. H.; Noh, T. W.; Jung, R.; Lee, J.-C.; and Bu, S. D. Appl. Phys. Lett., 2005, 86, 041913.

[37] Seah, M.P., et al., Towards a Single Recommended Optimal Convolutional Smoothing Algorithm for Electron and Other Spectroscopies. Journal of Physics E-Scientific Instruments, 1988. 21(4): p. 351-363.

# CHAPTER SEVEN

## General Conclusions and Future Works

### 7.1 General Conclusions

The work in this dissertation is part of a continuous effort in our group to understand the surface reactions taking place at the initial stage of film formation involved in chemical vapor deposition (CVD) and atomic layer deposition (ALD) from the point view of surface science. A lot of work has been done in our lab related to issues occurred during these chemical type depositions to provide insights into the reaction mechanisms at a molecular level [1-7]. ALD is a promising technique for producing uniform precious metal nanoparticles on high surface area surface because of its unique feature of sequential, self-limiting surface reactions. The goal of this project is to investigate the surface reactions taking place at the initial stage of film formation. This work is anticipated to form the basis for the exploration of the growth mechanisms for the atomic layer deposited platinum taking places on the targeted surfaces. Platinum films were deposited by alternating doses of (methylcyclopentadienyl)trimethylplatinum ($MeCpPtMe_3$) and oxygen ($O_2$) as co-reactants.

Pt thin films were grown on $SiO_2$ with assistance of electron impact activation and have shown a significant enhancement in uptake of film depositions, while the reference set

conducted at pure thermally driven process was suffered from steric hindrance. The intact of the cyclopentadinyl ligand was examined by the C:Pt ratios from quantified XPS results, where a value of ~7:1 suggests that the presence of protecting ligand remained bounded on the main complex. A more detailed investigation on fragmentation pattern of $MeCpPtMe_3$ was reproduced by quadrupole mass spectrometry, and has established that the precursor were partially decomposed and activated in a selective manner. The viable of this approach not only demonstrates that the formation of highly reactive species from the original organometallic complexes facilitates the ALD process, but also reveals possibility to conduct the entire deposition process at lower temperature.

An ALD process window was explored and optimized by firstly defining saturation conditions of $MeCpPtMe_3$ exposure required. The ALD process dependence on substrate temperature was investigated, where the Si(100) with native oxide revealed a temperature window from 250 °C to 300 °C and the 300 nm $SiO_2$ showed an unsaturated CVD-type growth. The growth rate of the thick oxide conducted in identical dosing conditions shows a significant dominant result in amount of Pt deposits in initial growing stage. In addition, the film thickness of 300 nm $SiO_2$ was exhibiting a linear dependence on the length of exposures, along with posing a constant growth rate of 0.09 nm per dose (1.8 x $10^5$ L); on the other hand, the insignificant leveling off of the Si signals observed on native oxide reveals a lower surface coverage compared with the former case. The $MeCpPtMe_3$ was adsorbed on both types of surface in form of metallic platinum. Multilayers of platinum were demonstrated by applying $O_2$ treatment to remove carbon

byproduct and to facilitate for preparation of new surface. The quantified results also suggest that the ALD of platinum first forms localized deposits possibly composed by a number of nanoclusters that grow slowly during the first few cycles. These islands later may merge to a complete film after larger exposures. An enhancement in nucleation behavior, in particular, at lower deposition temperature was presented by generating hydroxyl groups through precleaning the Si starting surface using piranha solution.

To implement the atomic layer deposition into the selective deposition which is commonly adapted in 3-D structure integrated in microelectronics, the viability of conducting silylation step in gas phase was studied by dosing vaporized HMDS molecules onto target substrate, the surface coverage corresponded to the percentage of deactivated adsorption sites was evaluated via quantified inhibited growth compared with the referenced unmodified starting surface. From the interpretation of C and Si XPS spectra, the HMDS was found more effectively chemisorbed on 300 nm $SiO_2$ than the native oxide on Si(100). Prior to the followed up HfO2 depositions, the contact angle measured via water droplet angle test was measured increased from 23$^{\circ}$ up to 77$^{\circ}$, in which the surface was posing relatively hydrophobic compared with the SC-1 precleaned starting surface, suggesting that the methyl groups from HMDS molecules were detached and were capped the nucleation sites. The site-capping effect is also evident from the XPS results of deposition of HfO2 on both silylated and reference samples, as all the silylated samples lead to reduced deposits compared with unmodified surfaces except the

case of 1st cycle; among all the samples, the set of silylated surface processed with 10 cycles of ALD Hf posed the most significant effect in rejecting the TDMAH adsorption. Such growth differences in ALD deposition seen between both groups of the silicon substrate suggests that the HMDS-based layer deposited via gas phase partially blocks the surface functional groups, leading to reduced $HfO_2$ growth on final films.

## 7.2 Future Works

### 7.2.1 Studies on addition of surface adsorption sites

ALD on oxide substrates generally starts with a nucleation period which the growth rate does not meet to the ideal monolayer per cycle scheme, one of the commonly accepted explanations is the absence of the proper surface species on starting surface to react with the precursors leading to a dispersion of metal nanoclusters that will form a continuous film only when the metal islands have grown together after numerous ALD cycles. Thereby attempting of using different surface treatments on the basis of enhancement of nucleation sites may be applied into studies in the future.

From the aspect of thin film deposition the Pt growth in form of nanoclusters on an oxide surface during the nucleation stage of ALD may not be highly desired, on the other hand, such phenomenon resembles the structure of oxide supported Pt catalysts, which has been intensively studied in the field of surface science for the purpose of maximizing the reactivity to improve its utilize efficiency in catalytic converter. Consequently, the

understanding of the nucleation behavior of Pt ALD can be improved on the basis of results from relevant surface science studies.

### 7.2.2 Studies on platinum thin films grown by ALD using H2O or H2 as counter reactant

The ligand removal steps are believed to be another critical factor that determines the efficiency for preparation of next cycle, the oxygen used in this study demonstrates but doesn't lead to immediate film growth by cycle numbers, suggesting that partial protecting ligands were not completely combusted, and thereby inhibit the subsequent adsorptions of source molecules. Such issue could possibly partially alleviate by utilizing stronger oxidizer as the counter reactant to facilitate reaction kinetics, for instance, water ($H_2O$) or hydrogen peroxide ($H_2O_2$) in vapor phase.

### 7.2.3 Attempting of different silylation agent for efficient employment of inhibiting layer on starting surface

It should be noted that the initial test used for the effectiveness of our approach to achieve selective ALD, the growth of $HfO_2$ films on silylated $SiO_2$/Si(100) surfaces, is not yet mature for microelectronic applications. Future work will be directed to test the silylation of films using liquid phase, and compare it with the gas phase deposition in terms of passivation. XPS analysis and followed up quantifications of those samples should reveal the relative coverage of nucleation sites after (vs. before) silylation: The signal of metal element corresponds to the amount of adsorption sites available on the surface, while the N XPS indicates how much silylation agent is deposited.

In addition, attempting using different silylation agent to achieve higher surface capping layer coverage leading to completely inhibited growth will be another objective. The ultimate goal is to utilize the nature of the surface to manipulate the deposition outcome in the ALD performance. We would like to be able to manipulate that.

## 7.3 References

[1] Sun, H.; Qin, X.; and Zaera, F. Chemical Nature of the Thin Films that Form on $SiO_2$/Si(100) Surfaces Upon Manganese Deposition. J. Phys. Chem. Lett., 2011, 2 (20), pp 2525–2530. DOI: 10.1021/jz201177w.

[2] Sun, H.; Qin, X.; and Zaera, F. Activation of Metal–Organic Precursors by Electron Bombardment in the Gas Phase for Enhanced Deposition of Solid Films. J. Phys. Chem. Lett., 2012, 3 (17), pp 2523–2527. DOI: 10.1021/jz3011332.

[3] Slavov, S.V.; Sanger, A.R.; and Chuang, K.T. Mechanism of Silation of Silica with Hexamethyldisilazane. J. Phys. Chem. B, 2000, 104 (5), pp 983–989. DOI: 10.1021/jp991715v.

[4] Guo, L.; Qin, X.; and Zaera, F. Chemical Treatment of Low-k Dielectric Surfaces for Patterning of Thin Solid Films in Microelectronic Applications. ACS Appl. Mater. Interfaces, 2016, 8 (9), pp 6293–6300. DOI: 10.1021/acsami.6b00495.

[5] Guo, L.; Lee, I.; and Zaera, F. Patterning of Solid Films via Selective Atomic Layer Deposition Based on Silylation and UV/Ozonolysis. ACS Appl. Mater. Interfaces, 2016, 8 (30), pp 19836–19841. DOI: 10.1021/acsami.6b07192.

[6] Tiznado, H.; and Zaera, F. Surface Chemistry in the Atomic Layer Deposition of TiN Films from $TiCl_4$ and Ammonia. J. Phys. Chem. B, 2006, 110 (27), pp 13491–13498. DOI: 10.1021/jp062019f.

[7] Guo, L.; and Zaera, F. Spatial resolution in thin film deposition on silicon surfaces by combining silylation and UV/ozonolysis. Nanotechnology, Volume 25(50), Nov. 2014.